Electronic Supplementary Information

Co-assembly Mediated Biosupramolecular Catalysis: Thermodynamic insights into Nucleobase-Specific (Oligo)nucleotide Attachment and Cleavage

Priyanka,[a] Subhabrata Maiti* [a]

[a] Department of Chemical Sciences, Indian Institute of Science Education and Research (IISER) Mohali, Knowledge City, Manauli 140306, India

*Email: smaiti@iisermohali.ac.in

Table of Contents

1. Materials and Methods:

All commercially available reagents were used as received without any further purification. The chemicals sodium phosphate dibasic (Na_2HPO_4), hexadecyl bromide ($C_{16}H_{33}Br$), 1-bromododecane ($C_{12}H_{25}Br$), 1-bromooctane ($C_8H_{15}Br$), 1-bromobutane (C_4H_9Br), Dipotassium phosphate (K_2HPO_4), Potassium dihydrogen phosphate (KH_2PO_4), Fluorescein isothiocyanate (FITC), HEPES (4-(2-hydroxyethyl)-1-piperazineethanesulfonic acid), Bovine Serum Albumin (BSA), Cetyltrimethyl ammonium bromide (CTAB), Guanosine 5′ monophosphate disodium salt (GMP), Thymidine 5′ monophosphate disodium salt (TMP), Adenosine, Guanosine, Cytidine and Thymidine were procured from Sisco Research Laboratory (SRL), India. All oligonucleotide sequences, Adenosine 5′ triphosphate disodium salt (ATP), adenosine 5′ diphosphate disodium salt (ADP), Adenosine 5′ monophosphate disodium salt (AMP), di-picolyl amine, coumarin 153, Bis(4-nitrophenyl) phosphate (BPNPP), para-nitrophenyl phosphate (PNPP) and alkaline phosphatase (ALP) of bovine origin were purchased from Sigma-Aldrich. Cytidine 5′ monophosphate disodium salt (CMP) was purchased from TCI Chemicals India. The chemicals potassium carbonate (K_2CO_3), potassium iodide (KI), Formic acid (HCOOH) and para-nitrophenol (PNP) were also purchased from SRL India, and magnesium nitrate was obtained from Molychem. HPLC grade methanol and acetonitrile purchased from Sigma-Aldrich were used in synthesis and HPLC.

The Dynamic Light Scattering (DLS) data was recorded on Horiba Scientific Nanoparticle Analyzer SZ100V2.

Stock solutions of enzyme/dye were prepared both by weight and by UV–visible spectroscopy using molar extinction ε_{280} (alkaline phosphatase from calf intestine) = 106 400 $M^{-1}cm^{-1}$, ε_{364} (Laurdan) = 20 000 M^{-1} cm^{-1} (in methanol), ε_{430}(C153)=20000 $M^{-1}cm^{-1}$ (in ethanol), ε_{310} (PNPP)=9800 $M^{-1}cm^{-1}$, ε_{290} (BPNPP)=18000 $M^{-1}cm^{-1}$, ε_{259} (AM/D/TP)=15400 $M^{-1}cm^{-1}$, ε_{253}(GMP)=13700 $M^{-1}cm^{-1}$, ε_{267}(TMP)=10200 $M^{-1}cm^{-1}$, ε_{272}(CMP)=9100 $M^{-1}cm^{-1}$. UV-vis studies were performed using a Varian Cary 60 (Agilent Technologies) spectrophotometer. Product Formation (PNP) was calculated using ε_{400}(PNP)=11000 $M^{-1}cm^{-1}$. The total reaction volume in the cuvette was fixed at 1 ml, and a cuvette with a path length of 1 cm was used for the entire kinetic study. All measurements were performed at 25 °C.

Fluorescence measurements were performed using Cary Eclipse Fluorescence Spectro-fluorometer.

Circular Dichroism (CD) Measurements were performed using Chirascan Spectrophotometer (Applied Photophysics) using a 1 mm path length quartz cell. The spectra were recorded over a scan range of 200-300 nm. The concentration of alkaline phosphatase used for the CD measurement was 2 μM. All measurements were recorded in triplicate. The calculations of α-helix and β-sheet content were performed using the BeStSel (beta structure selection) method.[S1]

Melting temperature measurements were performed using a Cary-Eclipse 3500 (Agilent Technologies).

The transmission electron microscopy images were taken using a JEOL JEM-F200 microscope.

Time-correlated single-photon counting (TCSPC) was measured in (Horiba Jobin Yvon, NJ). The samples were excited using 440-nm and 480-nm NanoLED picosecond laser diodes.

The surfactant $C_{16}DPA{\bullet}Zn^{2+}$ was synthesized and characterized as reported in the literature.[S2]

2. Synthesis and Characterization

Synthesis of C_4DPA

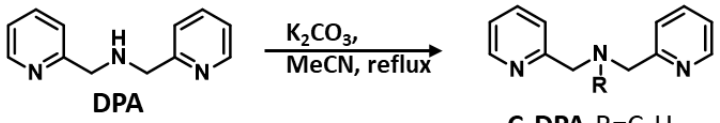

C_4DPA R=C_4H_9
C_8DPA R=C_8H_{17}
C_{12}DPA R=$C_{12}H_{25}$
C_{16}DPA R=$C_{16}H_{33}$

Di-(2-picolyl)amine (100 mg, 0.5 mmol) and 1-bromobutane (68.51mg, 0.5 mmol) were added to a suspension of K_2CO_3 in MeCN (10 ml). The suspension was refluxed and stirred for 24 h, after which it was filtered. After evaporation under reduced pressure, the crude product was purified using column chromatography (silica gel, eluent: hexane/EtOAc) yielded the product as a faintly yellow sticky oil (31%).

^{1}H NMR (δ ppm, $CDCl_3$, 298 K, 400 MHz): 8.52-8.51 (m, 2H), 7.67-7.63 (td, J = 8, 8 Hz, 2H), 7.56-7.54 (m, 2H), 7.15–7.12 (m, 2H), 3.81 (s, 4H), 2.54(m, 2H), 1.56-1.49 (m, 2H), 1.34-1.26 (m, 4H), 0.84 (t, J = 8 Hz, 3H).

^{13}C NMR (δ ppm, $CDCl_3$, 298 K, 100 MHz): 160.18, 148.90, 136.36, 122.80, 121.83, 60.48, 54.24, 29.70, 29.30, 20.50, 14.01.

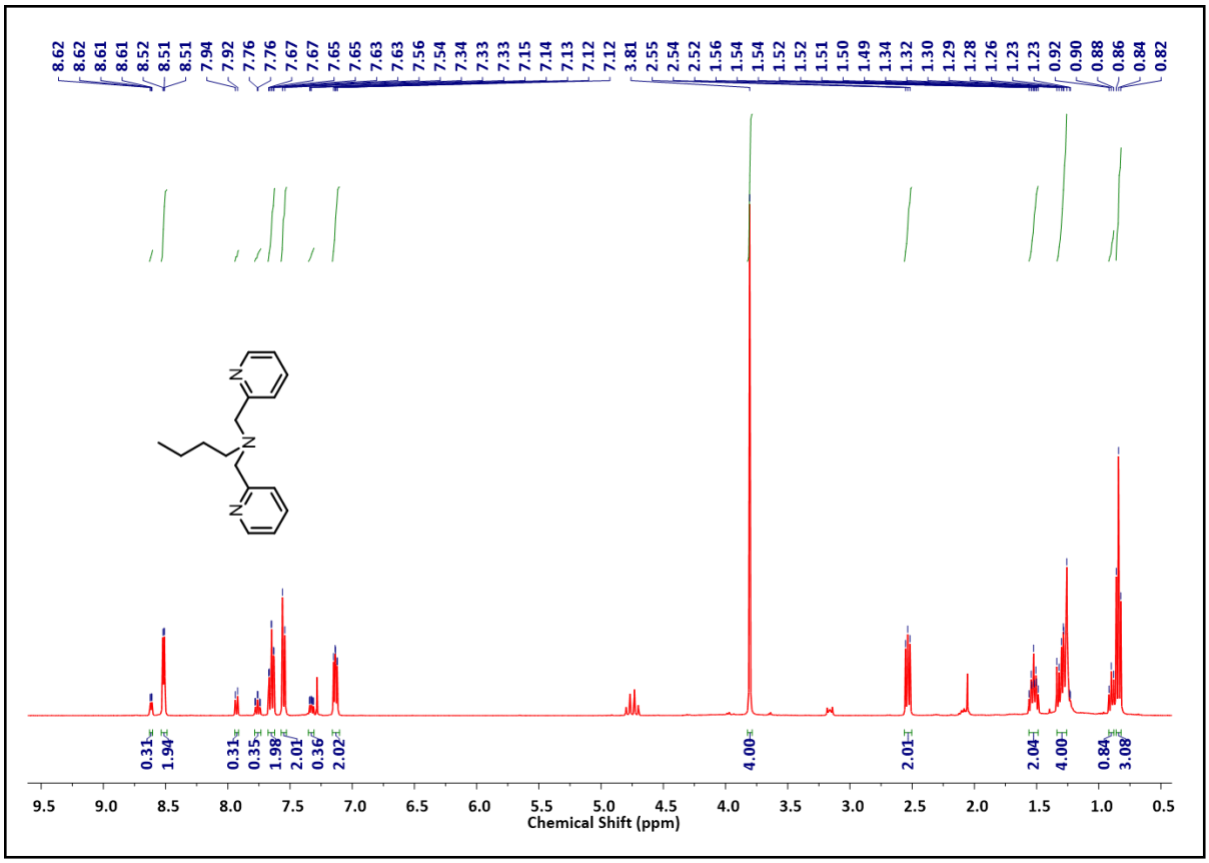

Fig. S1. ^{1}H-NMR Spectrum of Compound C_4DPA in CDCl3.

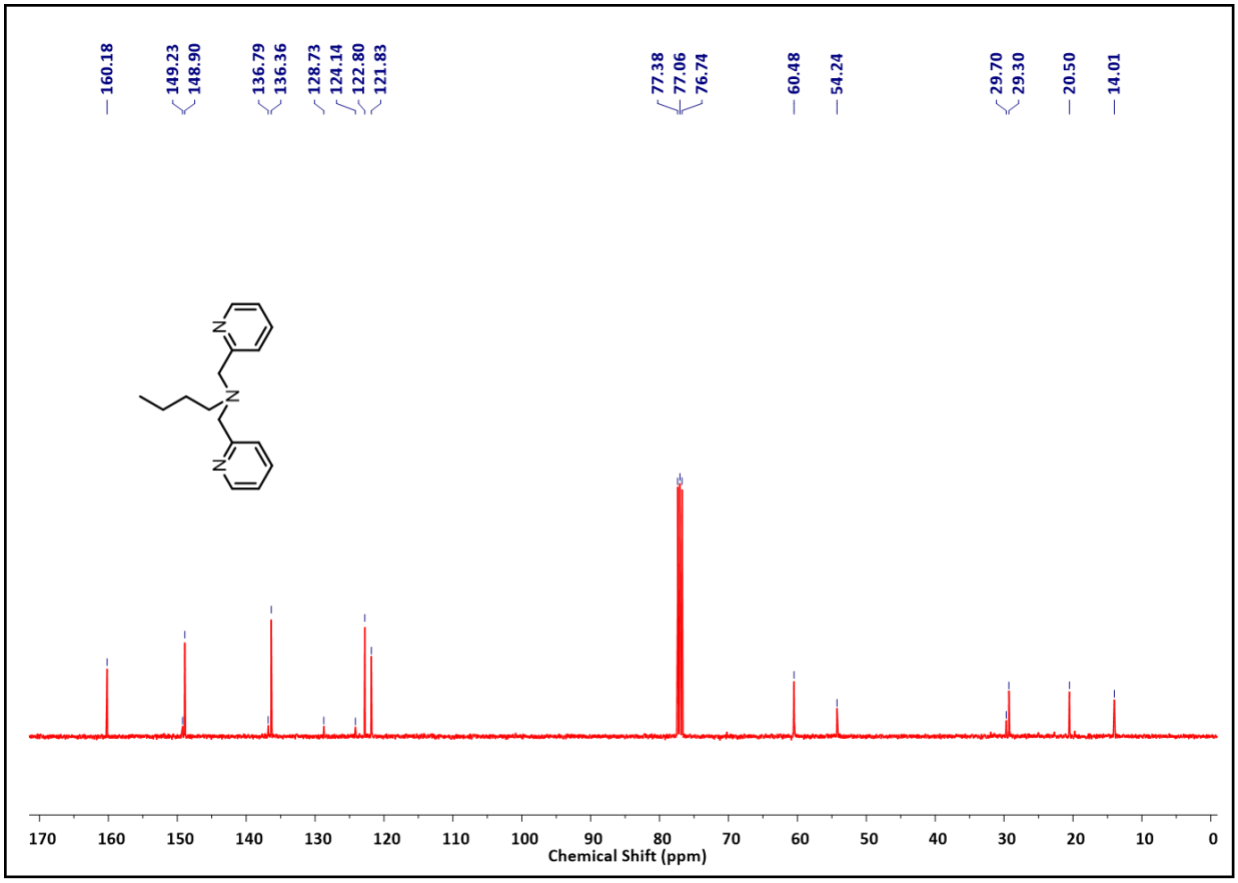

Fig. S2. ^{13}C-NMR Spectrum of Compound C_4DPA in CDCl3.

Synthesis of C_8DPA

Di-(2-picolyl)amine (100 mg, 0.5 mmol) and 1-bromooctane (96.56mg, 0.5 mmol) were added to a suspension of K_2CO_3 in MeCN (10 ml). The suspension was refluxed and stirred for 24 h, after which it was filtered. After evaporation under reduced pressure, the crude product was purified using column chromatography (silica gel, eluent: hexane/EtOAc) yielded the product as a faintly yellow sticky oil (58%).

^{1}H NMR (δ ppm, $CDCl_3$, 298 K, 400 MHz): 8.54-8.53 (m, 2H), 7.67 (td, J = 4 Hz, 8 Hz, 2H), 7.57-7.55 (m, 2H), 7.17–7.14 (m, 2H), 3.82 (s, 4H), 2.54(m, 2H), 1.56-1.53 (m, 2H), 1.30-1.23 (m, 10H), 0.88 (t, J = 8 Hz, 3H).

^{13}C NMR (δ ppm, $CDCl_3$, 298 K, 100 MHz): 160.10, 148.92, 136.36, 122.83, 121.85, 60.48, 54.72, 31.85, 29.44, 29.27, 27.32, 27.06, 22.66, 14.12.

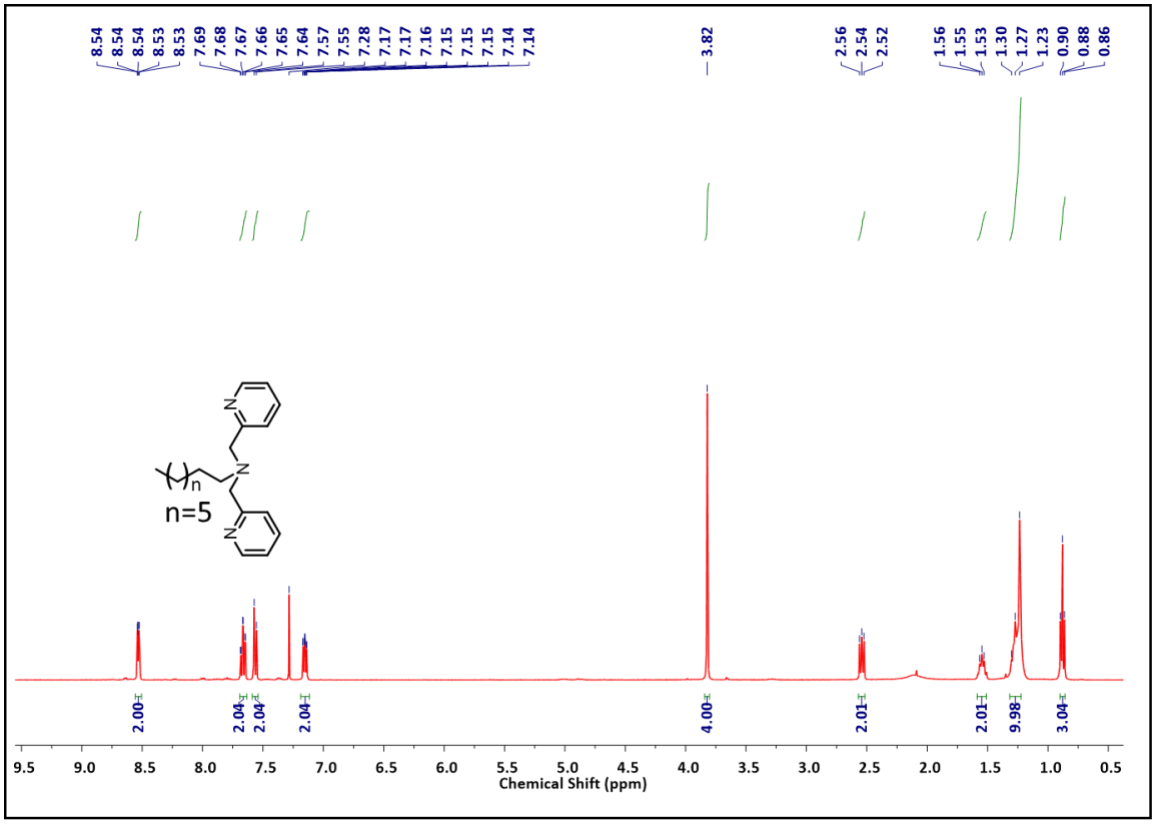

Fig. S3. ^{1}H-NMR Spectrum of Compound C_8DPA in CDCl3.

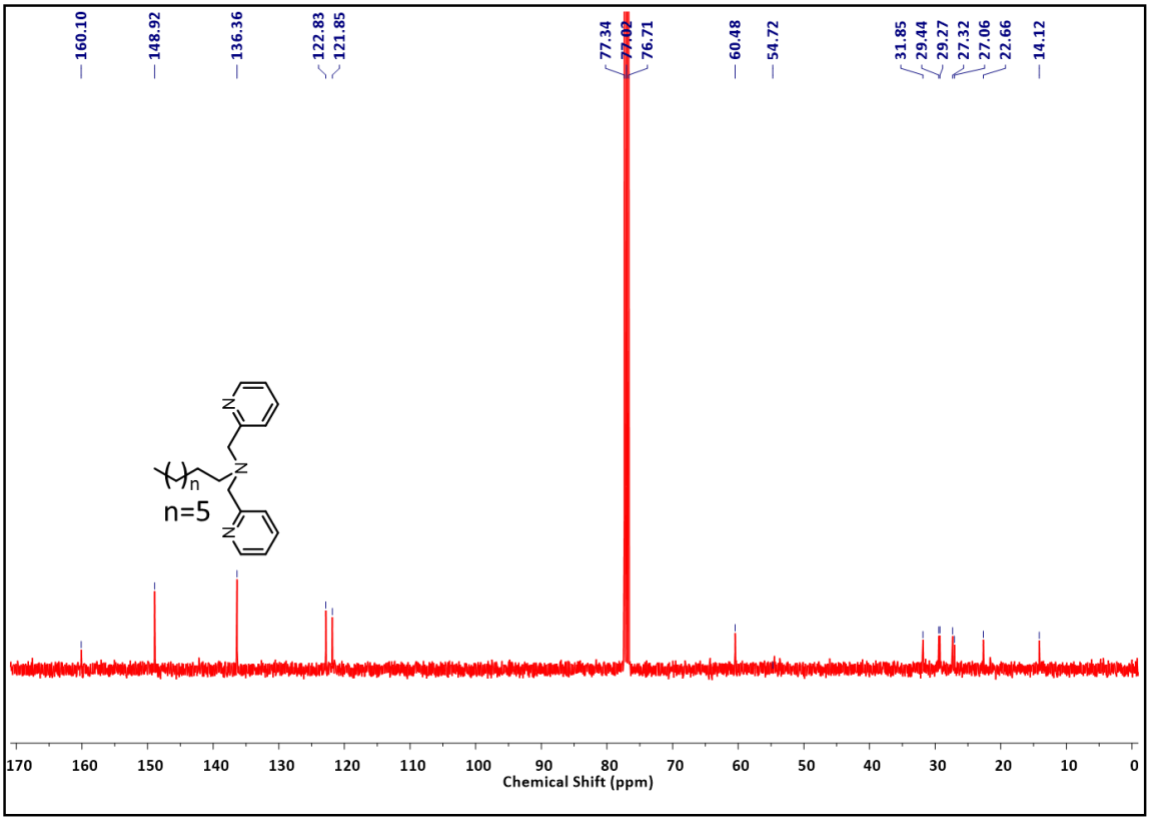

Fig. S4. ^{13}C-NMR Spectrum of Compound C_8DPA in CDCl3.

Synthesis of C_{12}DPA

C_{12}DPA was synthesized according to a literature protocol.[2] Di-(2-picolyl)amine (100 mg, 0.5 mmol) and 1-bromododecane (150mg, 0.5 mmol) were added to a suspension of K_2CO_3 in MeCN (10 ml). The suspension was refluxed and stirred for 24 h, after which it was filtered. After evaporation under reduced pressure, the crude product was purified using column chromatography (silica gel, eluent: hexane/EtOAc) yielded the product as a faintly yellow sticky oil (68%).

^{1}H NMR (δ ppm, $CDCl_3$, 298 K, 400 MHz): 8.53 (m, 2H), 7.67 (td, J = 4 Hz, 8 Hz, 2H), 7.58-7.56 (m, 2H), 7.17–7.14 (m, 2H), 3.84 (s, 4H), 2.55 (m, 2H), 1.57-1.54 (m, 2H), 1.33-1.23 (m, 18H), 0.89 (t, J = 8Hz, 3H).

^{13}C NMR (δ ppm, $CDCl_3$, 298 K, 100 MHz): 160.20, 148.91, 136.37, 122.81, 121.84, 60.50, 54.53, 31.93, 29.64, 29.50, 29.37, 27.33, 27.09, 22.71, 14.15.

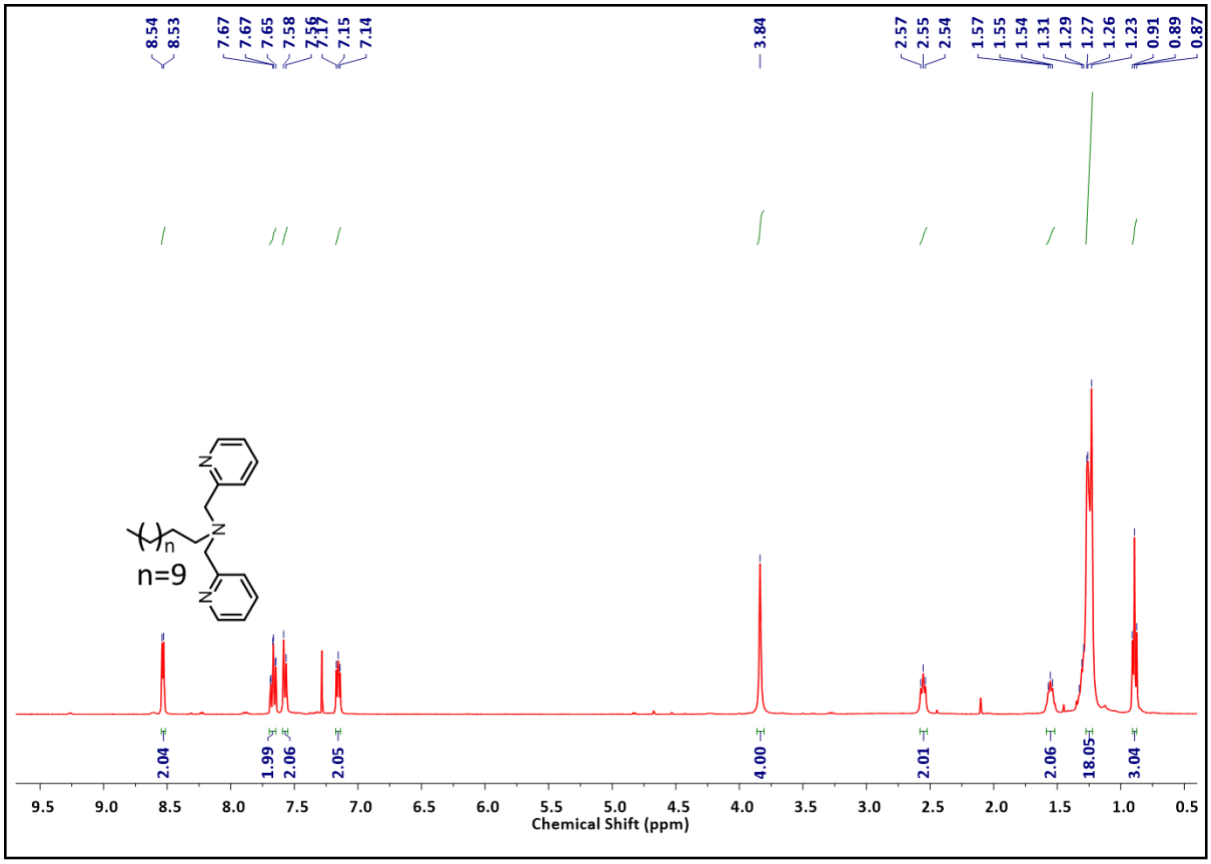

Fig. S5. ^{1}H-NMR Spectrum of Compound C_{12}DPA in CDCl3.

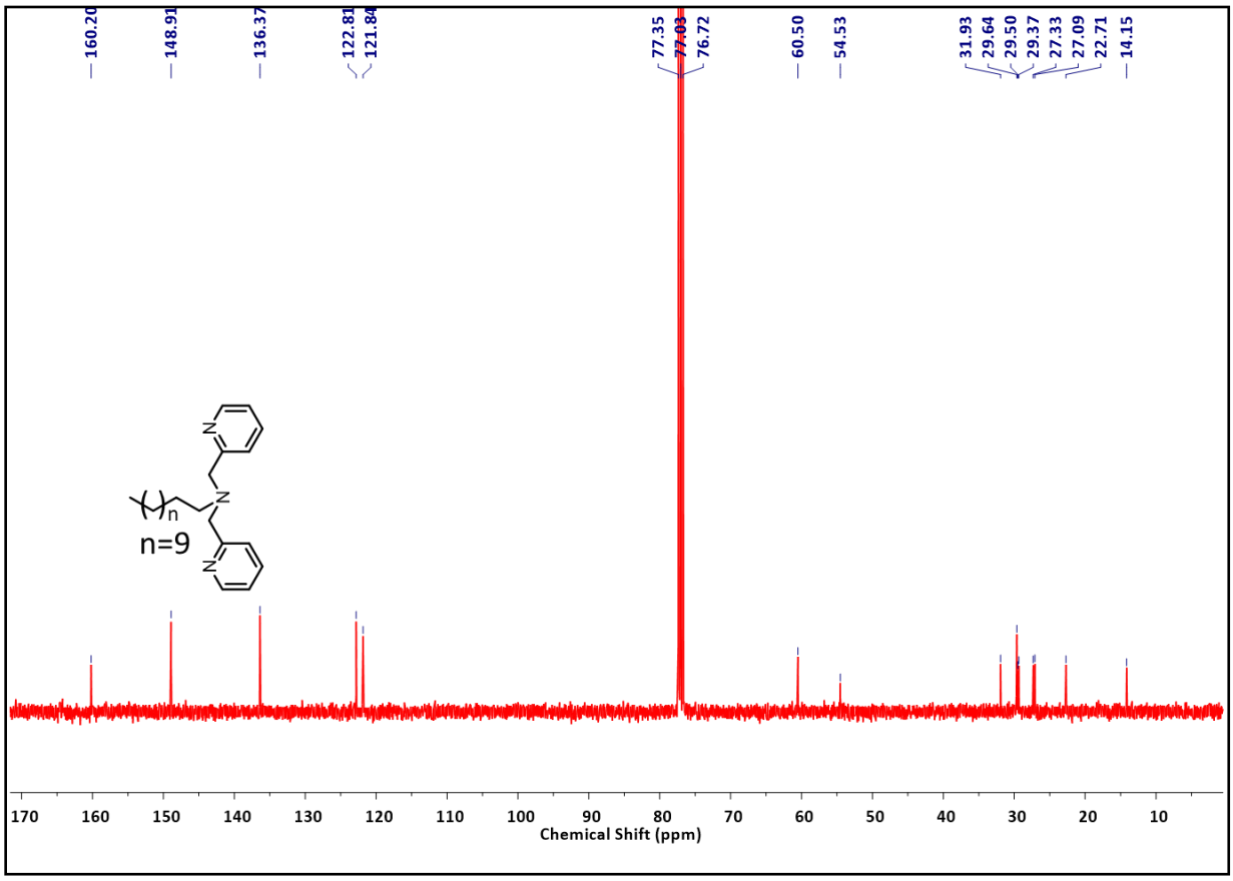

Fig. S6. ^{13}C-NMR Spectrum of Compound C_{12}DPA in CDCl3.

Synthesis of C_{16}DPA

C_{16}DPA was synthesized according to a literature protocol.[S2]

Preparation of $C_4DPA{\cdot}Zn^{2+}$

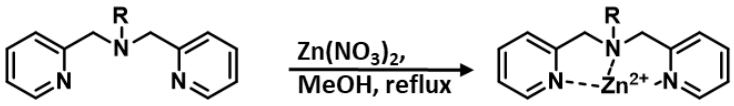

C_4DPA R=C_4H_9
C_8DPA R=C_8H_{17}
C_{12}DPA R=$C_{12}H_{25}$
C_{16}DPA R=$C_{16}H_{33}$

C_4DPA•Zn^{2+} R=C_4H_9
C_8DPA •Zn^{2+} R=C_8H_{17}
C_{12}DPA •Zn^{2+} R=$C_{12}H_{25}$
C_{16}DPA •Zn^{2+} R=$C_{16}H_{33}$

C_4DPA (40 mg, 0.16 mmol) and $Zn(NO_3)_2$ (47.6 mg, 0.16 mmol) were added to a round bottom flask and the reaction mixture was refluxed in MeOH for 3 h. The mixture was then evaporated to dryness under a vacuum in a rotatory evaporator yielding the product as a faint yellow solid, which was used for further observations without any purification.

Preparation of $C_8DPA{\cdot}Zn^{2+}$

C_8DPA (49.83 mg, 0.16 mmol) and $Zn(NO_3)_2$ (47.6 mg, 0.16 mmol) were added to a round bottom flask and the reaction mixture was refluxed in MeOH for 3 h. The mixture was then evaporated to dryness under a vacuum in a rotatory evaporator yielding the product as a faint yellow solid, which was used for further observations without any purification.

Preparation of $C_{12}DPA{\cdot}Zn^{2+}$

C_{12}DPA (67.78 mg, 0.16 mmol) and $Zn(NO_3)_2$ (47.6 mg, 0.16 mmol) were added to a round bottom flask and the reaction mixture was refluxed in MeOH for 3 h. The mixture was then evaporated to dryness under a vacuum in a rotatory evaporator yielding the product as a faint yellow solid, which was used for further observations without any purification.

Preparation of the $C_{16}DPA{\cdot}Zn^{2+}$

C_{16}DPA was synthesized according to a literature protocol.[2]

3. Catalytic activity with PNPP and BPNPP

i. In Buffer

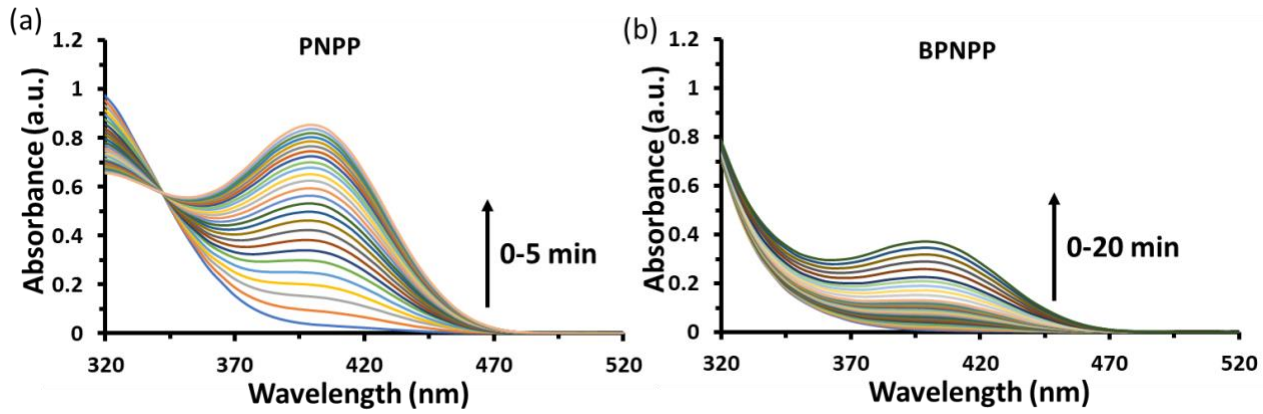

Fig. S7. Representative scanning kinetics images of (a) PNPP (b) BPNPP catalysis over time in presence of ALP. Experimental conditions: [PNPP] = 100 µM, [BPNPP] = 100 µM, [ALP] = 100 nM, [HEPES] = 5 mM, pH 7.0, T = 25 °C.

ii. **With $C_4DPA•Zn^{2+}$**

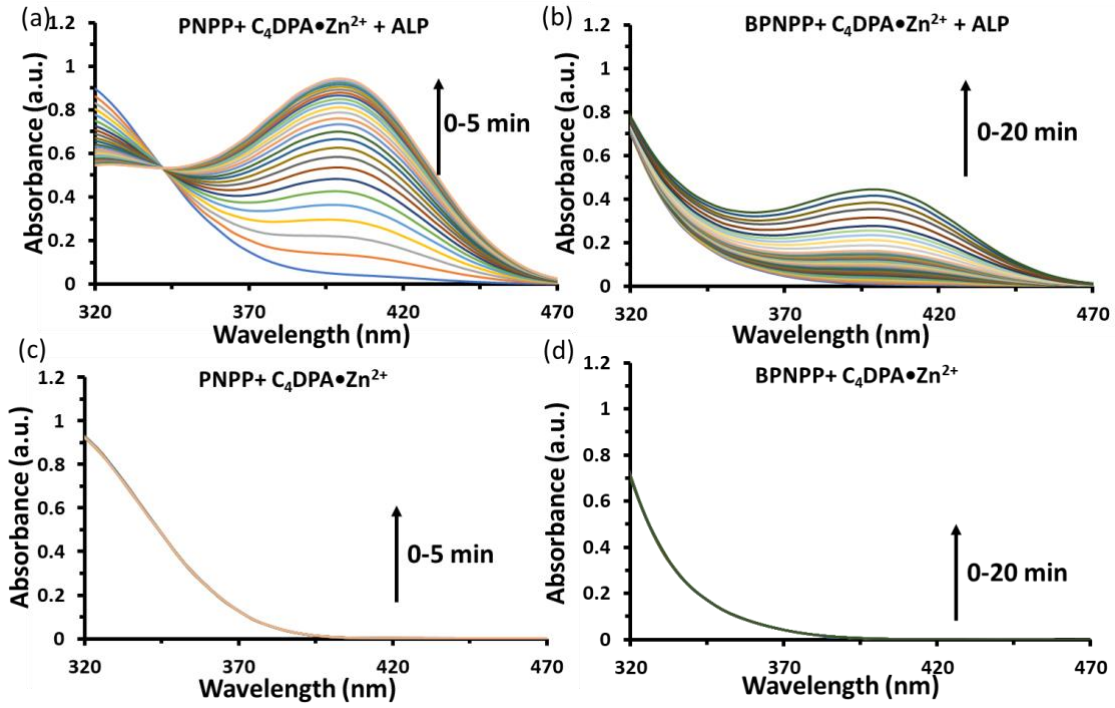

Fig. S8. Representative scanning kinetics images of catalysis of (a) PNPP (b) BPNPP with $C_4DPA•Zn^{2+}$ + ALP conjugate and (c) PNPP (d) BPNPP with $C_4DPA•Zn^{2+}$ over time. Experimental conditions: [PNPP] = 100 µM, [BPNPP] = 100 µM, [ALP] = 100 nM, [$C_4DPA•Zn^{2+}$] = 50 µM, [HEPES] = 5 mM, pH 7.0, T = 25 °C.

iii. With $C_8DPA•Zn^{2+}$

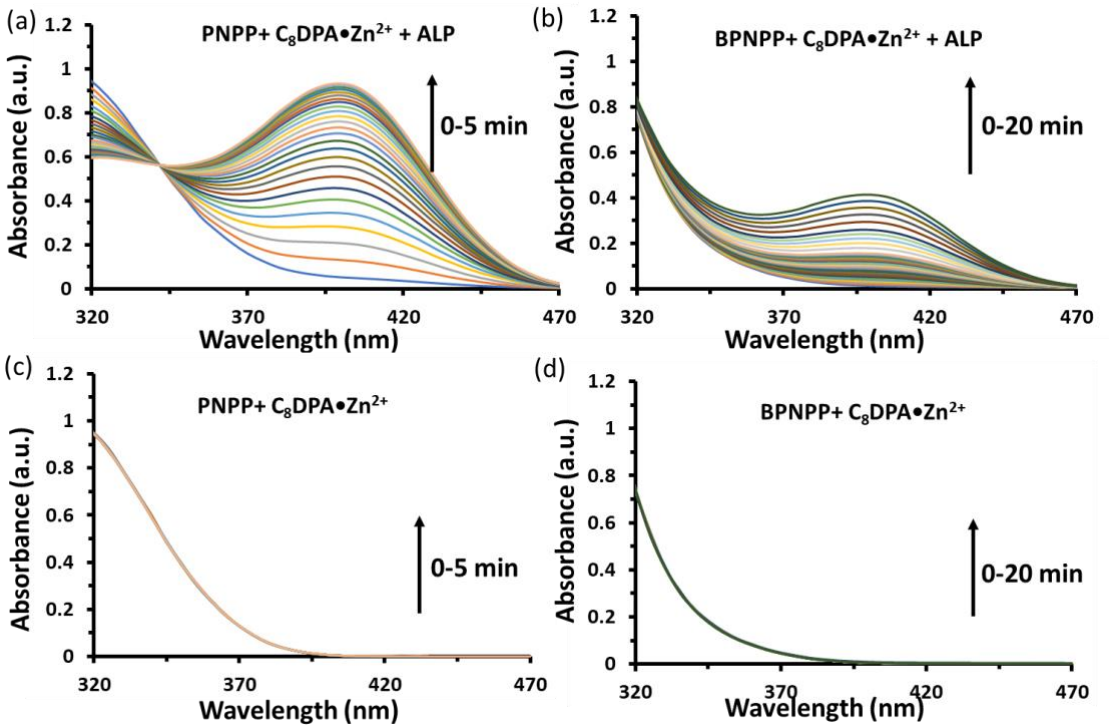

Fig. S9. Representative scanning kinetics images of catalysis of (a) PNPP (b) BPNPP with $C_8DPA•Zn^{2+}$ + ALP conjugate and (c) PNPP (d) BPNPP with $C_8DPA•Zn^{2+}$ over time. Experimental conditions: [PNPP] = 100 µM, [BPNPP] = 100 µM, [ALP] = 100 nM, [$C_8DPA•Zn^{2+}$] = 50 µM, [HEPES] = 5 mM, pH 7.0, T = 25 °C.

iv. With $C_{12}DPA•Zn^{2+}$

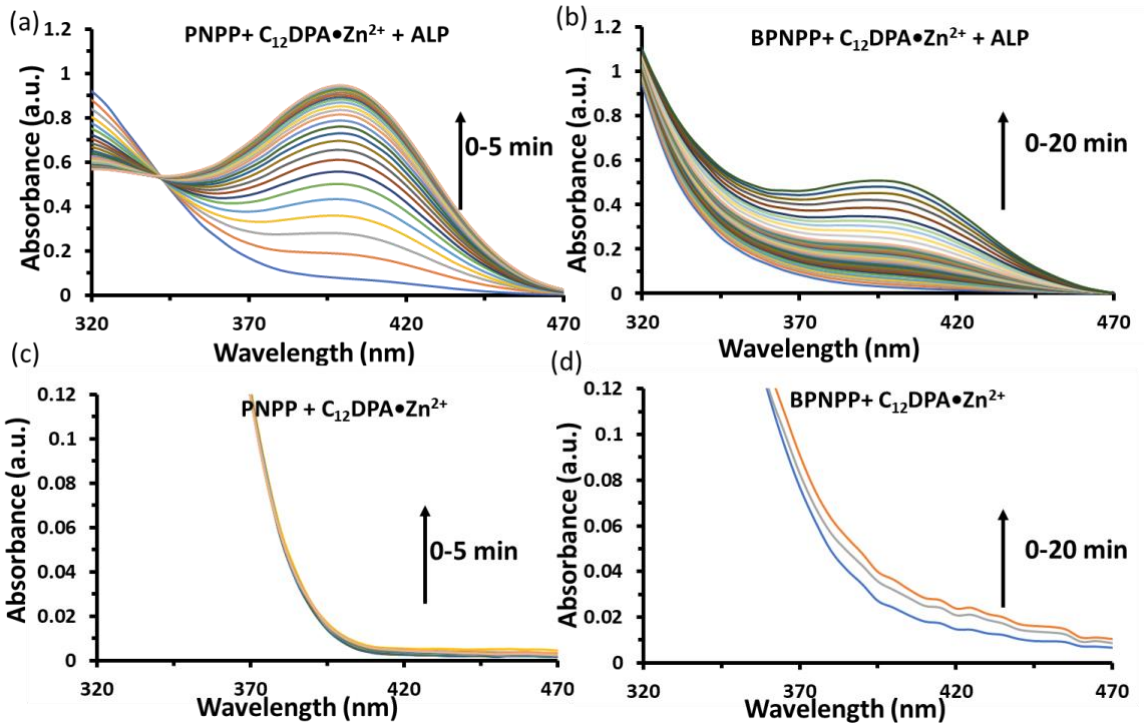

Fig. S10. Representative scanning kinetics images of catalysis of (a) PNPP (b) BPNPP with $C_{12}DPA•Zn^{2+}$ + ALP conjugate and (c) PNPP (d) BPNPP with $C_{12}DPA•Zn^{2+}$ over time. Experimental conditions: [PNPP] = 100 µM, [BPNPP] = 100 µM, [ALP] = 100 nM, [$C_{12}DPA•Zn^{2+}$] = 50 µM, [HEPES] = 5 mM, pH 7.0, T = 25 °C.

v. With $C_{16}DPA•Zn^{2+}$

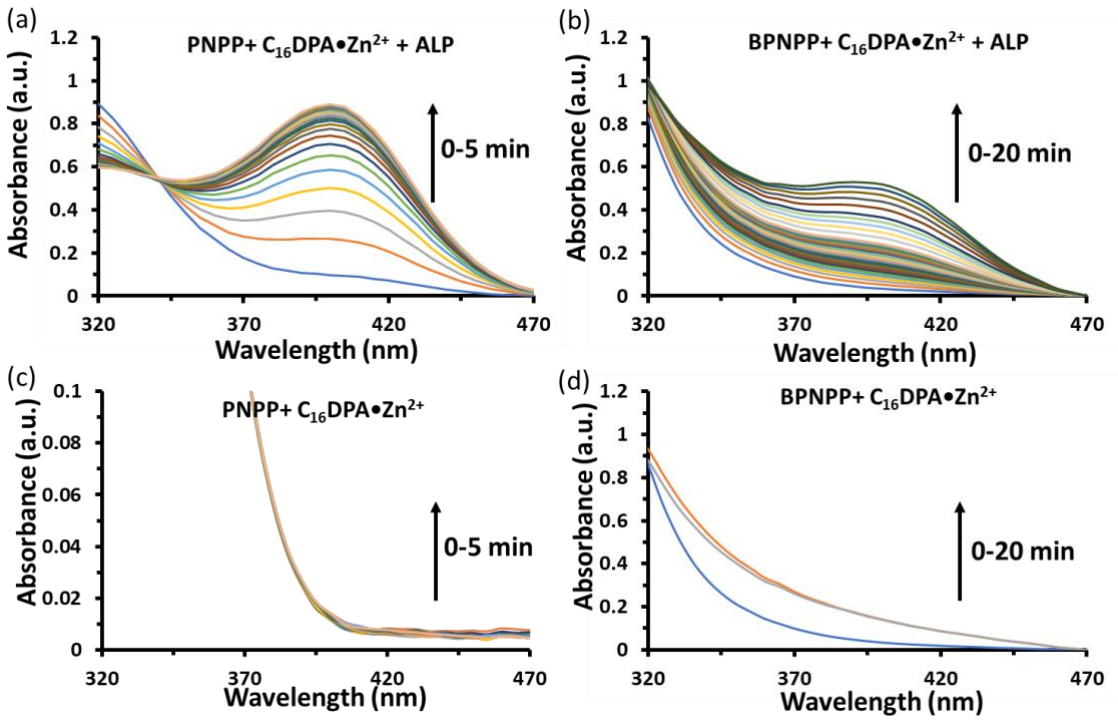

Fig. S11. Representative scanning kinetics images of catalysis of (a) PNPP (b) BPNPP with $C_{12}DPA•Zn^{2+}$ + ALP conjugate and (c) PNPP (d) BPNPP with $C_{12}DPA•Zn^{2+}$ over time. Experimental conditions: [PNPP] = 100 µM, [BPNPP] = 100 µM, [ALP] = 100 nM, [$C_{12}DPA•Zn^{2+}$] = 50 µM, [HEPES] = 5 mM, pH 7.0, T = 25 °C.

vi. With CTAB

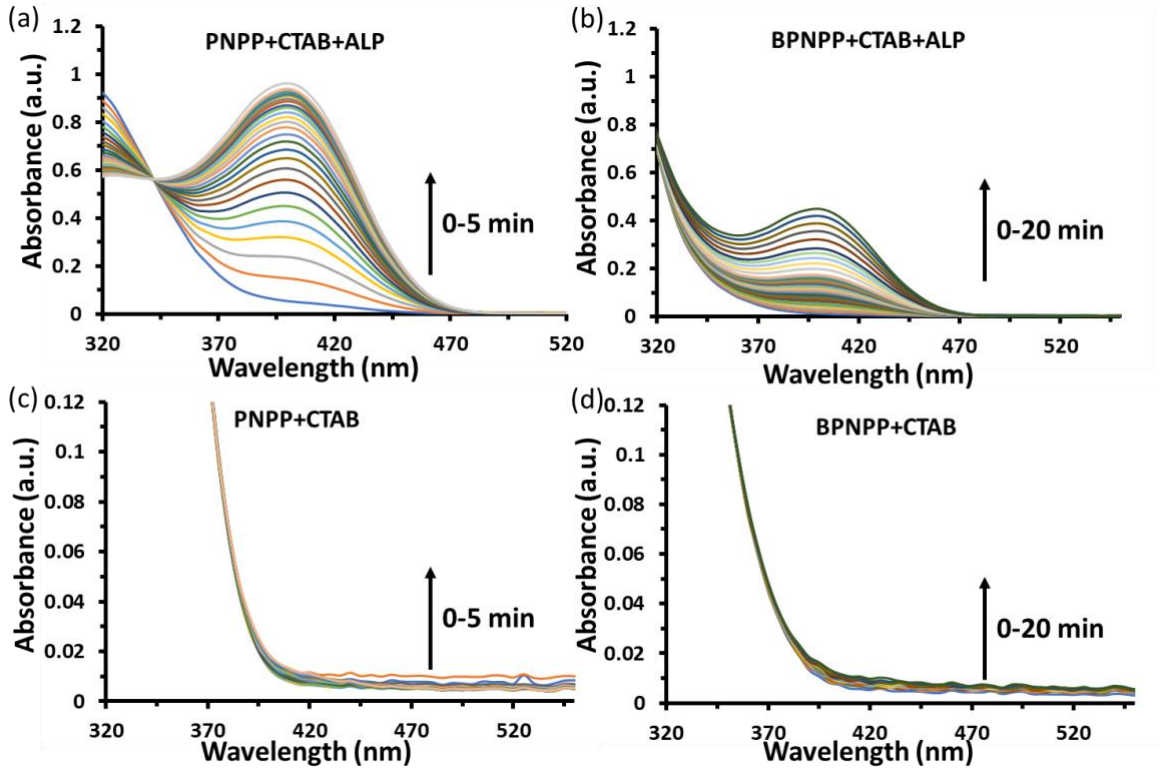

Fig. S12. Representative scanning kinetics images of catalysis of (a) PNPP (b) BPNPP with CTAB + ALP conjugate and (c) PNPP (d) BPNPP with CTAB over time. Experimental conditions: [PNPP] = 100 µM, [BPNPP] = 100 µM, [ALP] = 100 nM, [CTAB] = 50 µM, [HEPES] = 5 mM, pH 7.0, T = 25 °C.

vii. Catalytic activity of PNPP and BPNPP with Negatively Charged Protein BSA (Bovine Serum Albumin)

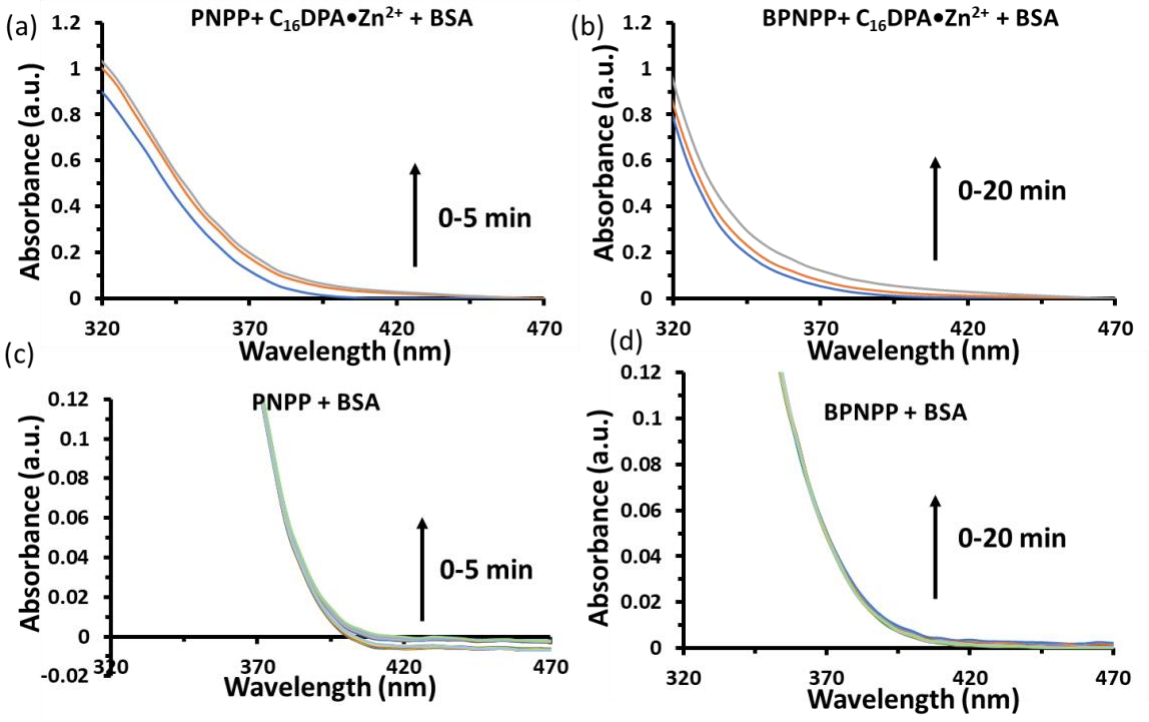

Fig. S13. Representative scanning kinetics images of catalysis of (a) PNPP (b) BPNPP with C_{16}DPA•Zn^{2+}+ ALB conjugate and (c) PNPP (d) BPNPP with BSA over time. Experimental conditions: [PNPP] = 100 µM, [BPNPP] = 100 µM, [BSA] = 1 µM, [C_{16}DPA•Zn^{2+}] = 50 µM, [HEPES] = 5 mM, pH 7.0, T = 25 °C.

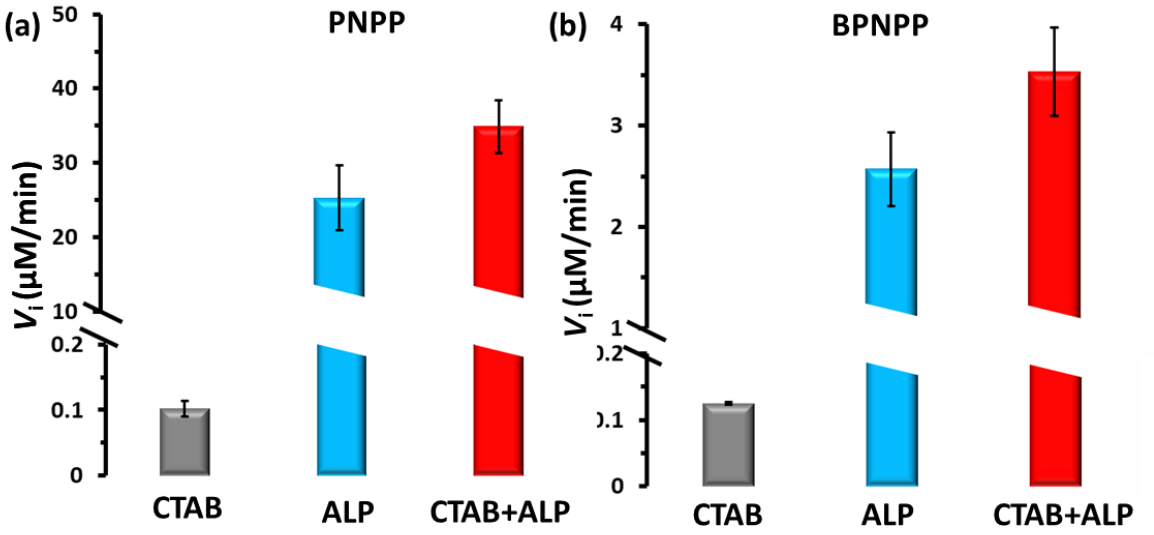

Fig. S14. Representative bar plot to show V_i of (a)PNPP and (b) BPNPP catalysis in the presence and absence of ALP with CTAB. Experimental conditions: [PNPP] = 100 μM, [BPNPP] = 100 μM, [ALP] = 100 nM, [CTAB] = 50 μM, [HEPES] = 5 mM, pH 7.0, T = 25 °C.

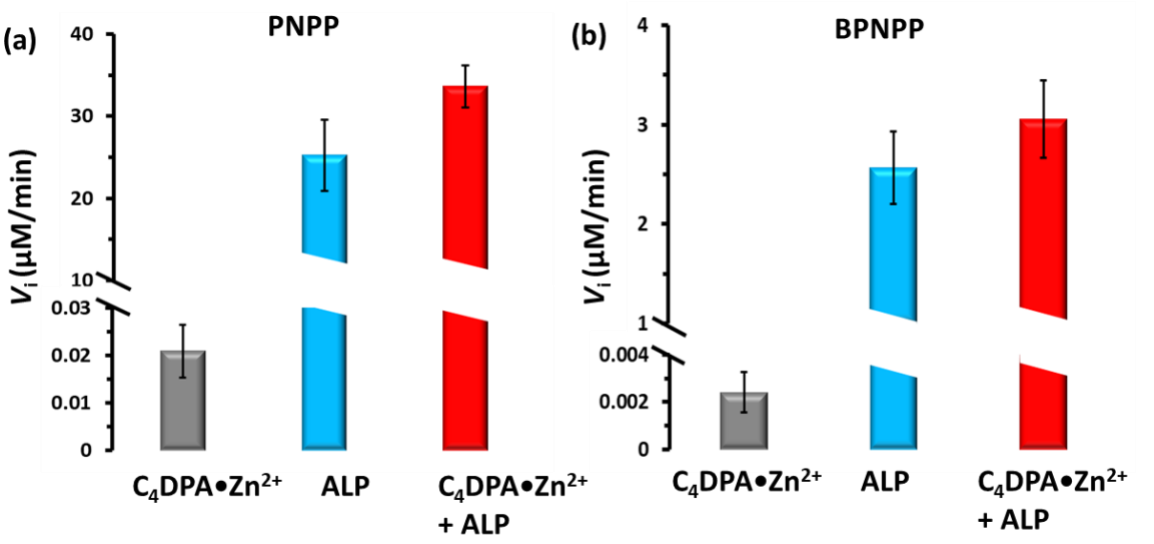

Fig. S15. Representative bar plot to show V_i of (a) PNPP and (b) BPNPP catalysis in the presence and absence of ALP with metallosurfactant. Experimental conditions: [PNPP] = 100 μM, [BPNPP] = 100 μM, [ALP] = 100 nM, [$C_4DPA•Zn^{2+}$] = 50 μM, [HEPES] = 5 mM, pH 7.0, T = 25 °C.

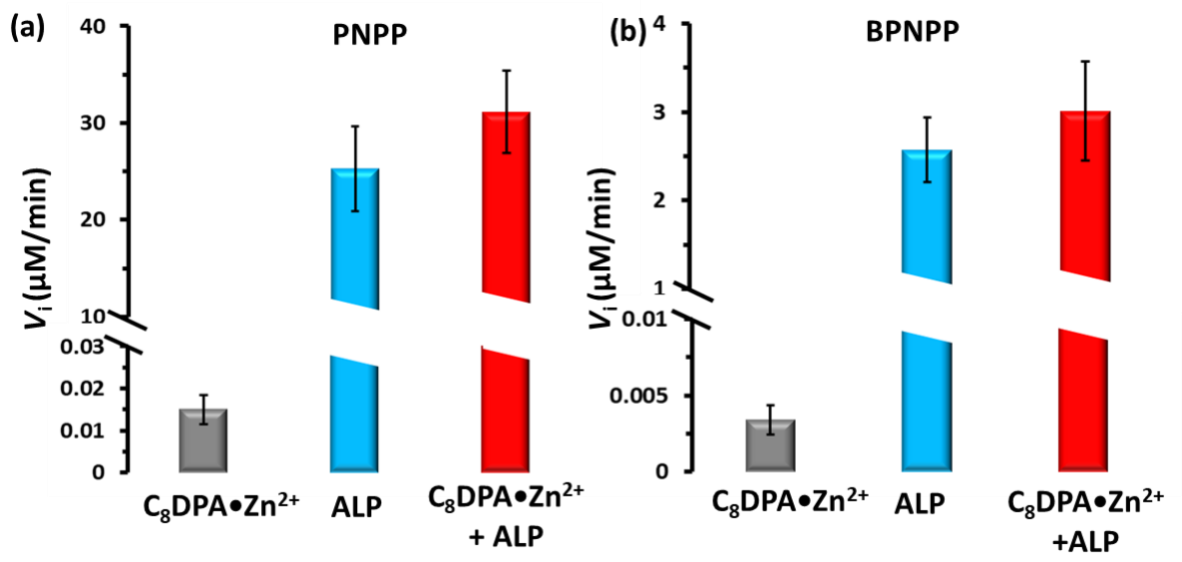

Fig. S16. Representative bar plot to show V_i of (a) PNPP and (b) BPNPP catalysis in the presence and absence of ALP with metallosurfactant. Experimental conditions: [PNPP] = 100 μM, [BPNPP] = 100 μM, [ALP] = 100 nM, [C_8DPA•Zn^{2+}] = 50 μM, [HEPES] = 5 mM, pH 7.0, T = 25 °C.

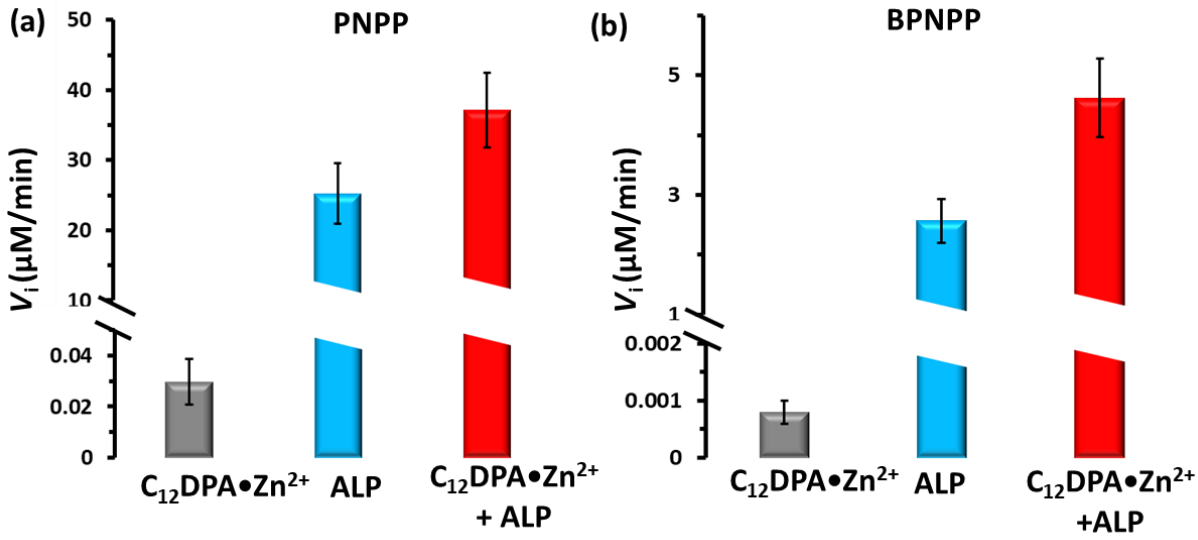

Fig. S17. Representative bar plot to show V_i of (a) PNPP and (b) BPNPP catalysis in the presence and absence of ALP with metallosurfactant. Experimental conditions: [PNPP] = 100 μM, [BPNPP] = 100 μM, [ALP] = 100 nM, [C_{12}DPA•Zn^{2+}] = 50 μM, [HEPES] = 5 mM, pH 7.0, T = 25 °C.

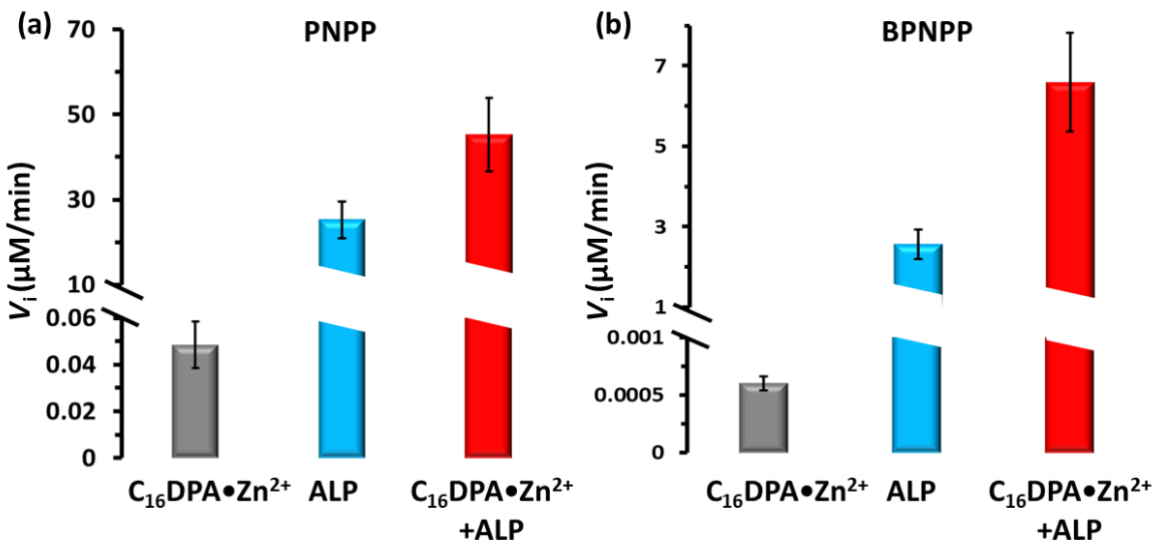

Fig. S18. Representative bar plot to show V_i of (a) PNPP and (b) BPNPP catalysis in the presence and absence of ALP with metallosurfactant. Experimental conditions: [PNPP] = 100 μM, [BPNPP] = 100 μM, [ALP] = 100 nM, [C_{16}DPA•Zn^{2+}] = 50 μM, [HEPES] = 5 mM, pH 7.0, T = 25 °C.

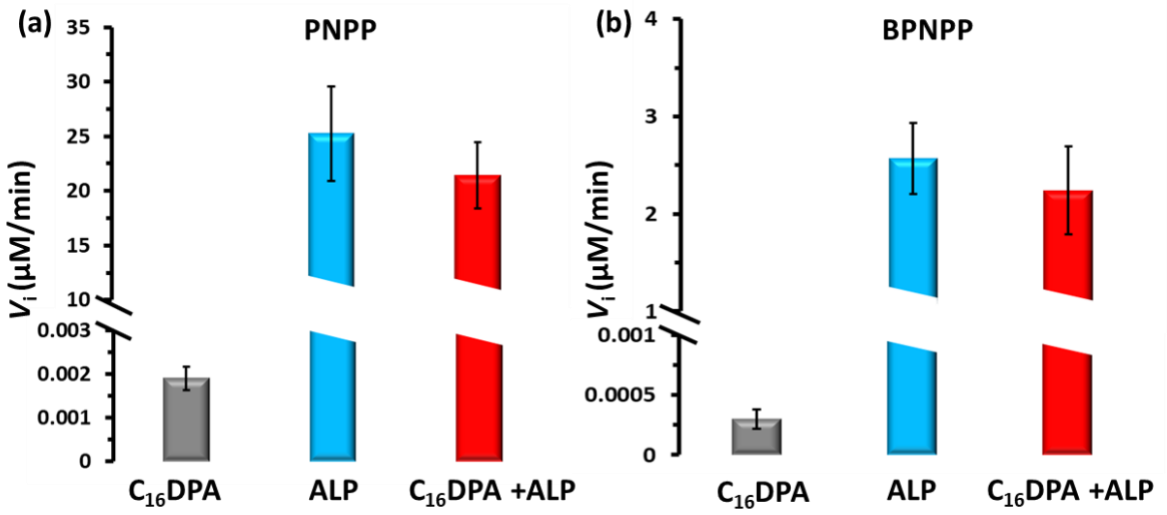

Fig. S19. Representative bar plot to show V_i of (a)PNPP and (b) BPNPP catalysis in the presence and absence of ALP with C_{16}DPA. Experimental conditions: [PNPP] = 100 μM, [BPNPP] = 100 μM, [ALP] = 100 nM, [C_{16}DPA] = 50 μM, [HEPES] = 5 mM, pH 7.0, T = 25 °C.

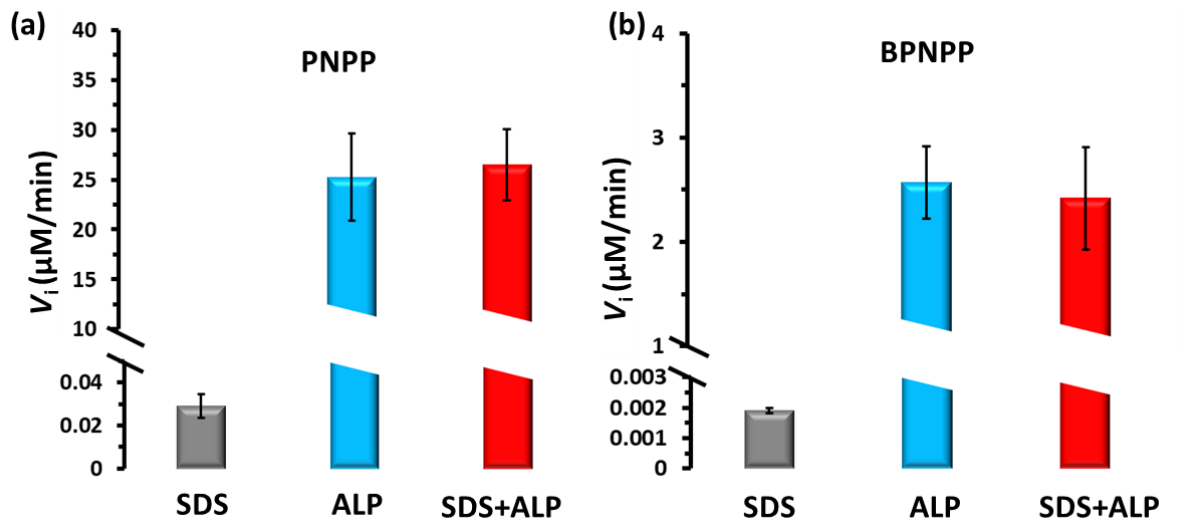

Fig. S20. Representative bar plot to show V_i of (a) PNPP and (b)BPNPP catalysis in the presence and absence of ALP with SDS. Experimental conditions: [PNPP] = 100 μM, [BPNPP] = 100 μM, [ALP] = 100 nM, [SDS] = 50 μM, [HEPES] = 5 mM, pH 7.0, T = 25 °C.

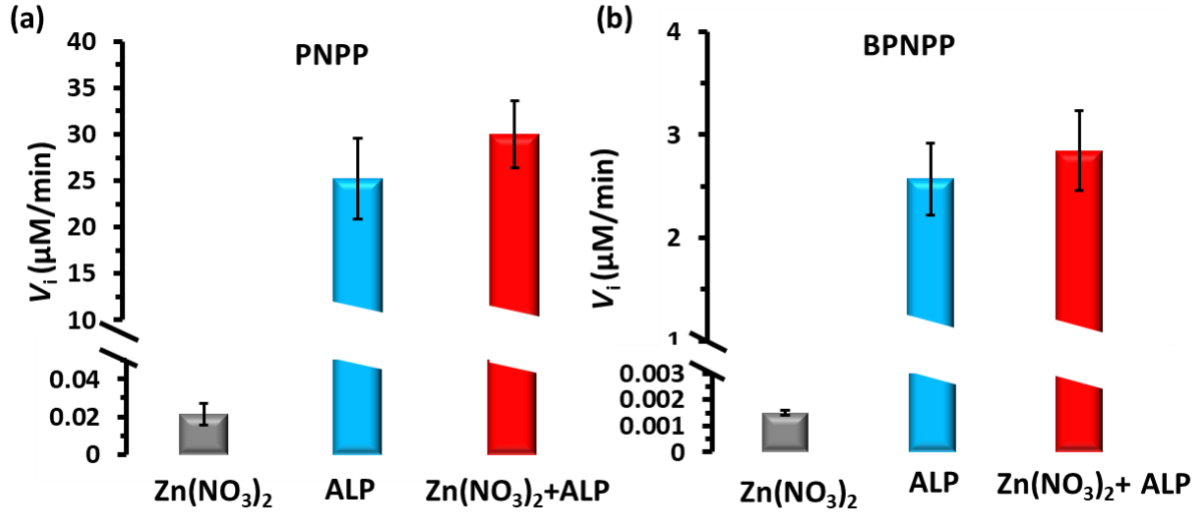

Fig. S21. Representative bar plot to show V_i of (a) PNPP and (b)BPNPP catalysis in the presence and absence of ALP with $Zn(NO_3)_2$. Experimental conditions: [PNPP] = 100 μM, [BPNPP] = 100 μM, [ALP] = 100 nM, [$Zn(NO_3)_2$] = 50 μM, [HEPES] = 5 mM, pH 7.0, T = 25 °C.

viii. With different Concentration of metallosurfactant

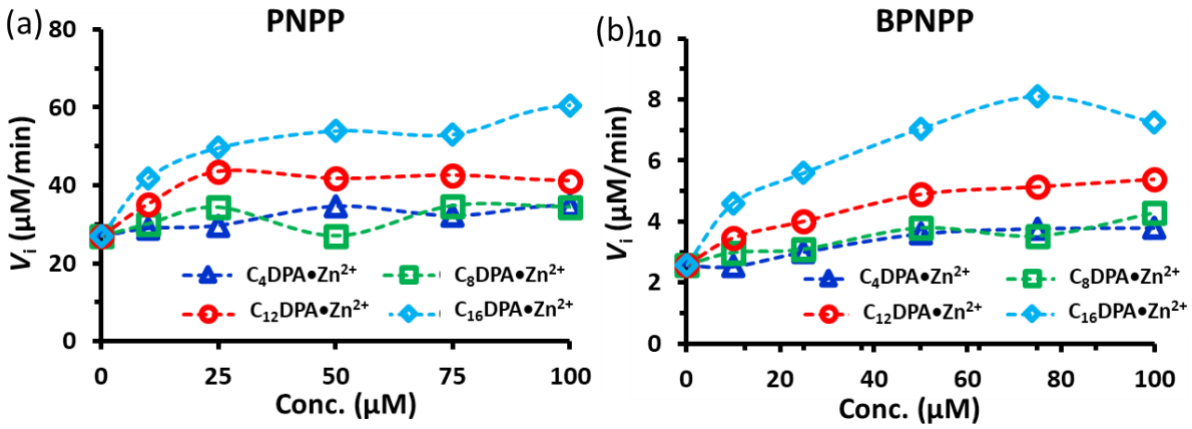

Fig. S22. Representative plot to show V_i of (a) PNPP (b) BPNPP catalysis in presence of ALP and different conc. of metallosurfactant. Experimental conditions: [PNPP] = 100 μM, [BPNPP] = 100 μM, [ALP] = 100 nM, [HEPES] = 5 mM, pH 7.0, T = 25 °C.

4. Complex Formation Study With ALP

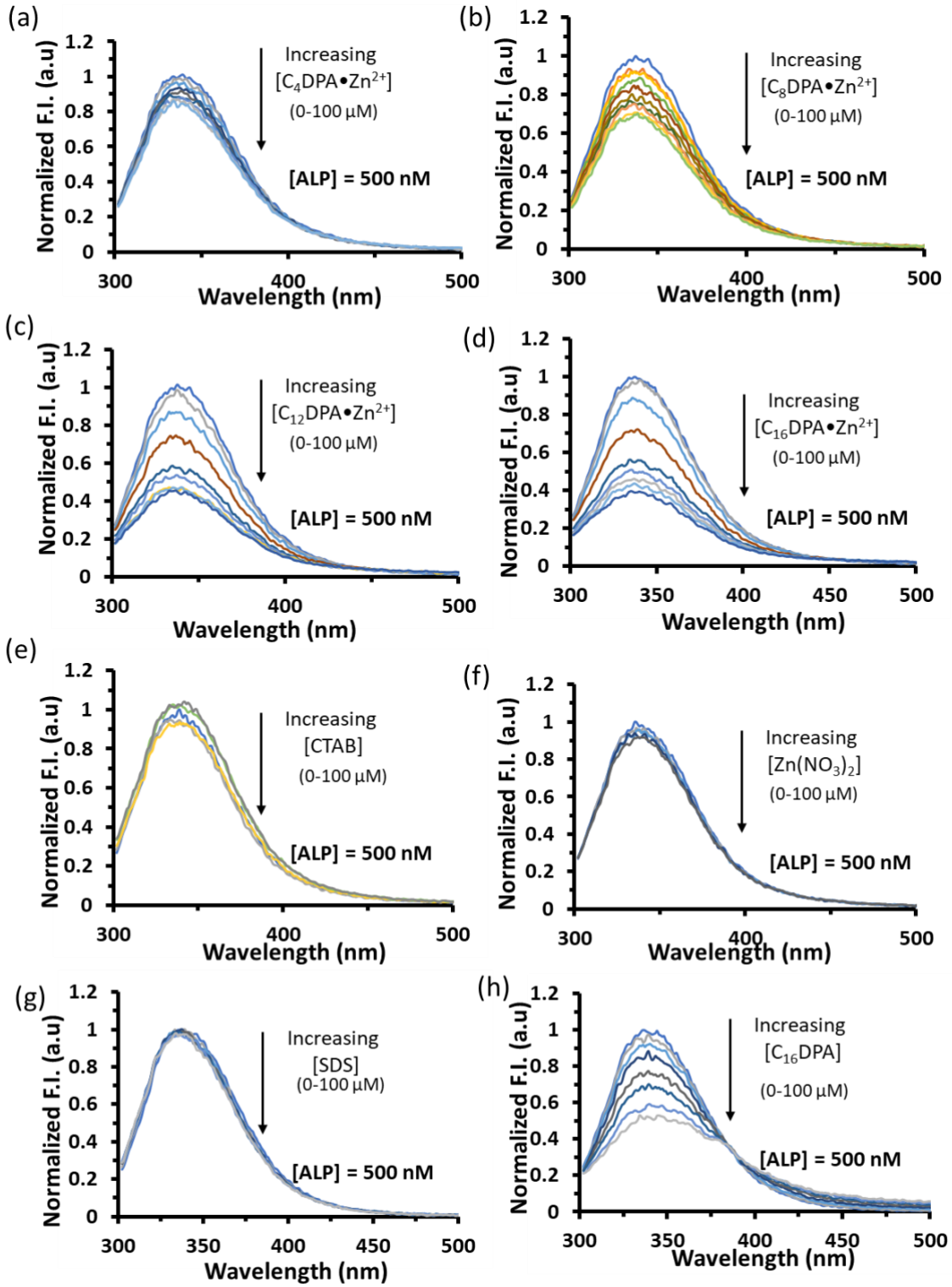

Fig. S23. Fluorescence emission spectra of ALP (500 nM) in the presence of (a) $C_4DPA•Zn^{2+}$ (b) $C_8DPA•Zn^{2+}$ (c) $C_{12}DPA•Zn^{2+}$ (d) $C_{16}DPA•Zn^{2+}$ (e) CTAB and (f) $Zn(NO_3)_2$ (g) SDS (h) $C_{16}DPA$ with the following concentrations: 0 µM, 1 µM, 5 µM, 10 µM, 20 µM, 35 µM, 50 µM, 75 µM and 100 µM. Experimental conditions: Slit Width ex/em = 5/5 nm, Excitation wavelength= 280nm, [HEPES] = 5 mM, pH 7.0, T = 25 °C.

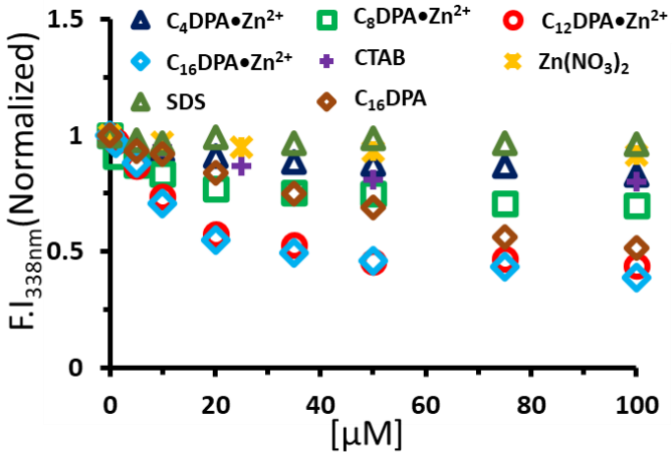

Fig. S24. Decrease in tryptophan fluorescence of native ALP in presence of metallosurfactant, CTAB, C_{16}DPA and $Zn(NO_3)_2$. Experimental conditions: Slit Width ex/em = 5/5 nm, Excitation wavelength= 280nm, [HEPES] = 5 mM, pH 7.0, T = 25 °C.

All the above-mentioned data mentioned in Fig. S7 to Fig. S17 suggest necessity of Zn^{2+} in the surfactant group for efficient binding of enzyme and substrate for enhanced catalytic phosphoester cleavage.

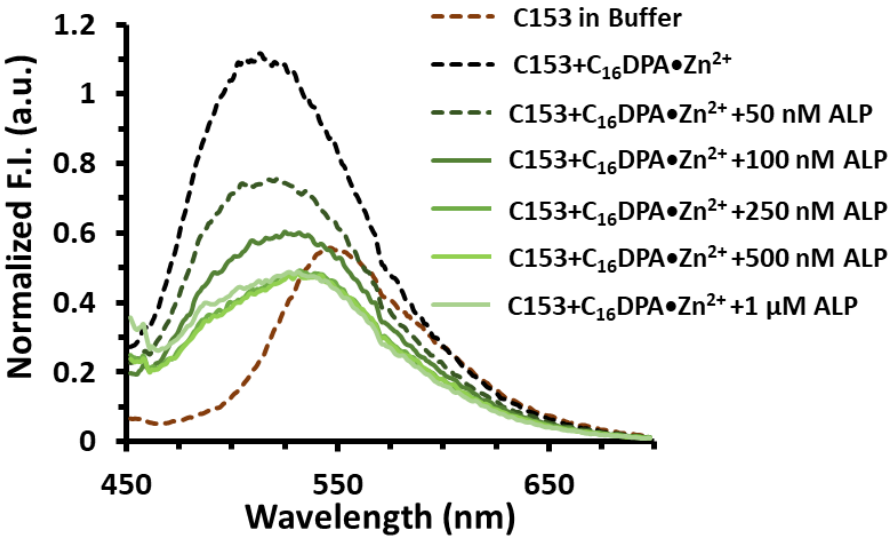

Fig. S25. Fluorescence emission spectra ALP in the presence of C_{16}DPA•Zn^{2+} using C153 as a hydrophobic probe. The blue shift of peaks in the presence of surfactant verifies the hydrophobic residence propensity of C153. Experimental conditions: [C_{16}DPA•Zn^{2+}] = 50 μM, [C153] = 1 μM, Slit Width ex/em = 5/5 nm, Excitation wavelength= 430nm, [HEPES] = 5 mM, pH 7.0, T = 25 °C.

5. Microscopic Images

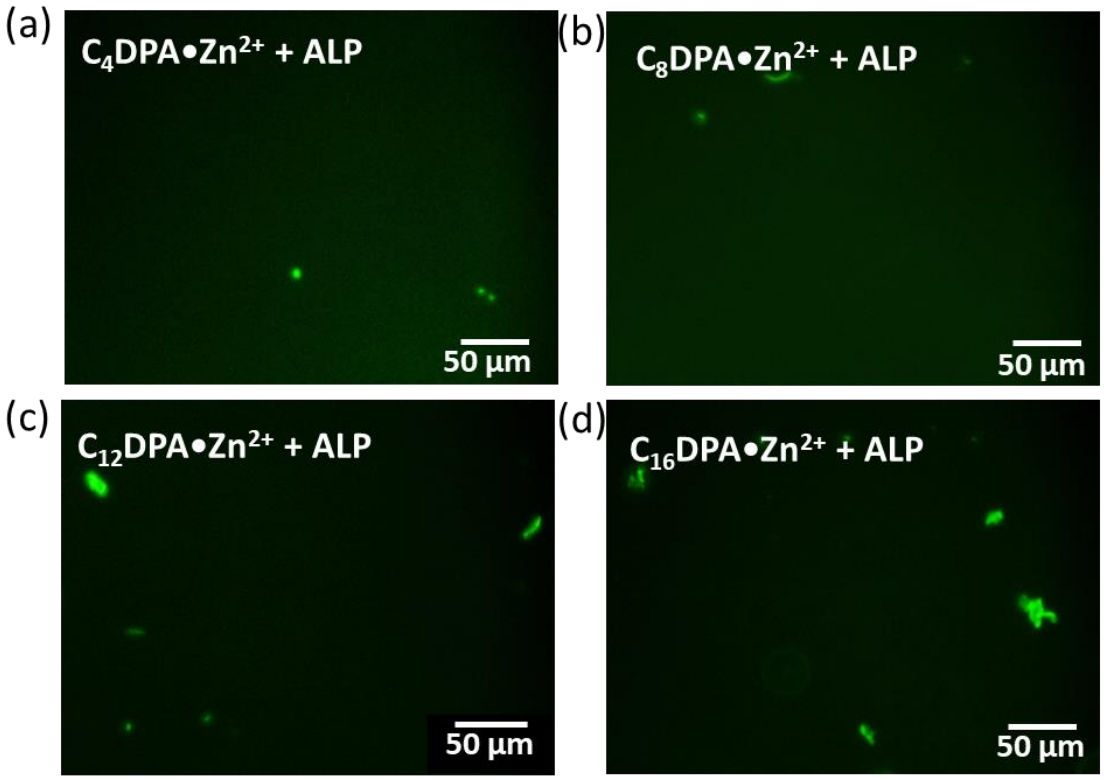

Fig. S26. Fluorescence microscopic images of conjugates of ALP with (a) $C_4DPA•Zn^{2+}$ (b) $C_8DPA•Zn^{2+}$ (c) $C_{12}DPA•Zn^{2+}$ (d) $C_{16}DPA•Zn^{2+}$ metallosurfactant. Images were captured after incubating the samples for 15 minutes. Experimental conditions: [ALP] = 1 µM, [C153] = 1 µM, [metallosurfactant] = 50 µM, [HEPES] = 5 mM, pH 7.0, T = 25 °C.

TEM Images

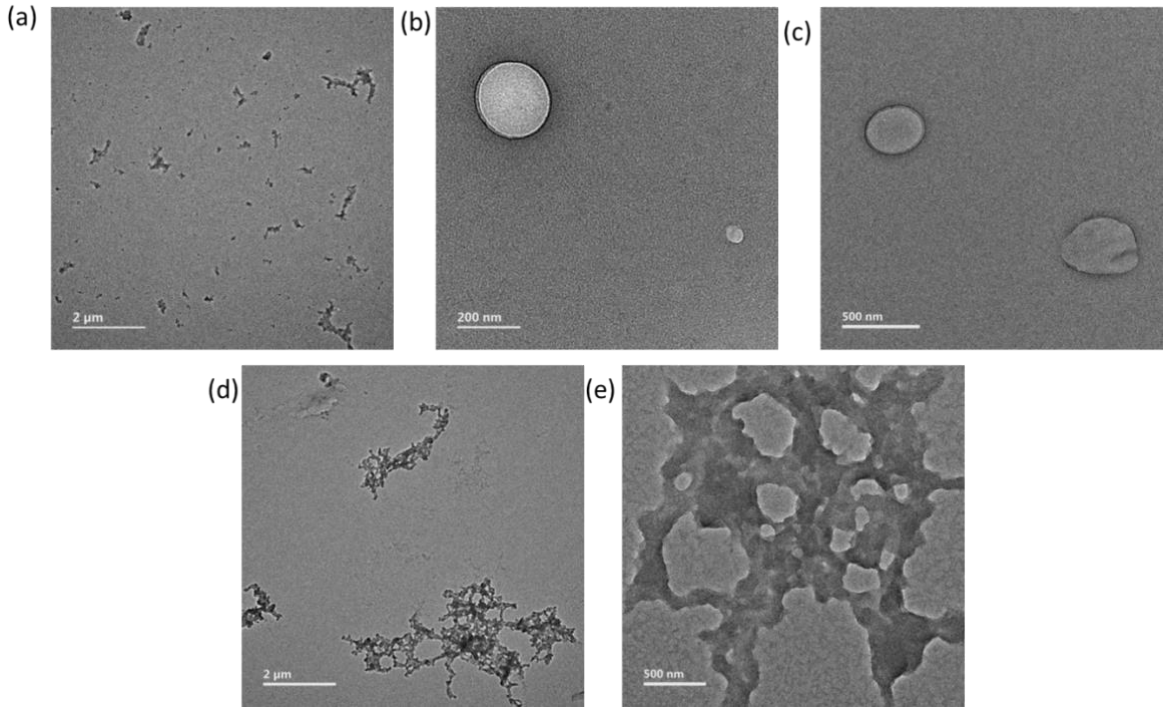

Fig. S27. TEM images of conjugates of C_{16}DPA•Zn^{2+} with (a) ALP (b) PNPP (c) BPNPP (d) PNPP+ALP (e) BPNPP+ALP. Images were captured after incubating the samples for 15 minutes. 0.1% uranyl acetate solution was used to stain the grid. Experimental conditions: [ALP] = 1 µM, [C_{16}DPA•Zn^{2+}] = 50 µM, [PNPP]= 100 µM, [BPNPP]= 100 µM, [uranyl acetate] = 0.1% [HEPES] = 5 mM, pH 7.0, T = 25 °C.

Table S1 Calculated K_{cat} ,K_M, V_{max} and K_{cat}/K_M values for PNPP and BPNPP

System	V_{max} (µM/min)	K_M (µM)	K_{cat} (/min)	K_{cat}/K_M (/µM/min)
PNPP (ALP)	63.26 ± 5	136 ± 9	632.55± 54	4.648
PNPP (C_{16}DPA•Zn^{2+} + ALP)	75.73 ± 4.3	36 ± 5	757.26± 43	20.779
BPNPP (ALP)	61.98 ± 6.2	190 ± 14	61.98 ± 6.2	0.3262
BPNPP (C_{16}DPA•Zn^{2+} + ALP)	72.07 ± 4.7	89 ± 7	72.07 ± 4.2	0.8097

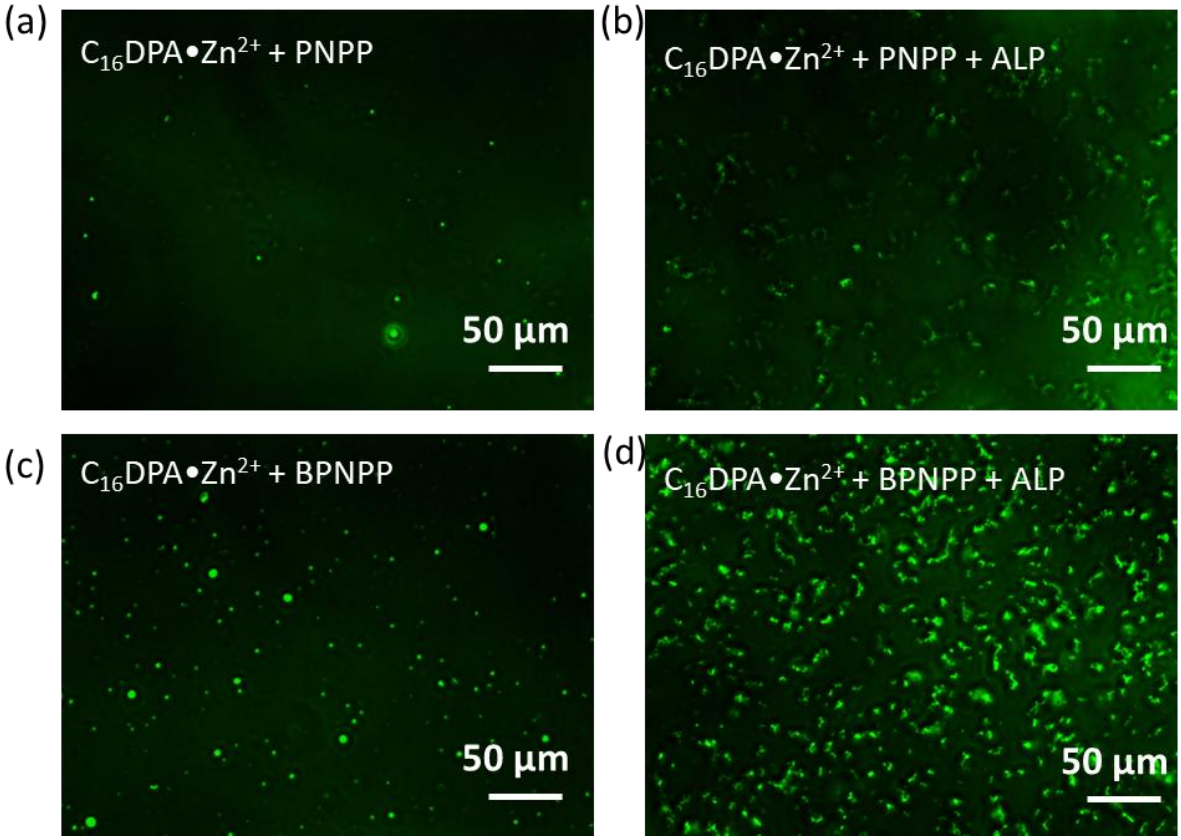

Fig. S28. Fluorescence Microscopic images of (a) C_{16}DPA•Zn^{2+} -PNPP (b) C_{16}DPA•Zn^{2+}- PNPP in presence of ALP images were taken after 1h of ALP addition (c) C_{16}DPA•Zn^{2+} -BPNPP (d) C_{16}DPA•Zn^{2+}- BPNPP in presence of ALP images were taken after 1h of ALP addition. Experimental conditions: [ALP] = 1 µM, [C_{16}DPA•Zn^{2+}] = 50 µM, [PNPP]= 100 µM, [BPNPP]= 100 µM, [C153] = 1 µM, [HEPES] = 5 mM, pH 7.0, T = 25 °C.

DLS Study

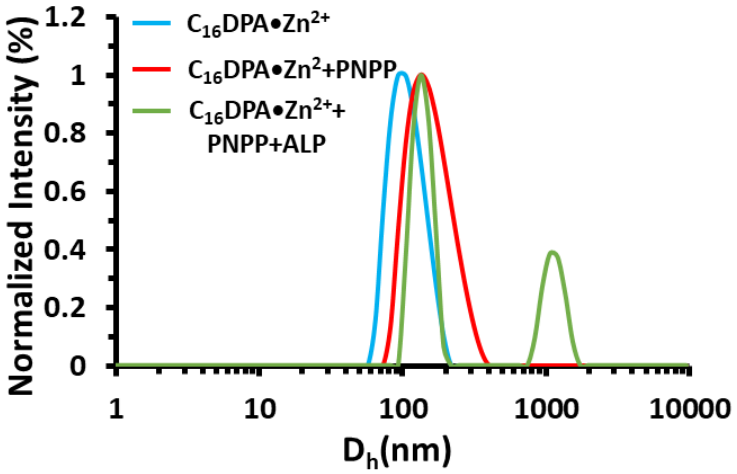

Fig. S29. DLS plot shows D_h (hydrodynamic diameter) of C_{16}DPA•Zn^{2+}, C_{16}DPA•Zn^{2+} + ALP (after 1h), C_{16}DPA•Zn^{2+} + ALP + PNPP (after 1h). Experimental conditions: [ALP] = 100 nM, [C_{16}DPA•Zn^{2+}] = 50 µM, [PNPP]= 100 µM, [HEPES] = 5 mM, pH 7.0, T = 25 °C.

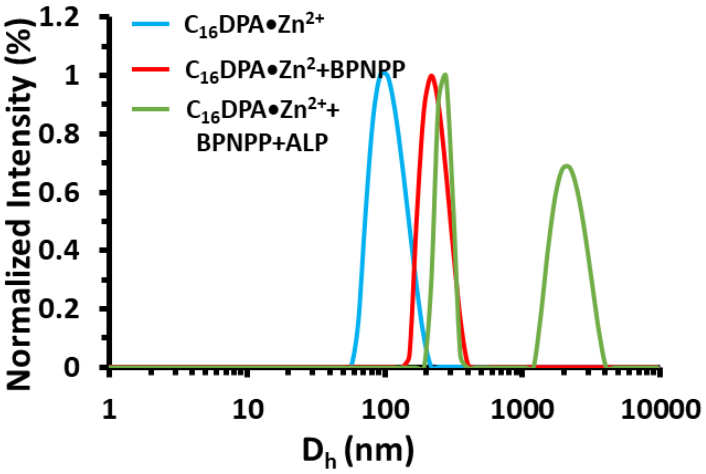

Fig. S30. DLS plot shows Dh (hydrodynamic diameter) of C_{16}DPA•Zn^{2+}, C_{16}DPA•Zn^{2+} + ALP (after 1h), C_{16}DPA•Zn^{2+} + ALP + BPNPP (after 1h). Experimental conditions: [ALP] = 100 nM, [C_{16}DPA•Zn^{2+}] = 50 µM, [BPNPP]= 100 µM, [HEPES] = 5 mM, pH 7.0, T = 25 °C.

6. Catalytic Activity with Nucleotides-HPLC Study

Calibration Plots:

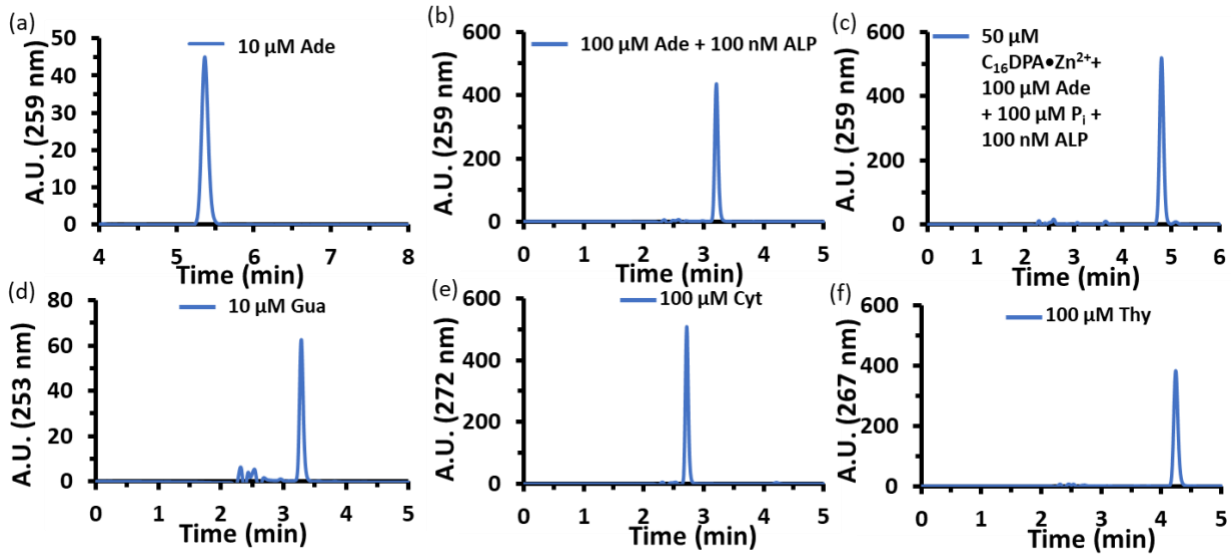

Fig. S31. HPLC Calibration Plot of (a) 10 µM Adenosine (b) 100 µM Adenosine with ALP (c) 100 µM Adenosine in presence of $C_{16}DPA•Zn^{2+}$, Na_2HPO_4, and ALP (d) 10 µM Guanosine (e) 100 µM Cytidine (f) 100 µM Thymidine. Experimental conditions: [ALP] = 100 nM, [$C_{16}DPA•Zn^{2+}$] = 50 µM, [Na_2HPO_4] = 100 µM [HEPES] = 5 mM, pH 7.0, T = 25 °C.

Table. S2 HPLC Retention Time of Nucleosides

Nucleosides	Retention Time (min)
Adenosine	5.2
Guanosine	3.3
Cytidine	2.8
Thymidine	4.2
Adenosine + ALP (in buffer)	3.2
$C_{16}DPA•Zn^{2+}$ + Adenosine + P_i + ALP	4.9

Binding of ALP with Adenosine

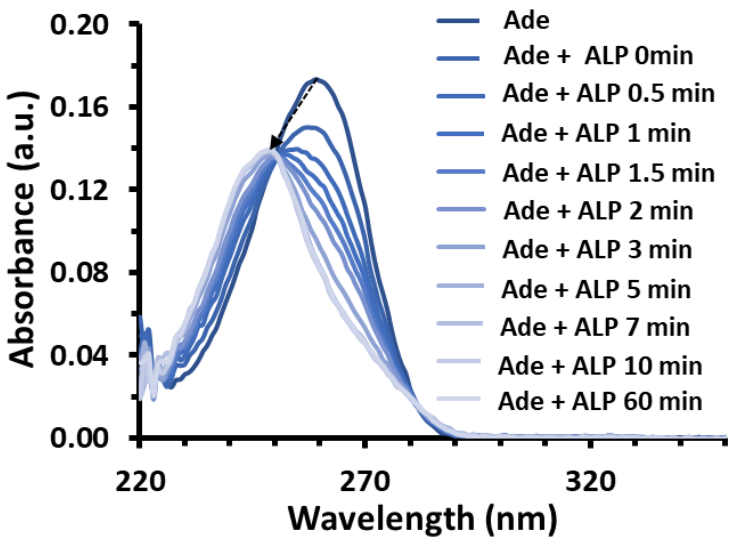

Fig. S32. Representative Absorbance Plot of Adenosine in the Presence of ALP. Experimental conditions: [ALP] = 100 nM, [Adenosine] = 10 µM [HEPES] = 5 mM, pH 7.0, T = 25 °C.

Control experiments of Catalytic activity of AMP with C_{16}DPA•Zn^{2+}:

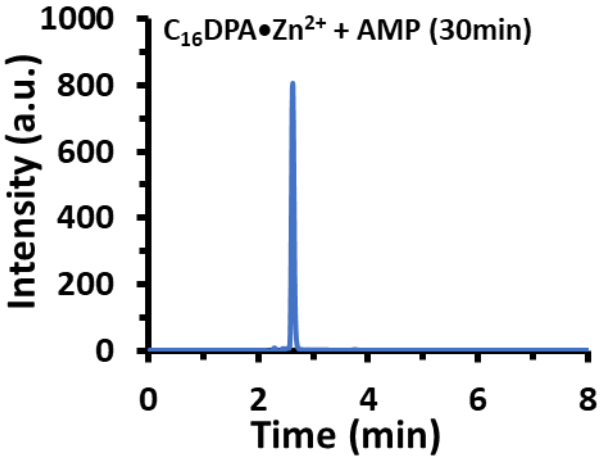

Fig. S33. HPLC Chromatogram of AMP catalysis with C_{16}DPA•Zn^{2+} after 30 min of incubation. No product formation was observed with only C_{16}DPA•Zn^{2+} The product was separated by C18 column using phosphate buffer/MeOH (80:20; v/v). Experimental conditions: [C_{16}DPA•Zn^{2+}] = 50 µM, [AMP] = 100 µM, [HEPES] = 5 mM, pH 7.0, T = 25

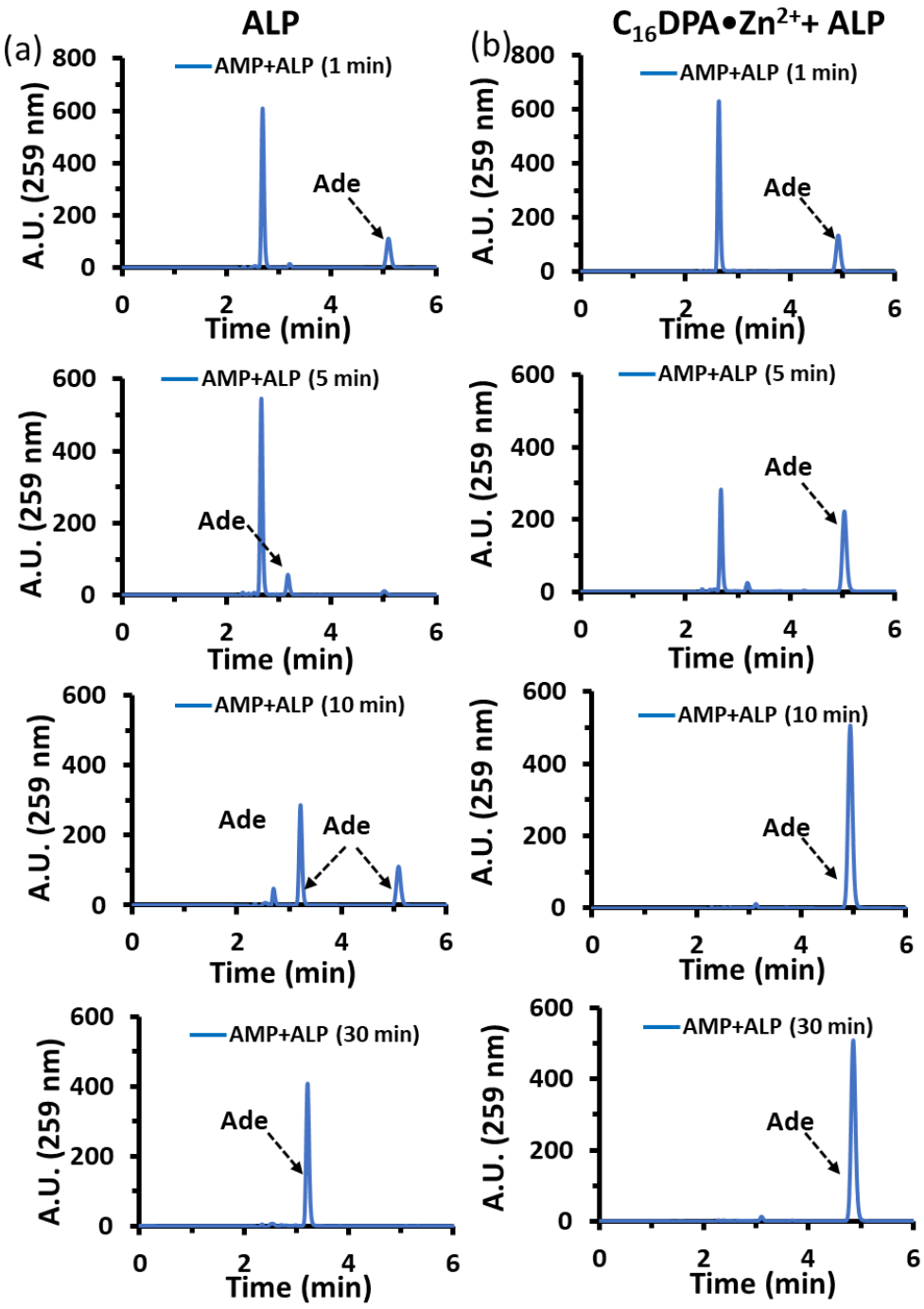

Fig. S34. HPLC Chromatogram of AMP catalysis over time with (a) ALP (b) C_{16}DPA•Zn^{2+} + ALP. The product was separated by C18 column using phosphate buffer/MeOH (80:20; v/v). Experimental conditions: [ALP] = 100 nM, [C_{16}DPA•Zn^{2+}] = 50 µM, [AMP] = 100 µM, [HEPES] = 5 mM, pH 7.0, T = 25 °C.

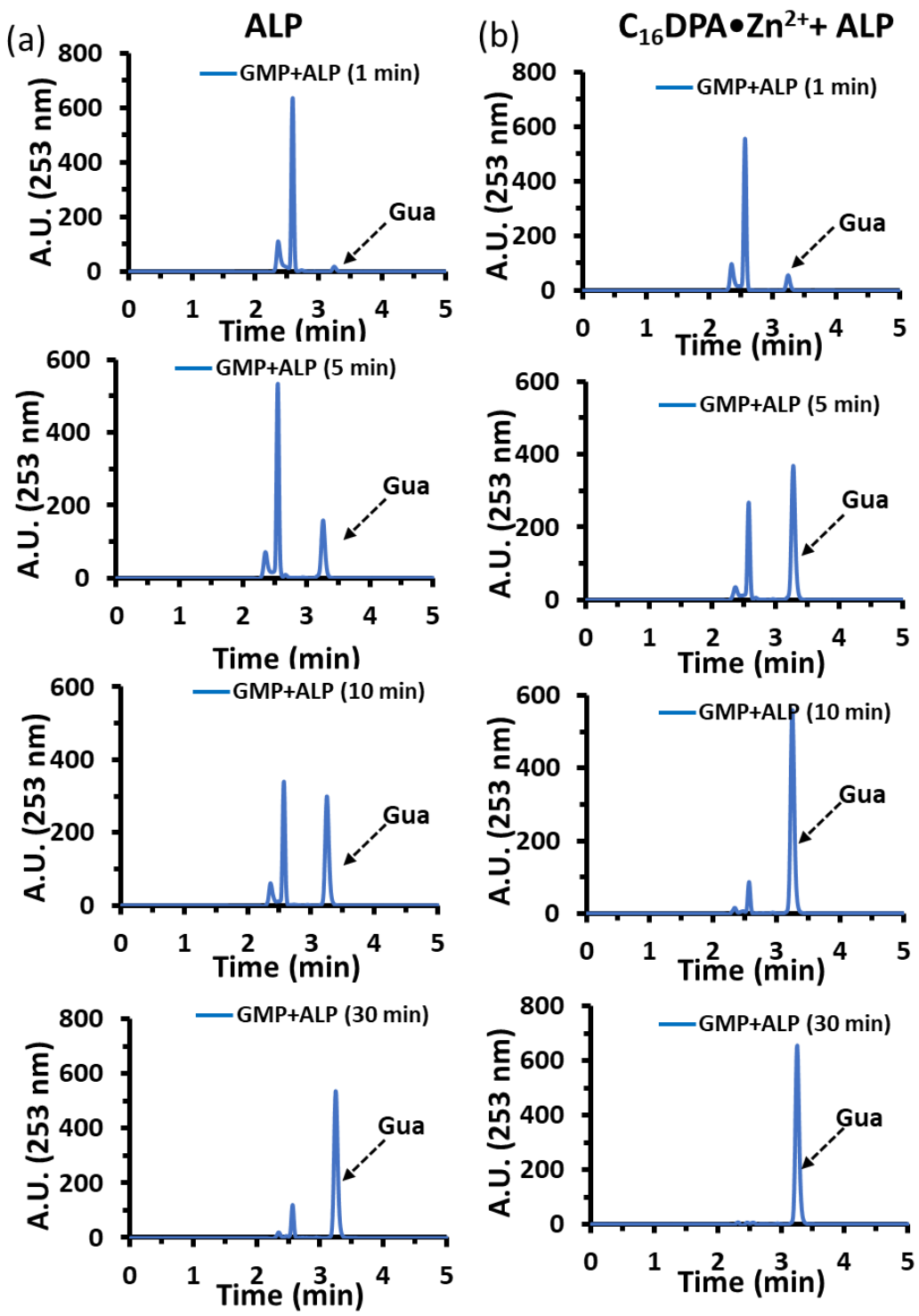

Fig. S35. HPLC Chromatogram of GMP catalysis over time with (a) ALP (b) C_{16}DPA•Zn^{2+} + ALP. The product was separated by C18 column using phosphate buffer/MeOH (80:20; v/v). Experimental conditions: [ALP] = 100 nM, [C_{16}DPA•Zn^{2+}] = 50 µM, [AMP] = 100 µM [HEPES] = 5 mM, pH 7.0, T = 25 °C.

Table S3 Calculated K_{cat} ,K_M, V_{max} and K_{cat}/K_M values for AMP and GMP

System	V_{max} (μM/min)	K_M (μM)	K_{cat} (/min)	K_{cat}/K_M (/μM/min)
AMP (ALP)	10.5 ± 2.2	90 ± 7	105 ± 22	1.17
AMP (C_{16}DPA•Zn^{2+} + ALP)	20.5 ± 1.8	10 ±1.4	205 ± 18	20.5
GMP (ALP)	17.5 ± 1.5	125 ± 9	175 ± 15	1.4
GMP (C_{16}DPA•Zn^{2+} + ALP)	18.2 ± 2.1	8 ± 1	182 ± 21	22.75

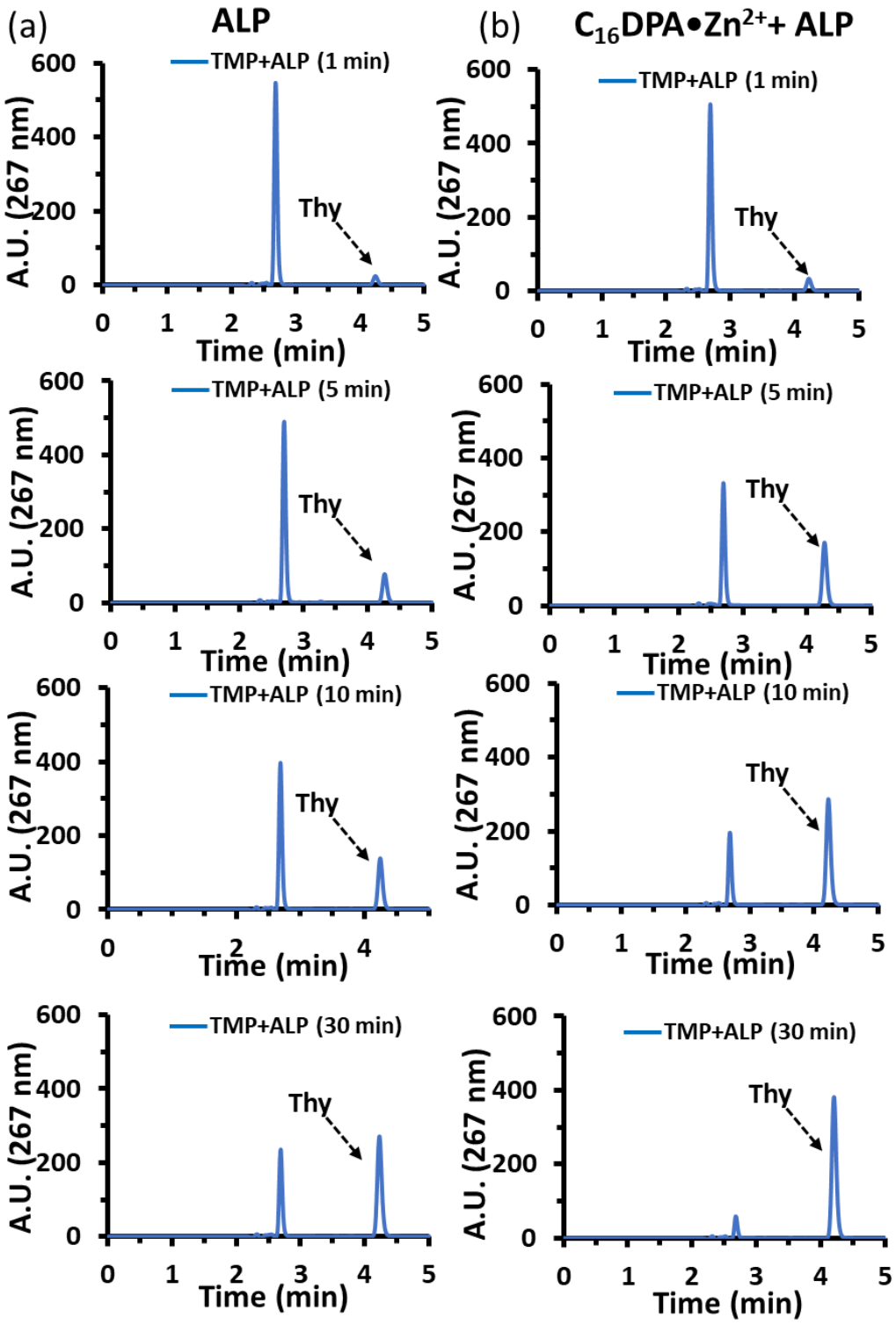

Fig. S36. HPLC Chromatogram of TMP catalysis over time with (a) ALP (b) C_{16}DPA•Zn^{2+} + ALP. The product was separated by C18 column using phosphate buffer/MeOH (80:20; v/v). Experimental conditions: [ALP] = 100 nM, [C_{16}DPA•Zn^{2+}] = 50 µM, [AMP] = 100 µM [HEPES] = 5 mM, pH 7.0, T = 25 °C.

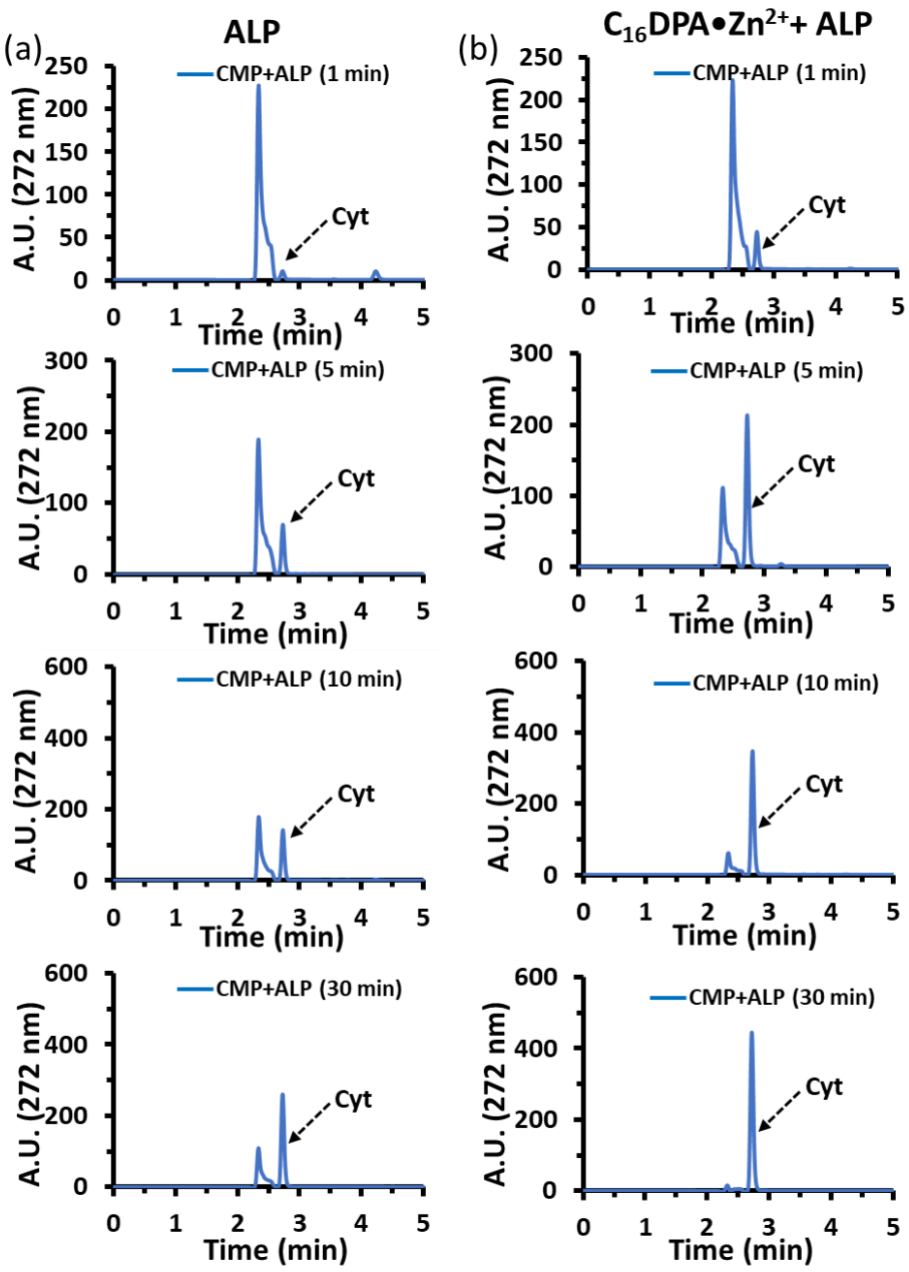

Fig. S37. HPLC Chromatogram of CMP catalysis over time with (a) ALP (b) C_{16}DPA•Zn^{2+} + ALP. The product was separated by C18 column using phosphate buffer/MeOH (80:20; v/v). Experimental conditions: [ALP] = 100 nM, [C_{16}DPA•Zn^{2+}] = 50 µM, [AMP] = 100 µM [HEPES] = 5 mM, pH 7.0, T = 25 °C.

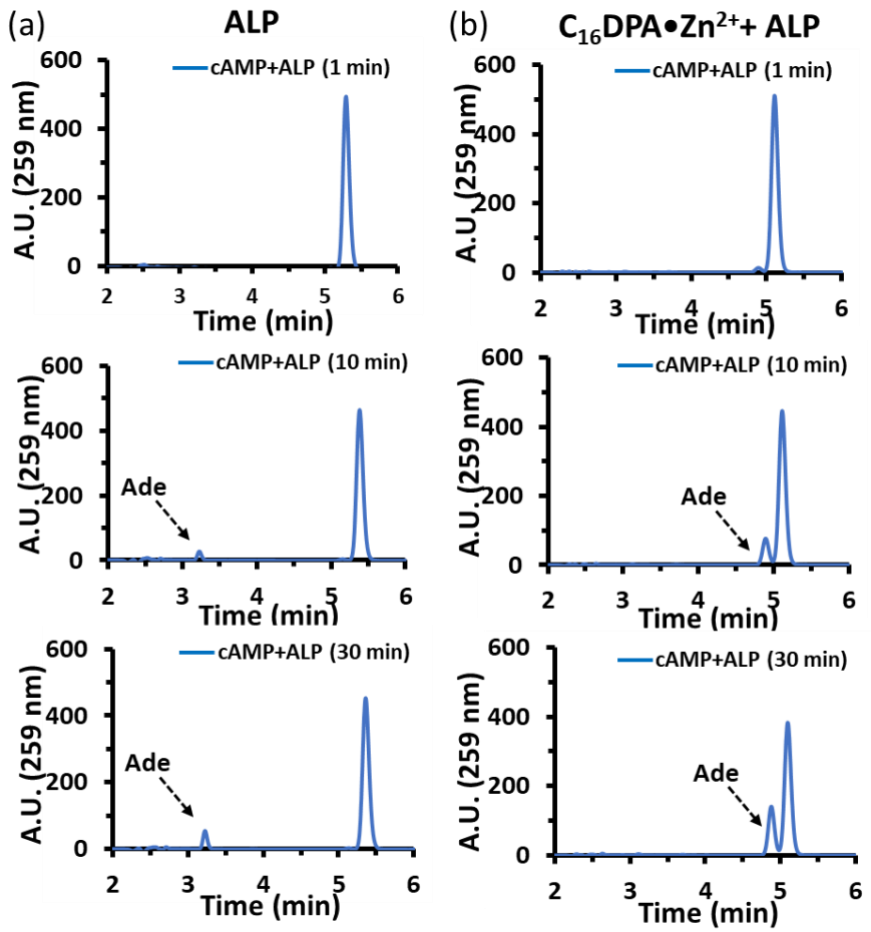

Fig. S38. HPLC Chromatogram of cAMP catalysis over time with (a) ALP (b) $C_{16}DPA•Zn^{2+}$ + ALP. The product was separated by C18 column using phosphate buffer/MeOH (80:20; v/v). Experimental conditions: [ALP] = 100 nM, [$C_{16}DPA•Zn^{2+}$] = 50 µM, [AMP] = 100 µM [HEPES] = 5 mM, pH 7.0, T = 25 °C.

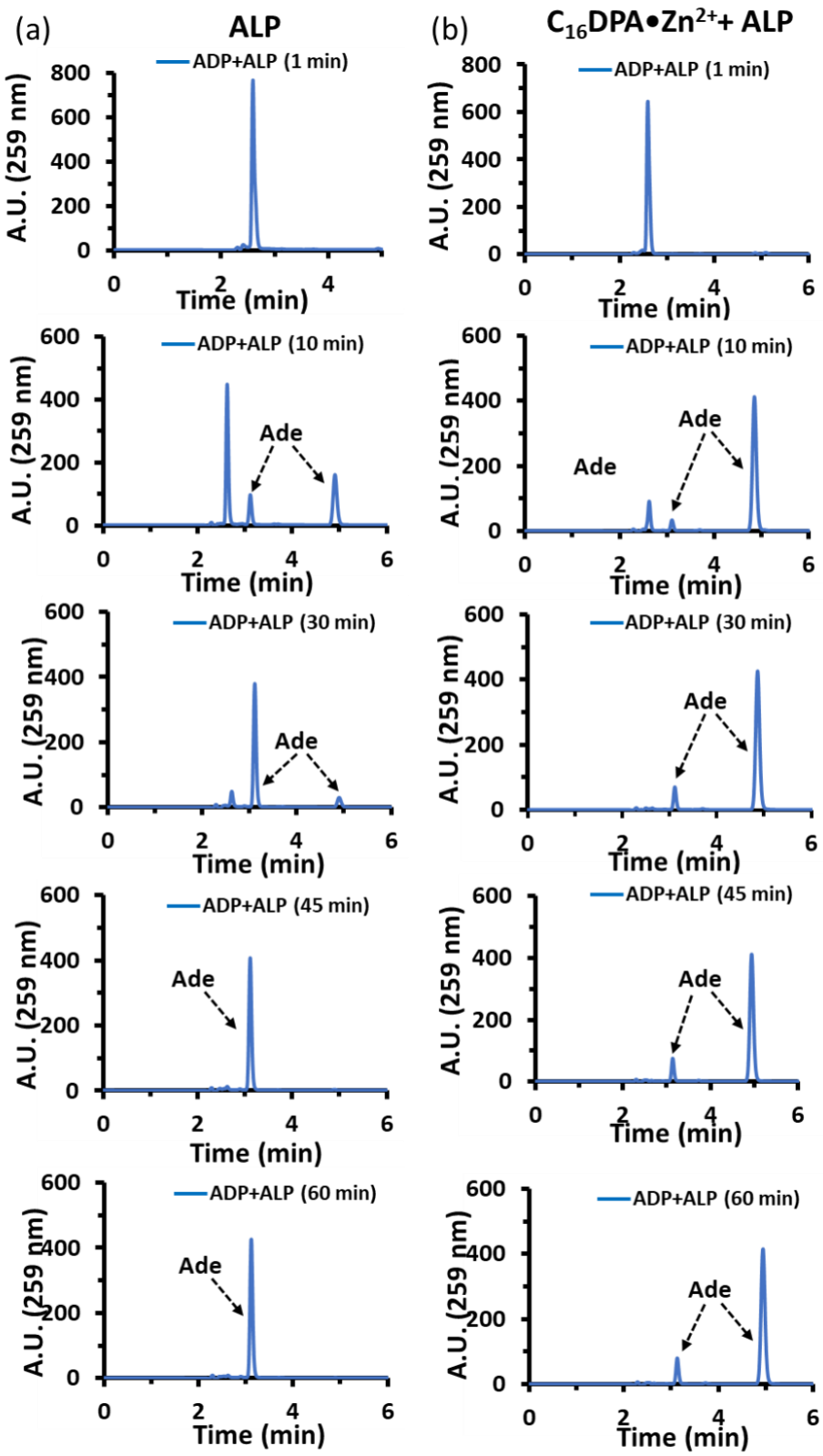

Fig. S39. HPLC Chromatogram of ADP catalysis over time with (a) ALP (b) $C_{16}DPA•Zn^{2+}$ + ALP. The product was separated by C18 column using phosphate buffer/MeOH (80:20; v/v). Experimental conditions: [ALP] = 100 nM, [$C_{16}DPA•Zn^{2+}$] = 50 µM, [AMP] = 100 µM [HEPES] = 5 mM, pH 7.0, T = 25 °C.

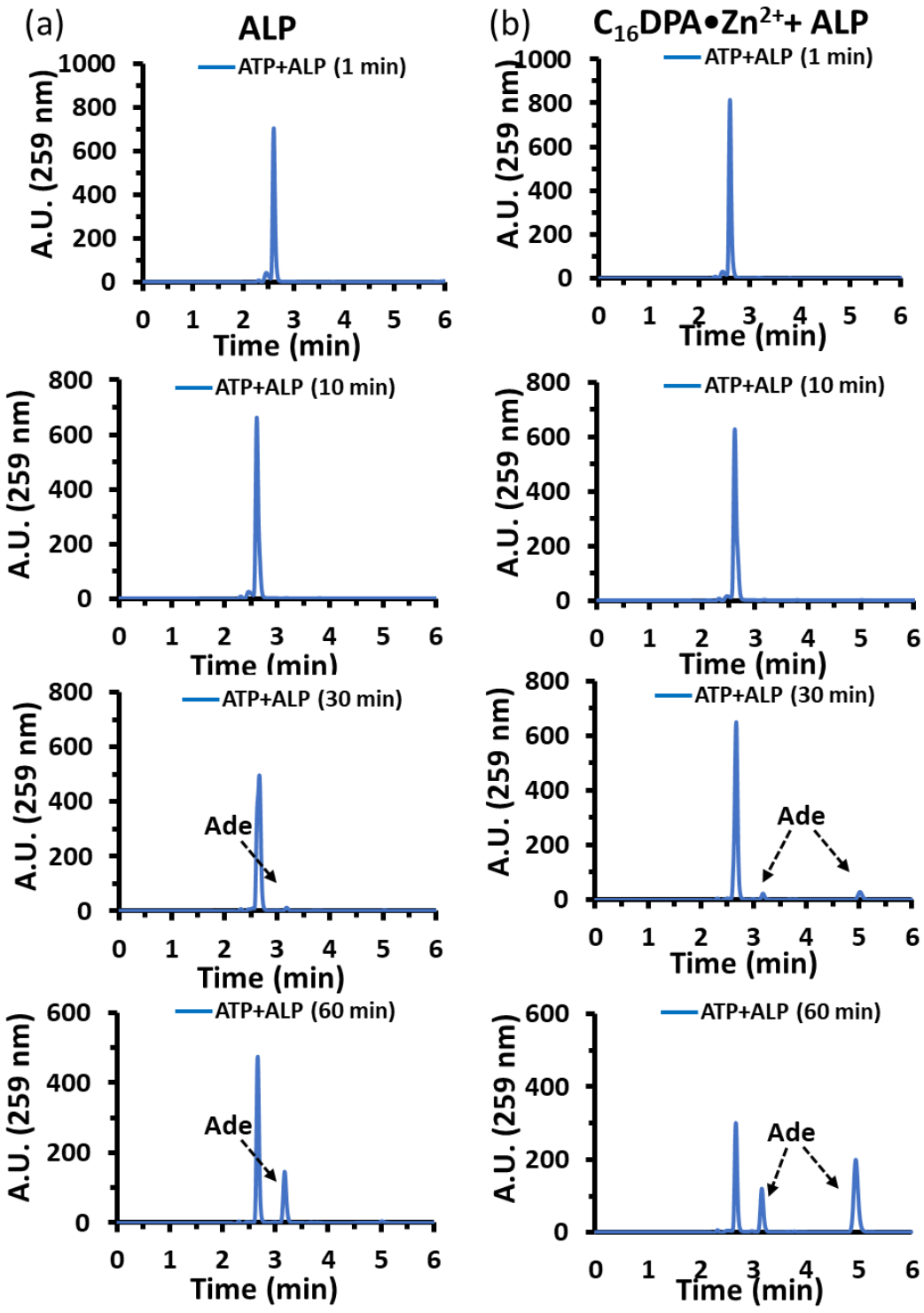

Fig. S40. HPLC Chromatogram of ATP catalysis over time with (a) ALP (b) C_{16}DPA•Zn^{2+} + ALP. The product was separated by C18 column using phosphate buffer/MeOH (80:20; v/v). Experimental conditions: [ALP] = 100 nM, [C_{16}DPA•Zn^{2+}] = 50 µM, [AMP] = 100 µM [HEPES] = 5 mM, pH 7.0, T = 25 °C.

7. Complex properties in the presence of nucleotides

CD Study

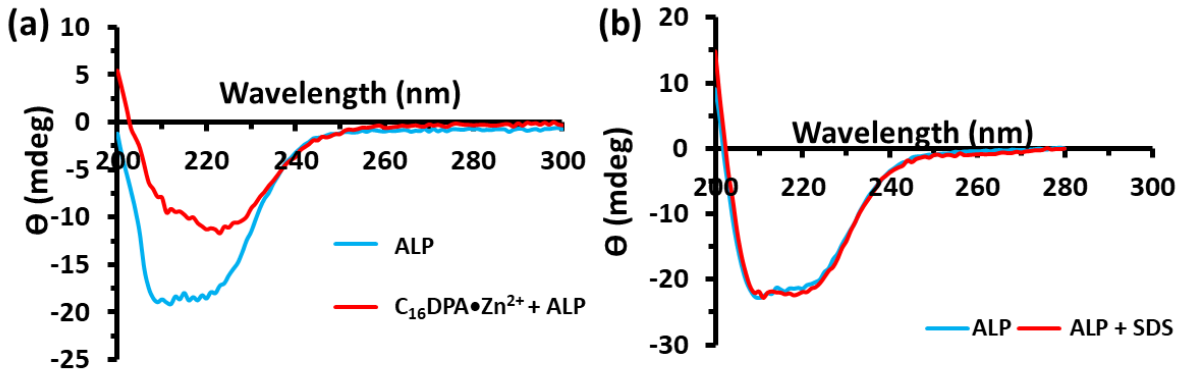

Fig. S41. Circular Dichroism (CD) spectra of (a) only ALP and C_{16}DPA•Zn^{2+}+ALP (b) only ALP (2 µM) and SDS + ALP. Experimental conditions: [ALP] = 2 µM, [C_{16}DPA•Zn^{2+}] = 50 µM, [SDS]= 50 µM, CD cuvette pathlength = 1mm, [HEPES] = 5 mM, pH 7.0, T = 25 °C. CD data suggest that the secondary structure of ALP remains intact in the presence of 50 µM SDS (used in our experiments).

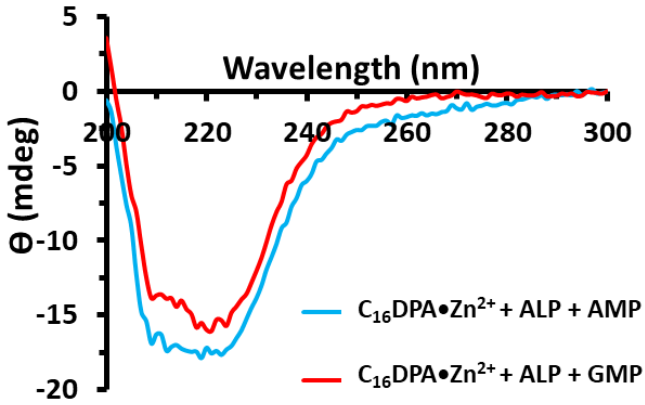

Fig. S42. Circular Dichroism (CD) spectra of C_{16}DPA•Zn^{2+} + ALP with AMP and GMP. Experimental conditions: [ALP] = 2 µM, [C_{16}DPA•Zn^{2+}] = 50 µM, [Nucleotides] = 100 µM, CD cuvette pathlength = 1mm, [HEPES] = 5 mM, pH 7.0, T = 25 °C.

Table. S4 Percentage content of alpha helix and beta sheet of ALP in coassembly with metallosurfactant and nucleotides

System	α- Helix	β- Sheets
ALP	39.8	18.2
C_{16}DPA•Zn^{2+} + ALP	6.6	13.7
C_{16}DPA•Zn^{2+} + ALP + AMP	36.3	19.2
C_{16}DPA•Zn^{2+} + ALP + GMP	30.8	17.9

Zeta Potential

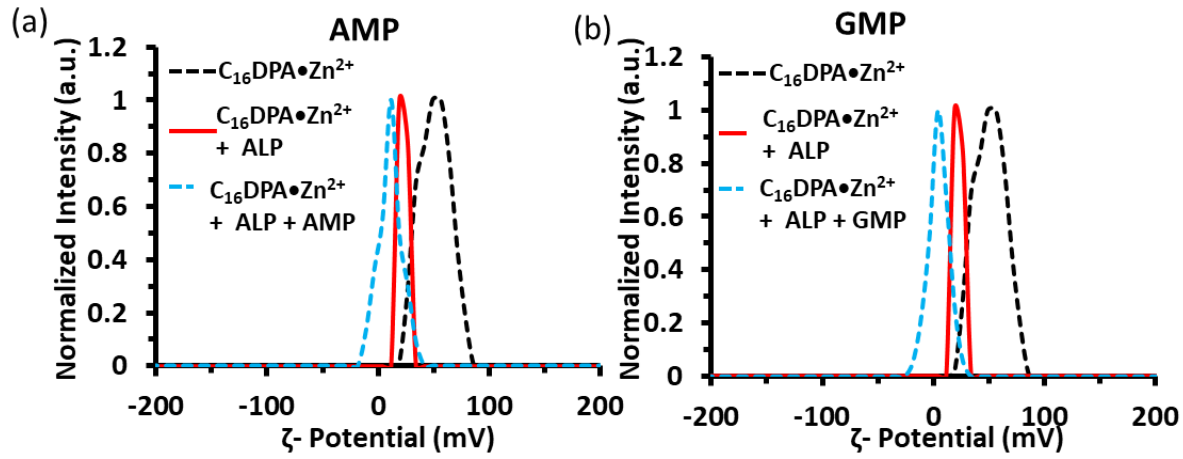

Fig. S43. Zeta potential of only $C_{16}DPA•Zn^{2+}$ and $C_{16}DPA•Zn^{2+}$-ALP in the presence of (a) AMP and (b) GMP. Experimental conditions: [ALP] = 100 nM, [$C_{16}DPA•Zn^{2+}$] = 50 µM, [AMP] = 100 µM, [GMP] = 100 µM, [HEPES] = 5 mM, pH 7.0, T = 25 °C.

Fluorescence Study

With C153

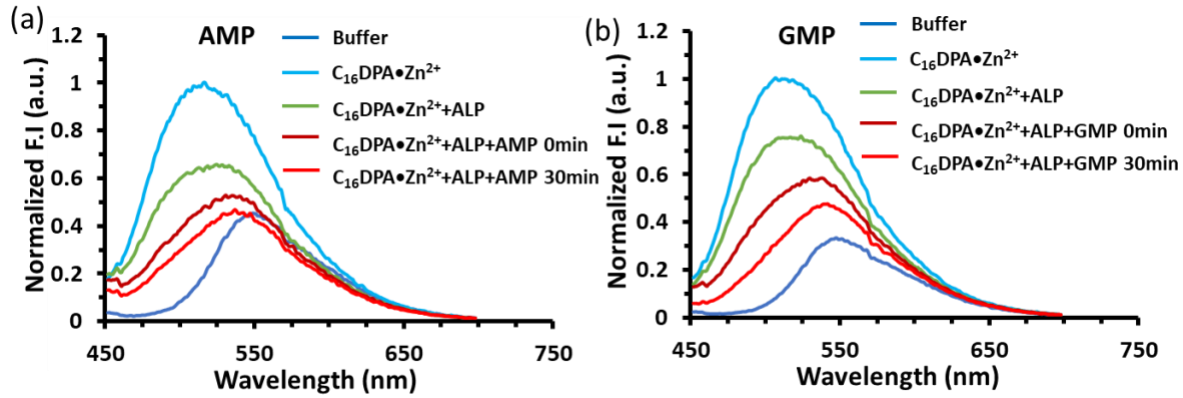

Fig. S44. Characteristic Fluorescence emission spectra of C153 in the presence of surfactant, ALP (a) AMP and (b) GMP showing coassembly. Experimental conditions: [ALP] = 100 nM, [C153] = 1 µM, [$C_{16}DPA•Zn^{2+}$] = 50 µM, [AMP] = 100 µM, [GMP] = 100 µM, slit width ex/em = 5/5 nm, Excitation wavelength = 430nm, [HEPES] = 5 mM, pH 7.0, T = 25 °C.

FRET Using FITC-ALP and Nile Red in the Presence of Nucleotides

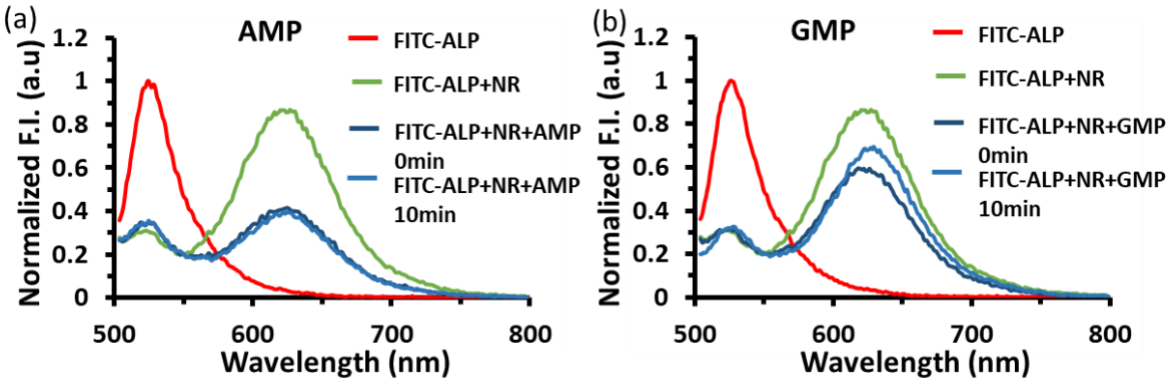

Fig. S45. Characteristic Fluorescence emission spectra showing FRET between FITC tagged ALP and Nile red in the presence of (a) AMP and (b) GMP. Experimental conditions: [FITC-ALP] = 100 nM, [Nile Red] = 500 nM, [C_{16}DPA•Zn^{2+}] = 50 µM, [AMP] = 100 µM, [GMP] = 100 µM, slit width ex/em = 5/5 nm, Excitation wavelength = 492nm, [HEPES] = 5 mM, pH 7.0, T = 25 °C.

E_{FRET} was calculated using the equation

$$E_{FRET} = \frac{(I_{619} - \sigma I_{525})}{(I_{525} + (I_{619} - \sigma I_{525}))}$$

Where I_{619} and I_{525} are the Fluorescence Intensity at 619nm and 525nm respectively, and $\sigma = \frac{I619}{I555}$

Table. S5 E_{FRET} in the Presence of Nucleotides.

	E_{FRET} (without Nucleotides)	E_{FRET} (with Nucleotides after 1 min)	E_{FRET} (with Nucleotides after 10 min)
With AMP	0.70 ± 0.04	0.53 ± 0.02	0.50 ± 0.03
With GMP	0.70 ± 0.04	0.65 ± 0.015	0.67 ± 0.02

Laurden GP value

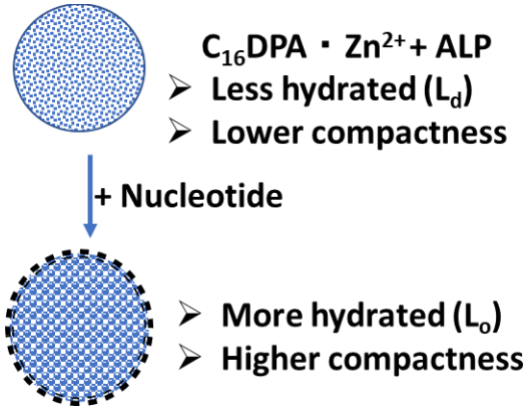

Fig. S46. Schematically showing transformation of complex environment in terms of hydration and compactness upon nucleotide binding.

8. Catalytic Oligonucleotide Digestion study - HPLC Study

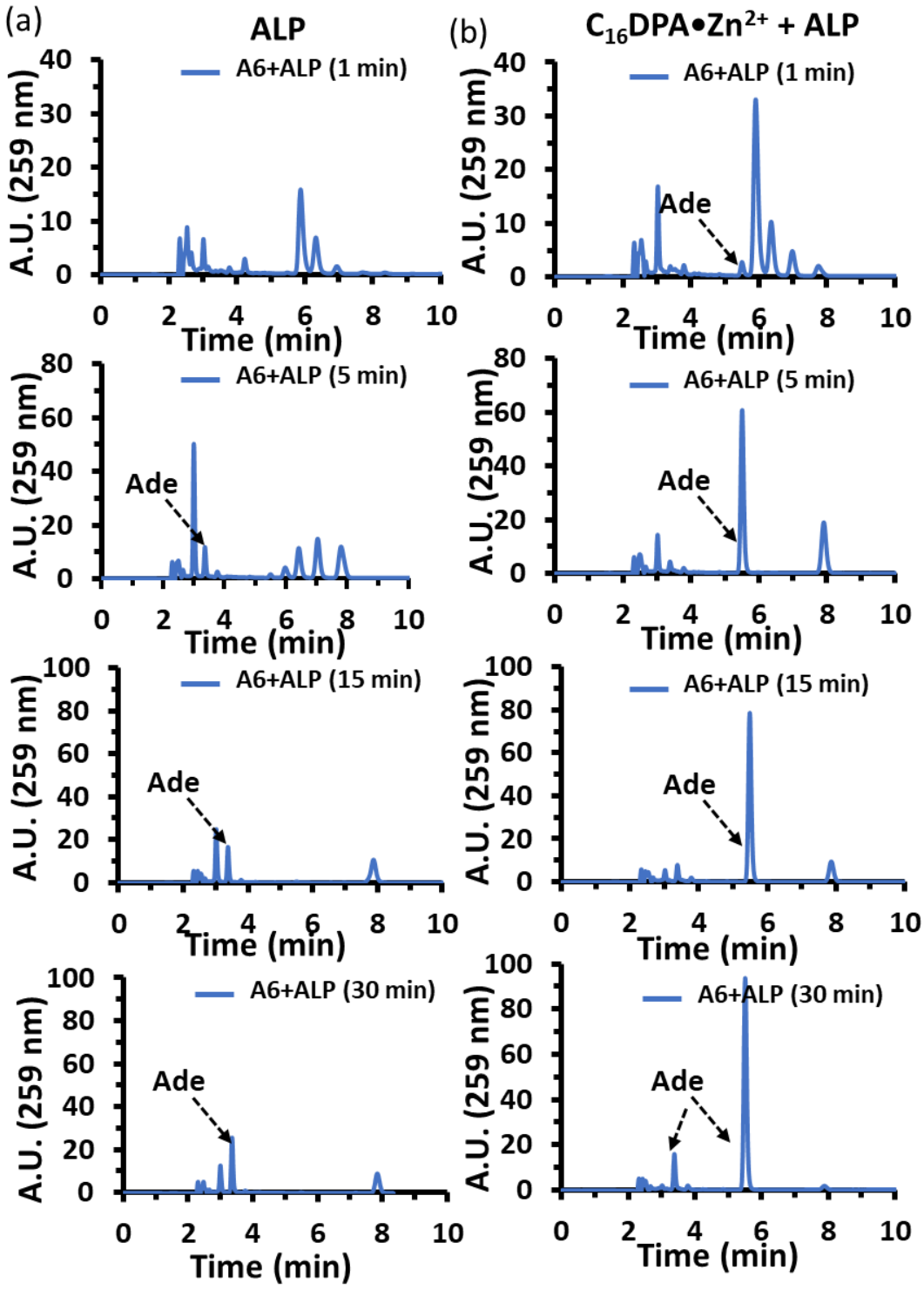

Fig. S47. HPLC Chromatogram of A6 catalysis over time with (a) ALP (b) C_{16}DPA•Zn^{2+} + ALP. The product was separated by C18 column using phosphate buffer/MeOH (80:20; v/v). Experimental conditions: [ALP] = 100 nM, [C_{16}DPA•Zn^{2+}] = 50 µM, [A6] = 5 µM [HEPES] = 5 mM, pH 7.0, T = 25 °C.

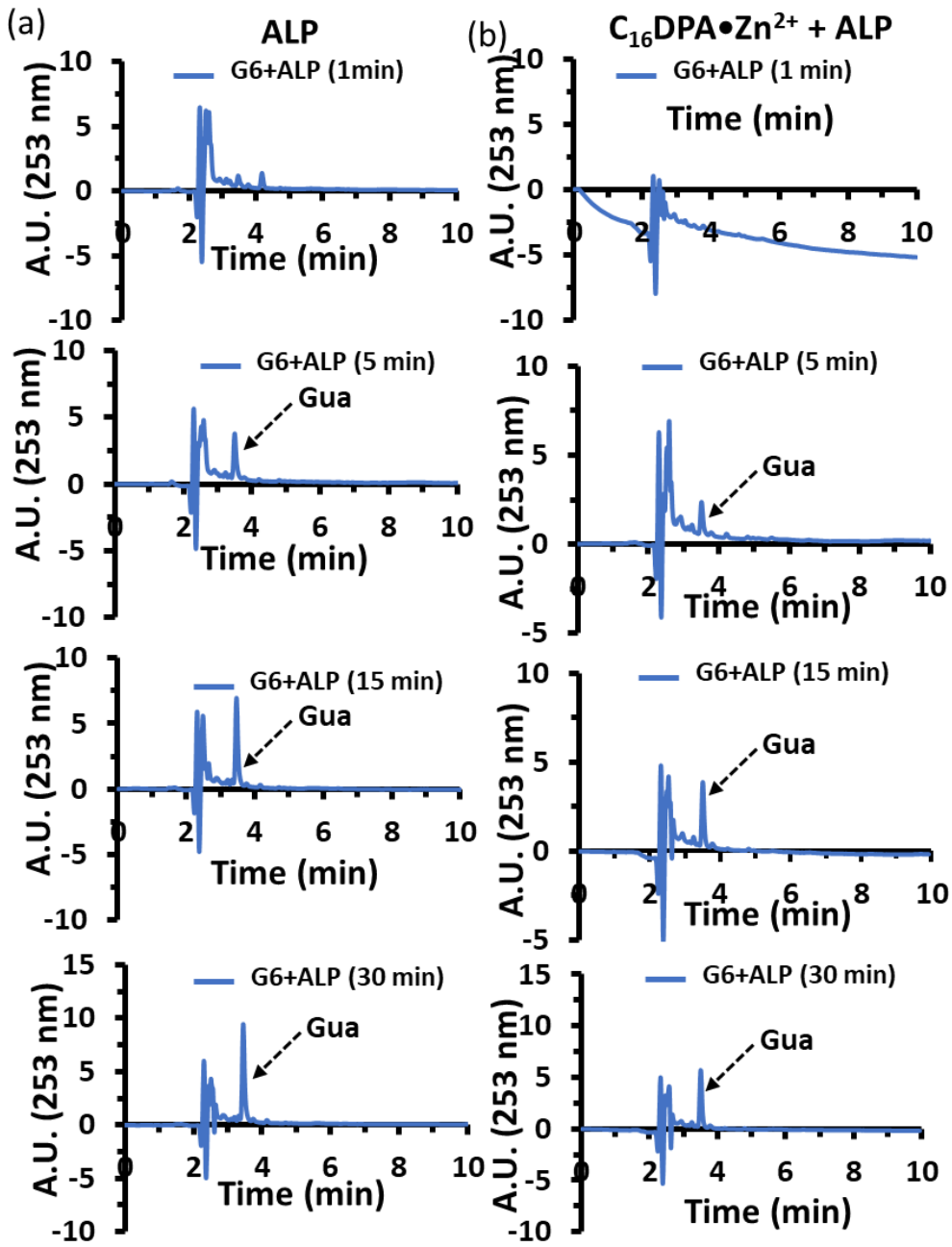

Fig. S48. HPLC Chromatogram of G6 catalysis over time with (a) ALP (b) C_{16}DPA•Zn^{2+} + ALP. The product was separated by C18 column using phosphate buffer/MeOH (80:20; v/v). Experimental conditions: [ALP] = 100 nM, [C_{16}DPA•Zn^{2+}] = 50 µM, [A6] = 5 µM [HEPES] = 5 mM, pH 7.0, T = 25 °C.

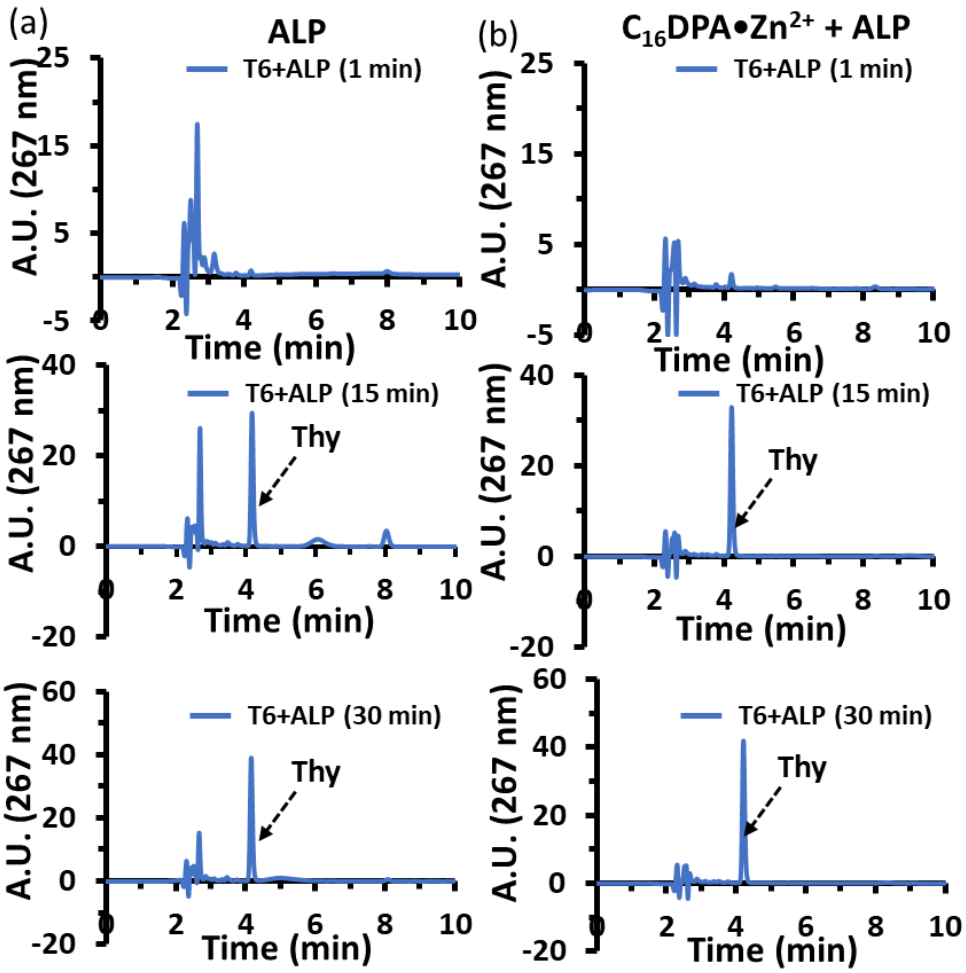

Fig. S49. HPLC Chromatogram of T6 catalysis over time with (a) ALP (b) C_{16}DPA•Zn^{2+} + ALP. The product was separated by C18 column using phosphate buffer/MeOH (80:20; v/v). Experimental conditions: [ALP] = 100 nM, [C_{16}DPA•Zn^{2+}] = 50 µM, [T6] = 5 µM [HEPES] = 5 mM, pH 7.0, T = 25 °C.

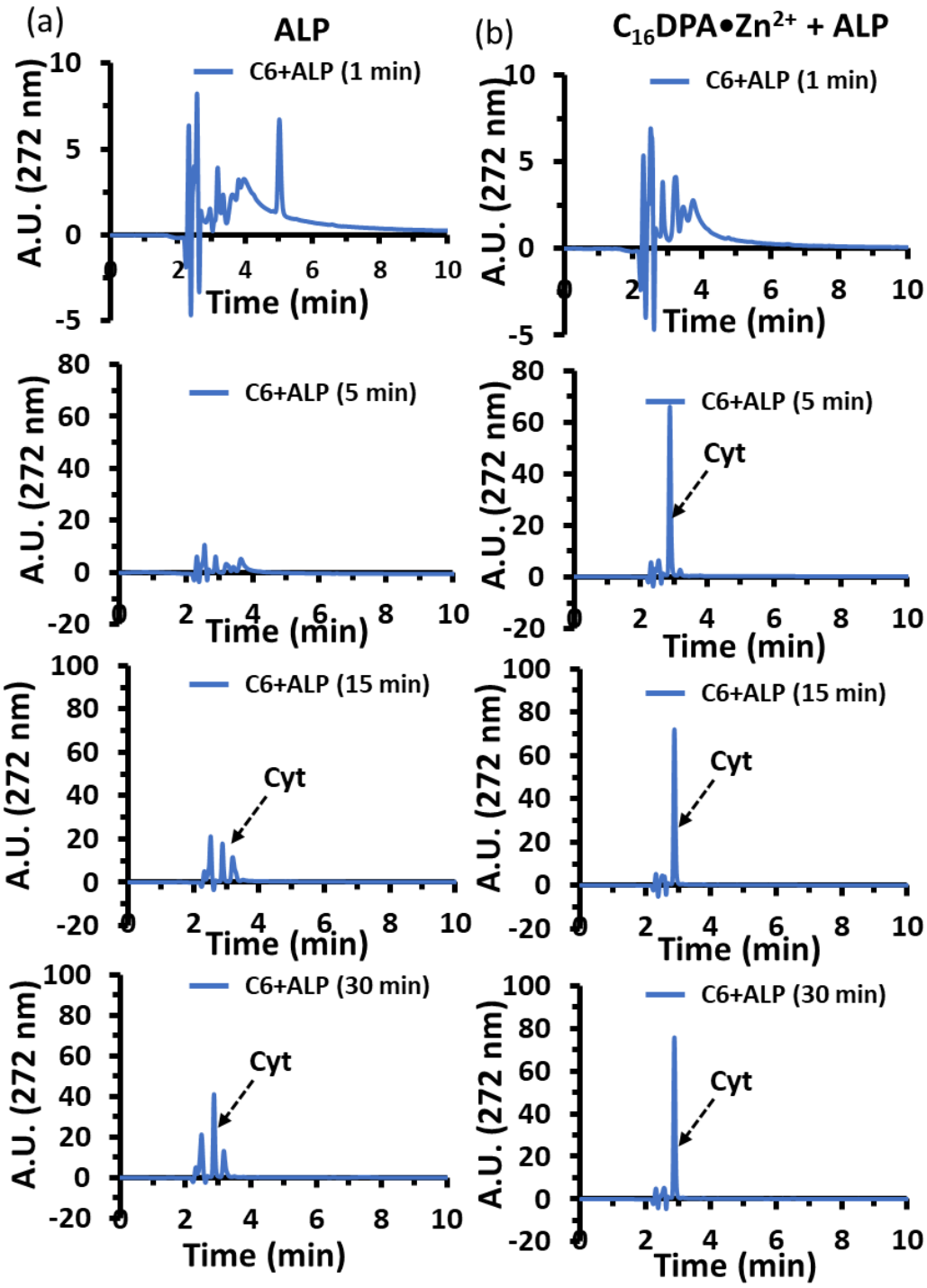

Fig. S50. HPLC Chromatogram of C6 catalysis over time with (a) ALP (b) $C_{16}DPA•Zn^{2+}$ + ALP. The product was separated by C18 column using phosphate buffer/MeOH (80:20; v/v). Experimental conditions: [ALP] = 100 nM, [$C_{16}DPA•Zn^{2+}$] = 50 µM, [C6] = 5 µM [HEPES] = 5 mM, pH 7.0, T = 25 °C.

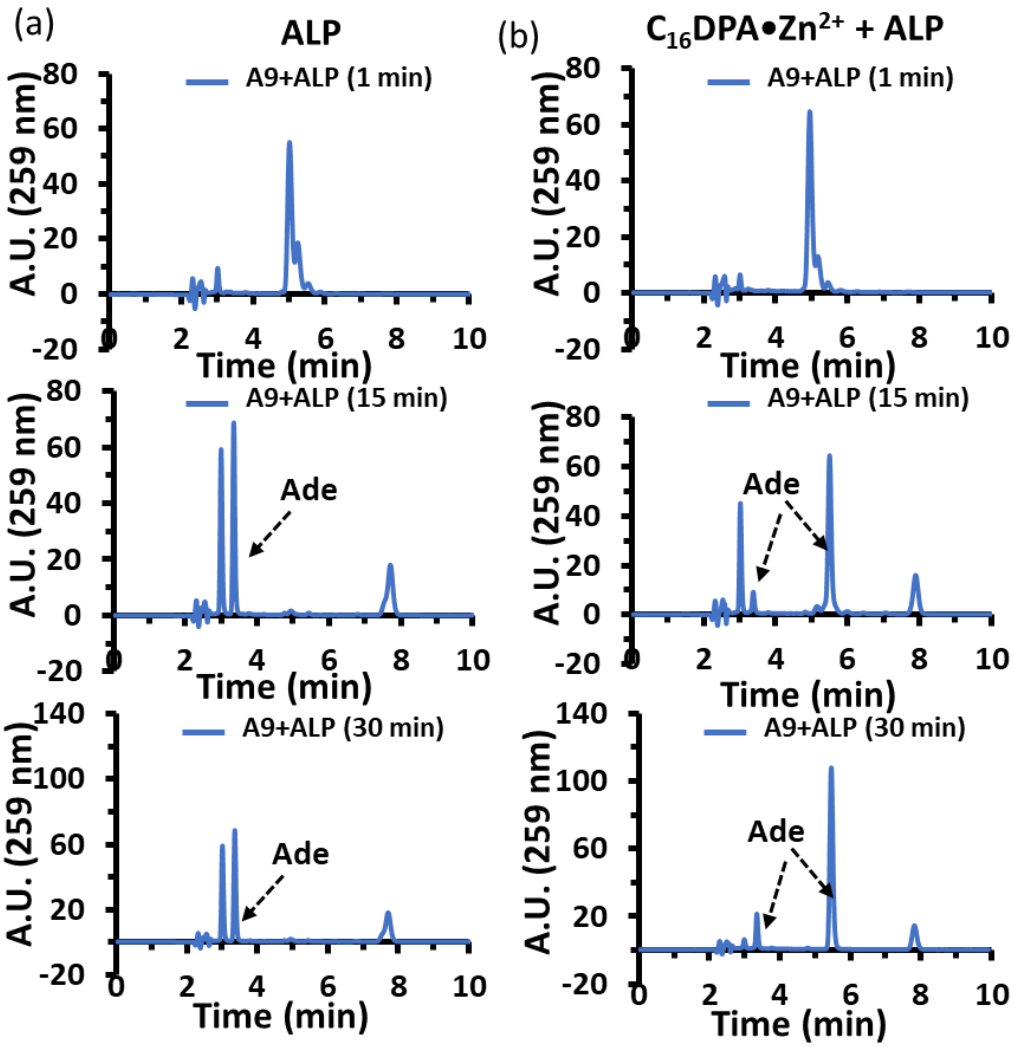

Fig. S51. HPLC Chromatogram of A9 catalysis over time with (a) ALP (b) $C_{16}DPA•Zn^{2+}$ + ALP. The product was separated by C18 column using phosphate buffer/MeOH (80:20; v/v). Experimental conditions: [ALP] = 100 nM, [$C_{16}DPA•Zn^{2+}$] = 50 µM, [A9] = 5 µM [HEPES] = 5 mM, pH 7.0, T = 25 °C.

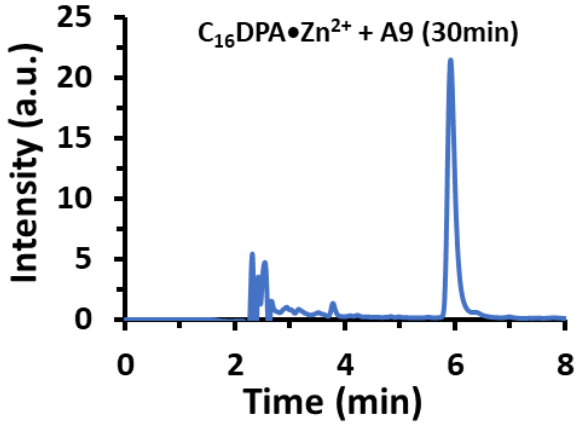

Fig. S52. HPLC Chromatogram of A9 catalysis with $C_{16}DPA•Zn^{2+}$ after 30 min of incubation. No product formation was observed with only $C_{16}DPA•Zn^{2+}$ The product was separated by C18 column using

phosphate buffer/MeOH (80:20; v/v). Experimental conditions: [C_{16}DPA•Zn^{2+}] = 50 µM, [A9] = 5 µM, [HEPES] = 5 mM, pH 7.0, T = 25

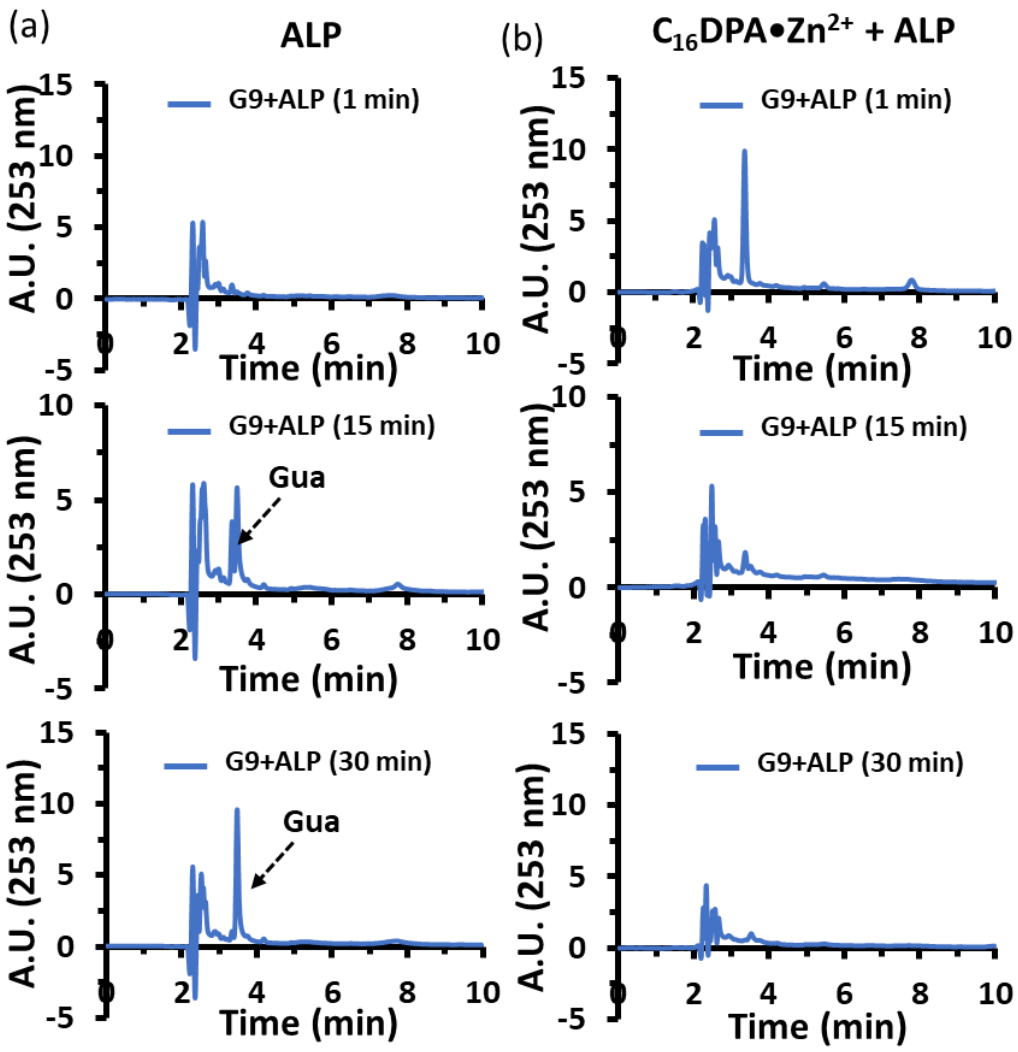

Fig. S53. HPLC Chromatogram of G9 catalysis over time with (a) ALP (b) C_{16}DPA•Zn^{2+} + ALP. The product was separated by C18 column using phosphate buffer/MeOH (80:20; v/v). Experimental conditions: [ALP] = 100 nM, [C_{16}DPA•Zn^{2+}] = 50 µM, [G9] = 5 µM [HEPES] = 5 mM, pH 7.0, T = 25 °C.

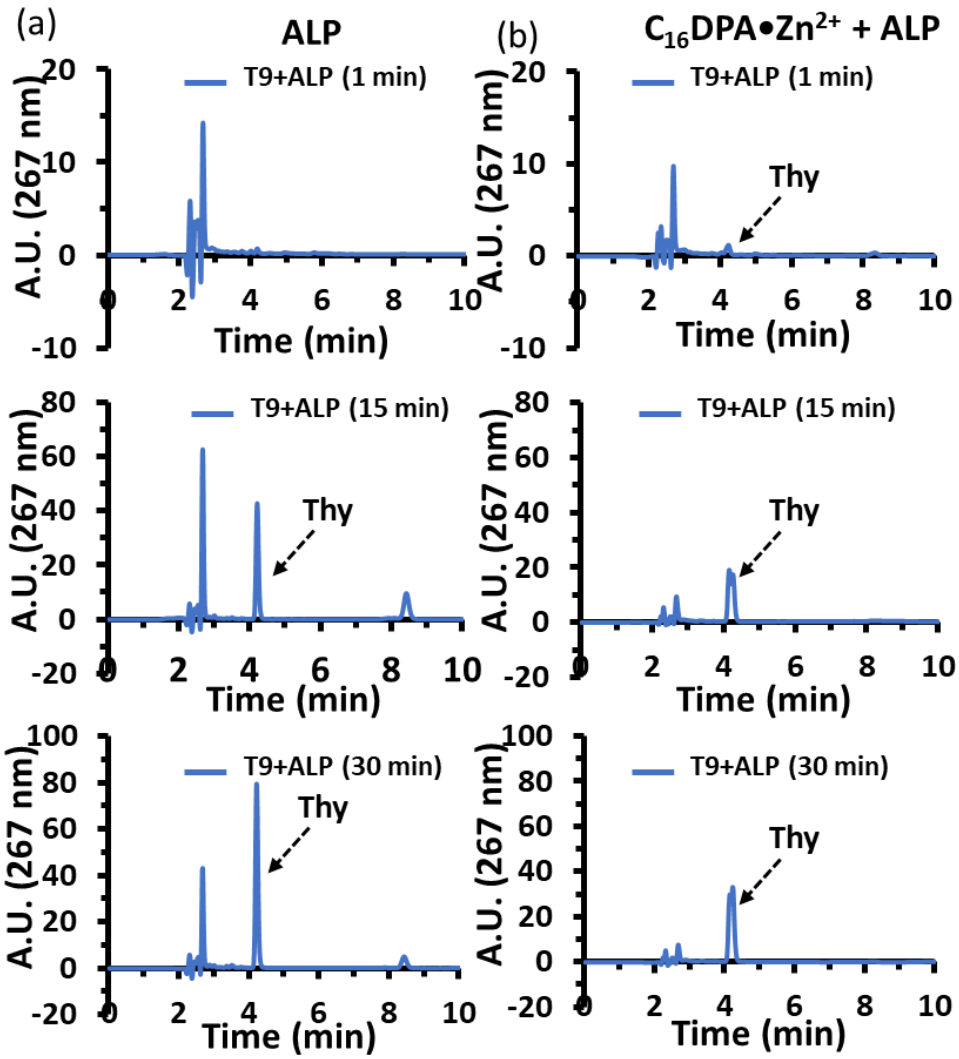

Fig. S54. HPLC Chromatogram of T9 catalysis over time with (a) ALP (b) C_{16}DPA•Zn^{2+} + ALP. The product was separated by C18 column using phosphate buffer/MeOH (80:20; v/v). Experimental conditions: [ALP] = 100 nM, [C_{16}DPA•Zn^{2+}] = 50 µM, [T9] = 5 µM [HEPES] = 5 mM, pH 7.0, T = 25 °C.

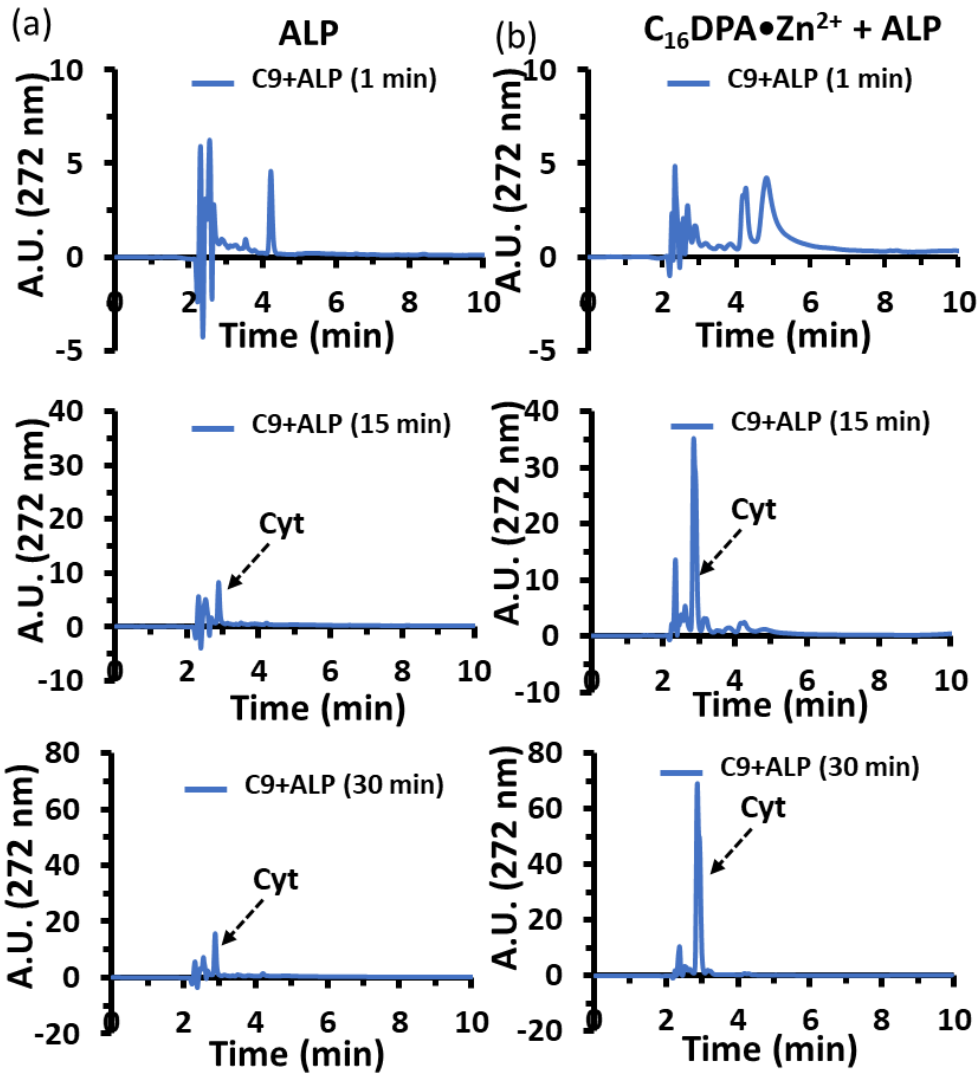

Fig. S55. HPLC Chromatogram of C9 catalysis over time with (a) ALP (b) $C_{16}DPA•Zn^{2+}$ + ALP. The product was separated by C18 column using phosphate buffer/MeOH (80:20; v/v). Experimental conditions: [ALP] = 100 nM, [$C_{16}DPA•Zn^{2+}$] = 50 µM, [C9] = 5 µM [HEPES] = 5 mM, pH 7.0, T = 25 °C.

9. Complex Properties in presence of different oligonucleotides

CD Study

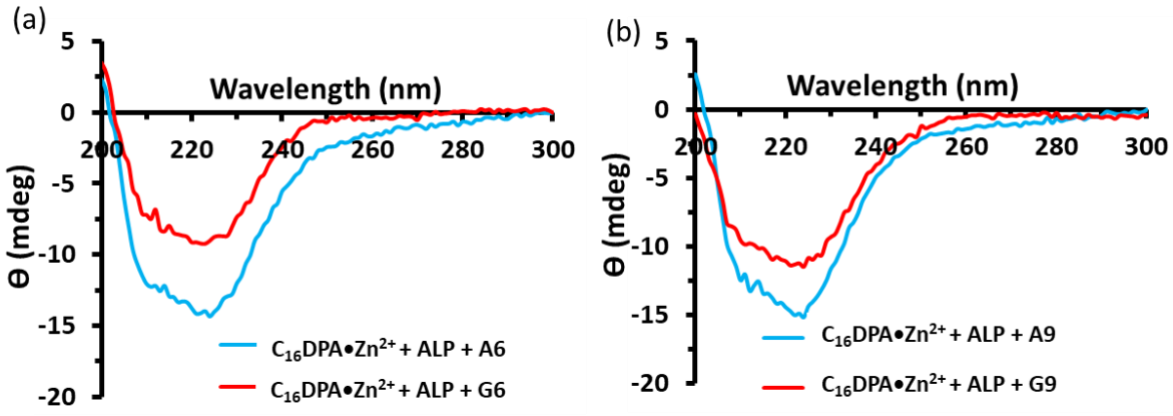

Fig. S56. Circular Dichroism (CD) spectra of $C_{16}DPA•Zn^{2+}$ + ALP with (a) A6, G6, and (b) A9, G9. Experimental conditions: [ALP] = 2 µM, [$C_{16}DPA•Zn^{2+}$] = 50 µM, For Fig. (a) and (b) [oligonucleotides] = 5 µM, Cuvette pathlength = 1mm, [HEPES] = 5 mM, pH 7.0, T = 25 °C.

Table. S6 Percentage content of alpha helix and beta sheet of ALP in coassembly with metallosurfactant and Oligonucleotides

System	α- Helix	β- Sheets
$C_{16}DPA•Zn^{2+}$ + ALP + A6	28.5	28.9
$C_{16}DPA•Zn^{2+}$ + ALP + G6	11.2	15.4
$C_{16}DPA•Zn^{2+}$ + ALP + A9	26.2	31.9
$C_{16}DPA•Zn^{2+}$ + ALP + G9	9.5	26.1
$C_{16}DPA•Zn^{2+}$ + ALP	6.6	13.7

Fluorescence Study

With C153

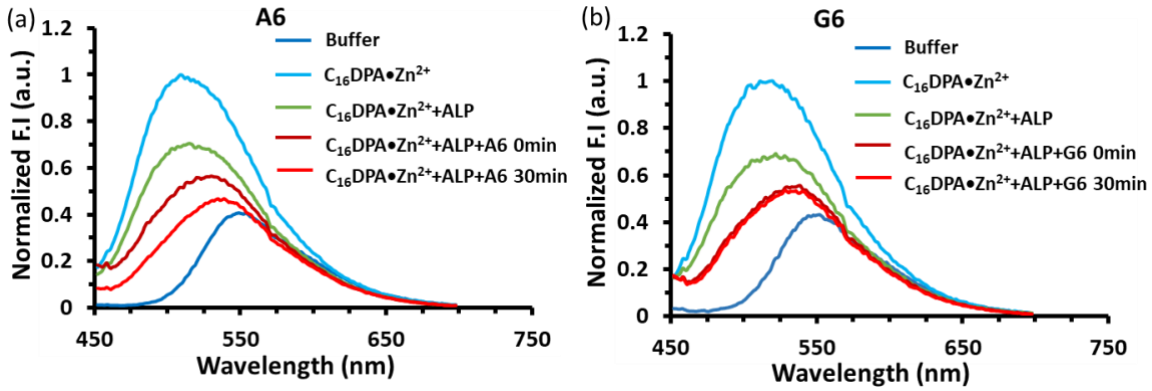

Fig. S57. Characteristic Fluorescence emission spectra of C153 in the presence of surfactant, ALP (a) A6 and (b) G6 showing coassembly. Experimental conditions: [ALP] = 100 nM, [C153] = 1 µM, [$C_{16}DPA•Zn^{2+}$] = 50 µM, [oligonucleotides] = 5 µM, slit width ex/em = 5/5 nm, Excitation wavelength = 430nm, [HEPES] = 5 mM, pH 7.0, T = 25 °C.

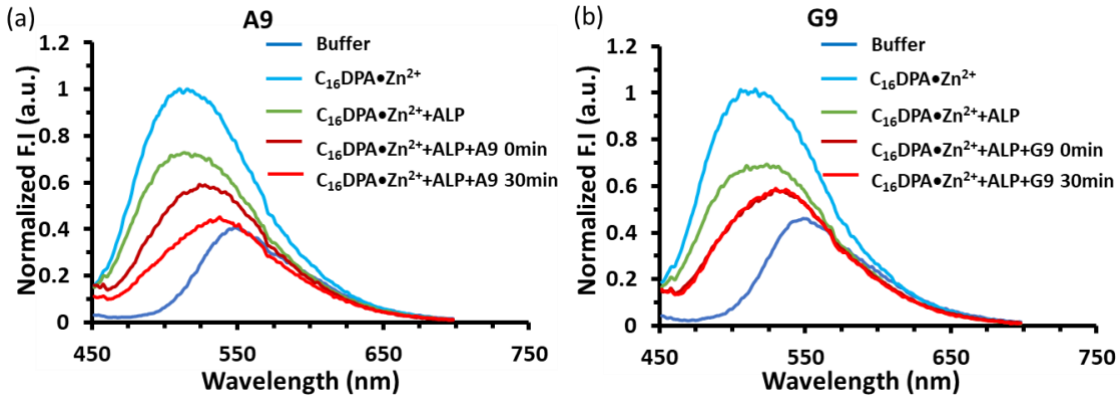

Fig. S58. Characteristic Fluorescence emission spectra of C153 in the presence of surfactant, ALP (a) A9 and (b) G9 showing coassembly. Experimental conditions: [ALP] = 100 nM, [C153] = 1 µM, [$C_{16}DPA•Zn^{2+}$] = 50 µM, [oligonucleotides] = 5 µM, slit width ex/em = 5/5 nm, Excitation wavelength = 430nm, [HEPES] = 5 mM, pH 7.0, T = 25 °C.

FRET Using FITC-ALP and Nile Red in the Presence of Oligonucleotides

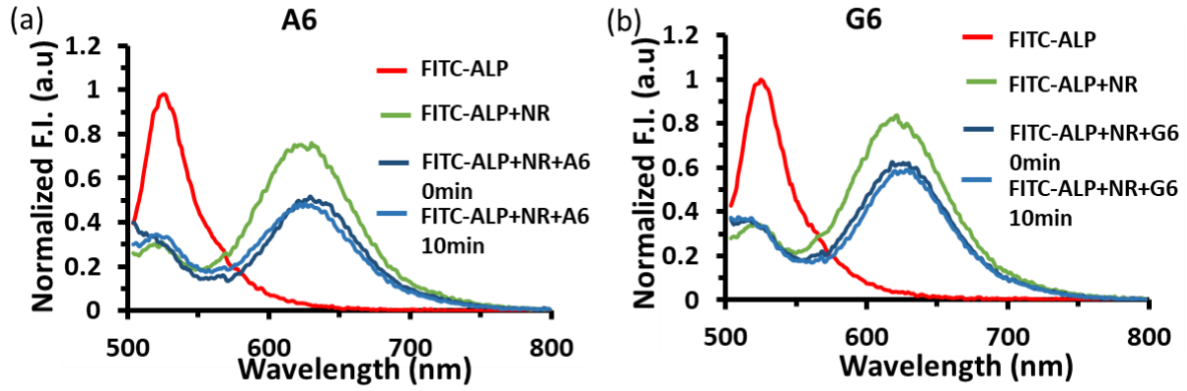

Fig. S59. Characteristic Fluorescence emission spectra showing FRET between FITC tagged ALP and Nile red in the presence of (a) A6 and (b) G6. Experimental conditions: [FITC-ALP] = 100 nM, [Nile Red] = 500 nM, [$C_{16}DPA•Zn^{2+}$] = 50 µM, [oligonucleotides] = 5 µM, slit width ex/em = 5/5 nm, Excitation wavelength = 492nm, [HEPES] = 5 mM, pH 7.0, T = 25 °C.

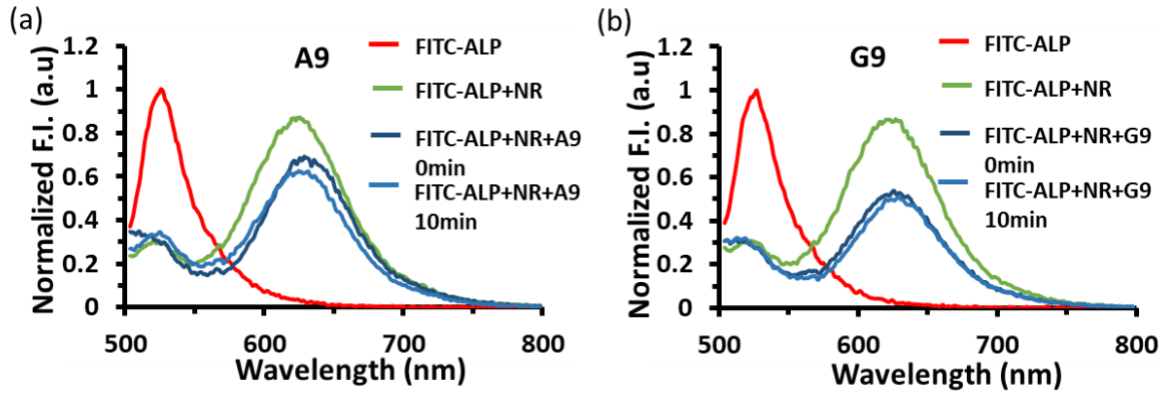

Fig. S60. Characteristic Fluorescence emission spectra showing FRET between FITC tagged ALP and Nile red in the presence of (a) A9 and (b)G9. Experimental conditions: [FITC-ALP] = 100 nM, [Nile Red] = 500 nM, [$C_{16}DPA•Zn^{2+}$] = 50 µM, [oligonucleotides] = 5 µM, slit width ex/em = 5/5 nm, Excitation wavelength = 492nm, [HEPES] = 5 mM, pH 7.0, T = 25 °C.

Table. S7 E_{FRET} in the Presence of Oligonucleotides.

	E_{FRET} (without Nucleotides)	E_{FRET} (with Oligonucleotides after 1 min)	E_{FRET} (with Oligonucleotides after 10 min)
With A6	0.70 ± 0.04	0.61 ± 0.016	0.58 ± 0.025
With G6	0.70 ± 0.04	0.65 ± 0.019	0.63 ± 0.024
With A9	0.70 ± 0.04	0.64 ± 0.02	0.51 ± 0.01
With G9	0.70 ± 0.04	0.65 ± 0.025	0.63 ± 0.032

Fluorescence Anisotropy

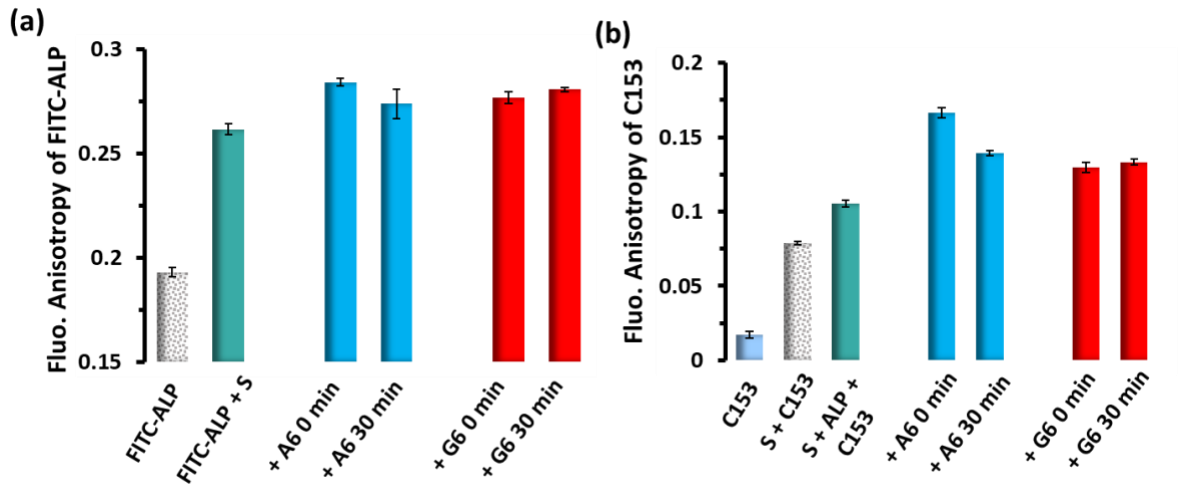

Fig. S61. Representative bar plot to show the Fluorescence Anisotropy values of (a) FITC-ALP (b) C153 with time after addition of A6 and G6 oligos. Experimental conditions: [FITC-ALP] = 100 nM, [C153] = 1 µM, [$C_{16}DPA•Zn^{2+}$] = 50 µM, [oligonucleotides] = 5 µM, slit width ex/em = 5/5 nm, Excitation wavelength = 492nm (for FITC-ALP), 430nm (for C153), [HEPES] = 5 mM, pH 7.0, T = 25 °C.

Fluorescence Lifetime

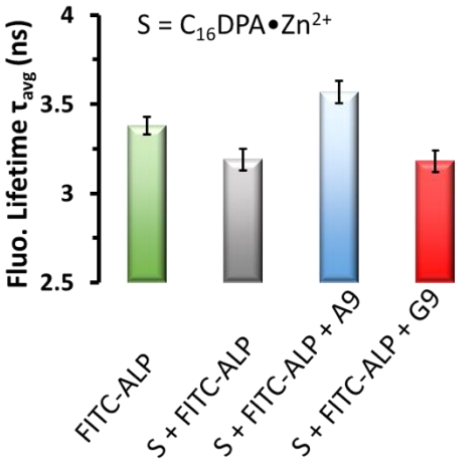

Fig. S62. Representative bar plot to show Fluorescence Lifetime of Oligos with FITC tagged ALP in the presence of surfactant. Experimental conditions: [FITC-ALP] = 100 nM, [$C_{16}DPA•Zn^{2+}$] = 50 µM, [oligonucleotides] = 5 µM, Excitation wavelength = 480nm, [HEPES] = 5 mM, pH 7.0, T = 25 °C.

Table. S8 Fluorescence Lifetime data of FITC-ALP with $C_{16}DPA•Zn^{2+}$ in the presence of oligonucleotides

Experimental conditions: [ALP-FITC] = 100 nM, [$C_{16}DPA•Zn^{2+}$] = 50 µM, [oligonucleotides] = 5 µM, [HEPES] = 5 mM, pH 7.0, T = 25 °C.

	τ_1 (ns)	τ_2 (ns)	τ_3 (ns)	α_1	α_2	α_3	τ_{avg} (ns)	χ^2
ALP-FITC	1.63	3.81	0.352	15.24	82.18	2.58	3.38 ± 0.05	1.02
$C_{16}DPA•Zn^{2+}$ + ALP-FITC	1.49	3.83	0.276	23.09	74.18	2.73	3.19 ± 0.06	1.14
ALP-FITC + A9	1.61	3.92	0.245	12.19	85.37	2.45	3.54 ± 0.048	1.12
$C_{16}DPA•Zn^{2+}$ + ALP-FITC + A9 initial	1.53	3.95	0.140	13.97	84.83	1.20	3.57 ± 0.063	0.986
$C_{16}DPA•Zn^{2+}$ + ALP-FITC + A9 after 2 min	1.63	3.87	0.077	16.04	82.83	1.62	3.47 ± 0.05	1.17
$C_{16}DPA•Zn^{2+}$ + ALP-FITC + A9 after 10 min	1.35	3.68	0.142	14.73	83.50	1.77	3.27 ± 0.045	1.08
$C_{16}DPA•Zn^{2+}$ + ALP-FITC + A9 after 12 min	1.55	3.81	0.232	17.97	80.14	1.88	3.34 ± 0.06	1.15

Table. S9 Fluorescence Lifetime data of FITC-ALP with $C_{16}DPA•Zn^{2+}$ in the presence of oligonucleotides

Experimental conditions: [ALP-FITC] = 100 nM, [$C_{16}DPA•Zn^{2+}$] = 50 µM, [oligonucleotides] = 5 µM, [HEPES] = 5 mM, pH 7.0, T = 25 °C.

	τ_1 (ns)	τ_2 (ns)	τ_3 (ns)	α_1	α_2	α_3	τ_{avg} (ns)	χ^2
ALP-FITC	1.63	3.81	0.352	15.24	82.18	2.58	3.38 ± 0.05	1.02
$C_{16}DPA•Zn^{2+}$ + ALP-FITC	1.49	3.83	0.276	23.09	74.18	2.73	3.19 ± 0.06	1.14
ALP-FITC + G9	1.65	4.03	0.273	20.56	76.86	2.58	3.44 ± 0.048	1.03
$C_{16}DPA•Zn^{2+}$ + ALP-FITC + G9 initial	1.26	3.68	0.137	16.40	80.66	2.95	3.18 ± 0.06	1.15
$C_{16}DPA•Zn^{2+}$ + ALP-FITC + G9 after 2 min	1.39	3.7	0.196	17.78	79.22	2.99	3.18 ± 0.03	1.13
$C_{16}DPA•Zn^{2+}$ + ALP-FITC + G9 after 10 min	1.14	3.59	0.085	14.75	82.28	2.97	3.12 ± 0.057	1.09
$C_{16}DPA•Zn^{2+}$ + ALP-FITC + G9 after 12 min	1.19	3.61	0.086	15.52	81.38	3.11	3.12 ± 0.049	1.24

DLS Study

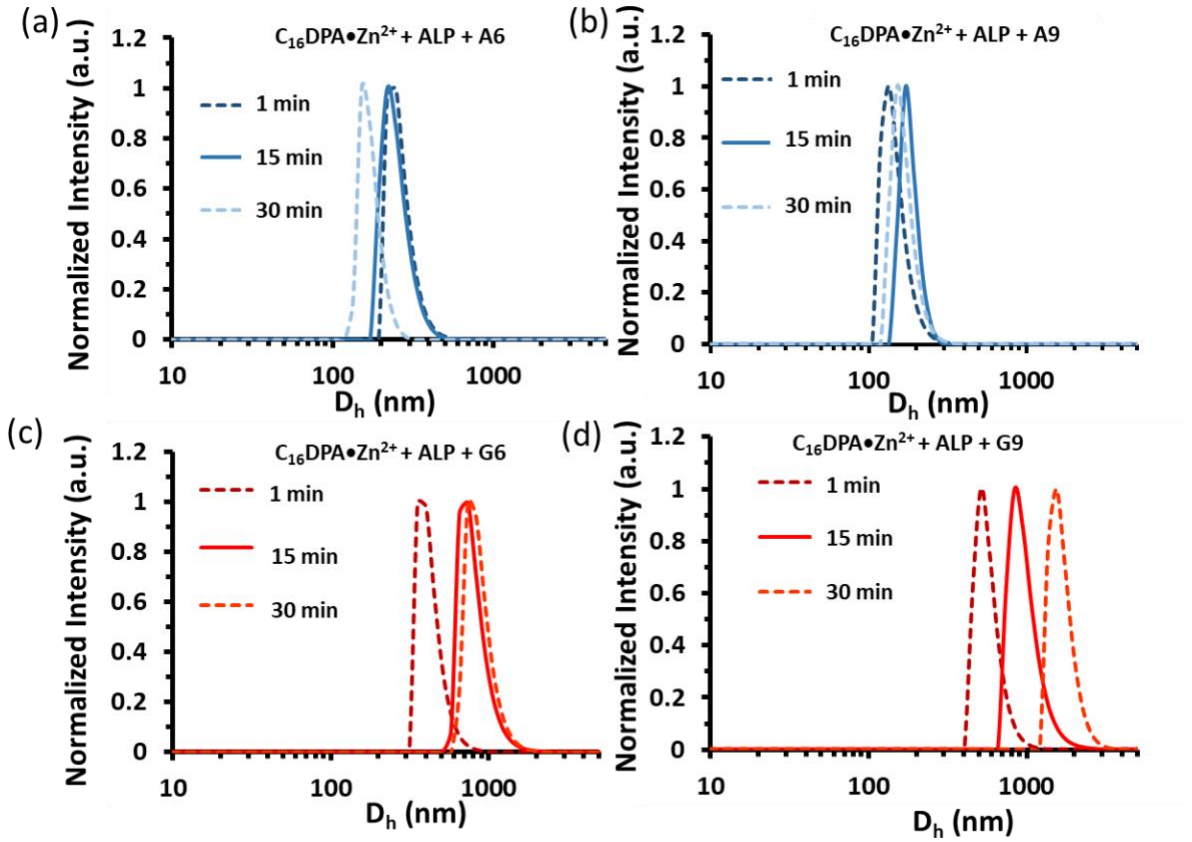

Fig. S63. DLS plot shows Dh (hydrodynamic diameter) of (a) $C_{16}DPA•Zn^{2+}$ + ALP + A6 (b) $C_{16}DPA•Zn^{2+}$ + ALP + A9 (c) $C_{16}DPA•Zn^{2+}$ + ALP + G6 (d) $C_{16}DPA•Zn^{2+}$ + ALP + G9 with time up to 30min. Experimental conditions: [ALP] = 100 nM, [$C_{16}DPA•Zn^{2+}$] = 50 µM, [oligonucleotides] = 5 µM, [HEPES] = 5 mM, pH 7.0, T = 25 °C.

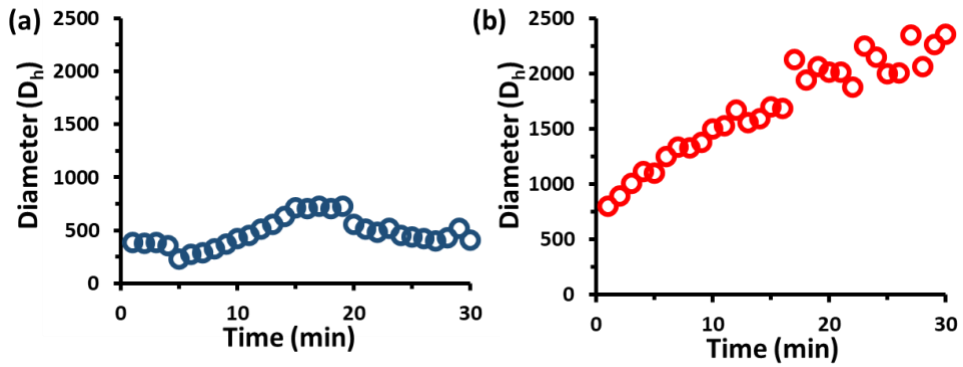

Fig. S64. DLS plot shows Dh (hydrodynamic diameter) of (a) $C_{16}DPA•Zn^{2+}$ + ALP + A9 (b) $C_{16}DPA•Zn^{2+}$ + ALP + G9 with time up to 30min. Experimental conditions: [ALP] = 100 nM, [$C_{16}DPA•Zn^{2+}$] = 50 µM, [oligonucleotides] = 5 µM, [HEPES] = 5 mM, pH 7.0, T = 25 °C.

For, A6 and A9, size of the complex initially increased and then decreased. For G6 and G9, with time it did not decrease rather increased or increased size remained constant.

CD Spectra of Oligo

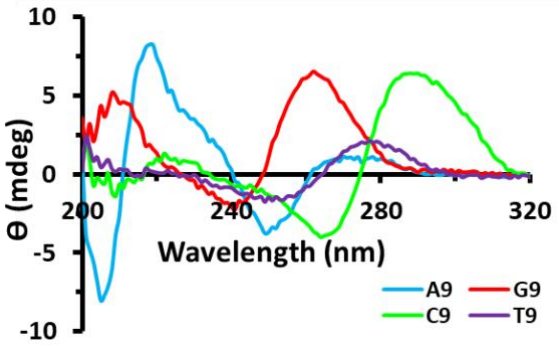

Fig. S65. Circular Dichroism (CD) spectra of Oligos A9, G9, C9 and T9 in absence of $C_{16}DPAZn^{2+}$. Experimental conditions: [oligonucleotides] = 10 µM, cuvette pathlenth = 2mm [HEPES] = 5 mM, pH 7.0, T = 25 °C.

Melting Temperature of Oligos

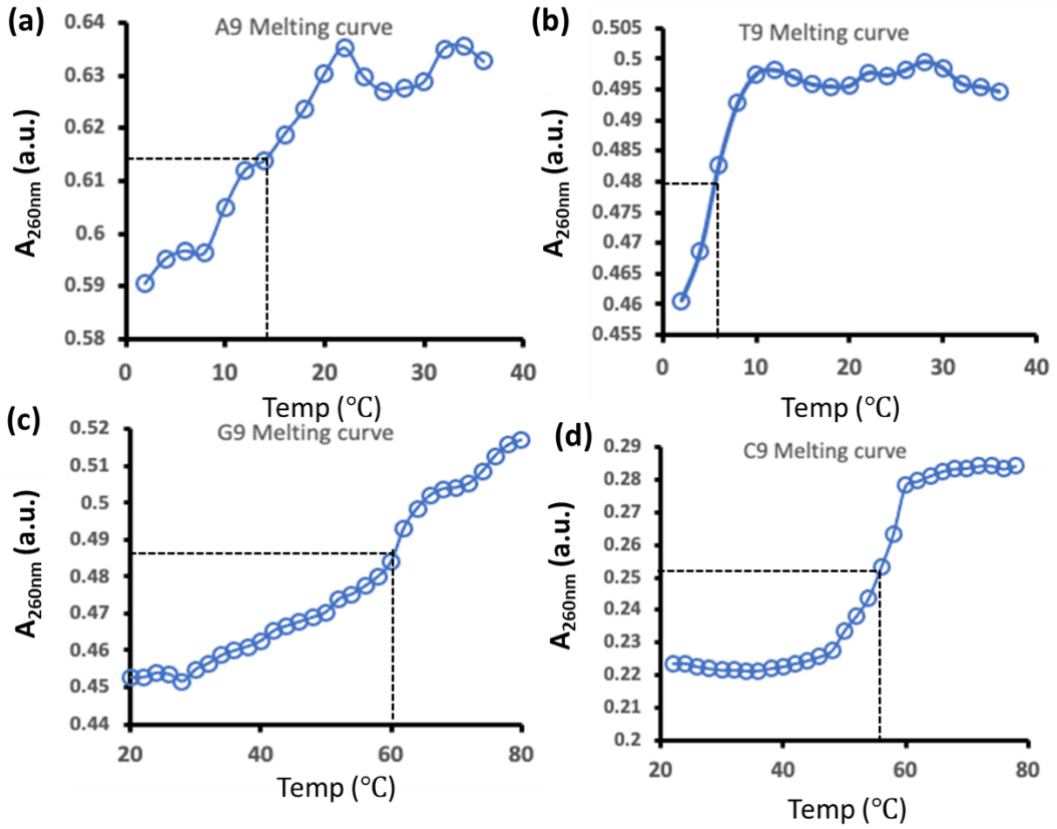

Fig. S66. Absorbance plots of Oligos (a) A9 (b) T9 at 260 nm as a function of temperature from 0-40°C (c) G9 and (d) C9 as a function of temperature from 20-80°C. Experimental conditions: [oligonucleotides] = 5 µM, [HEPES] = 5 mM, pH 7.0, T = 25 °C. From Fig. S66, experimentally found T_m° of A9, T9, G9 and C9 were 14 v, 6 °C, 60 °C, and 54 °C respectively.

Catalysis of Fluorophore-tagged oligonucleotides

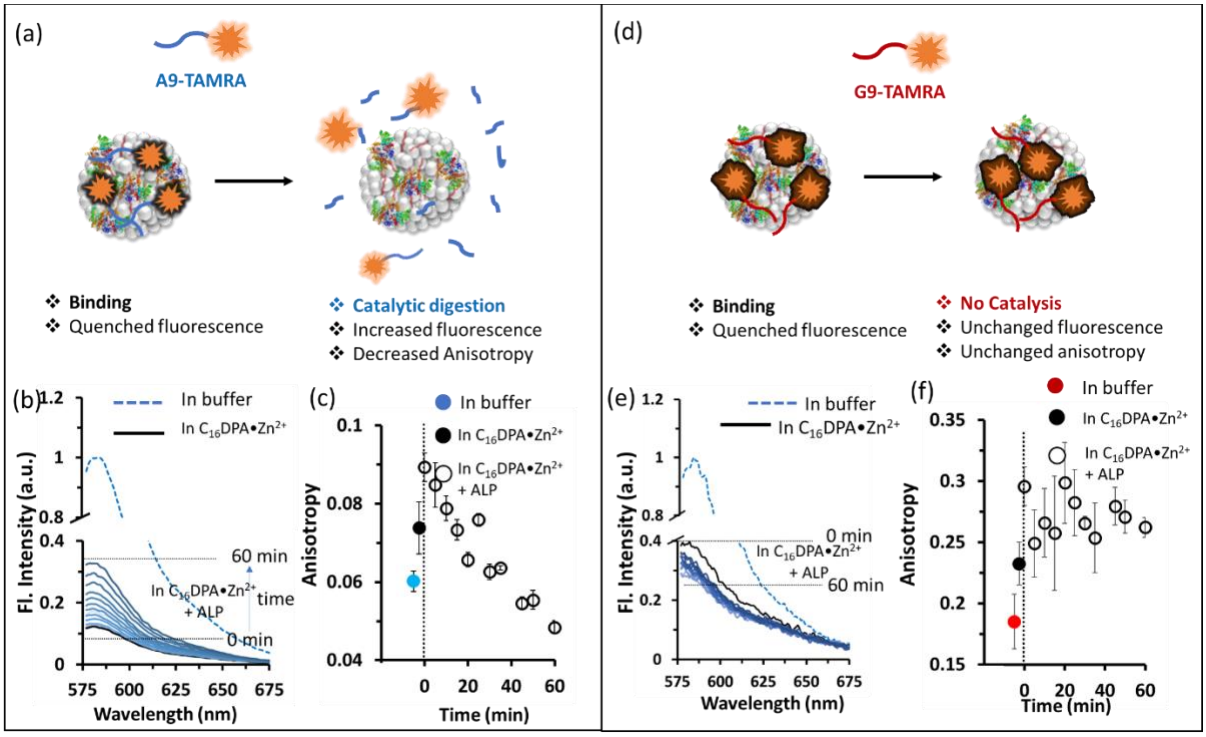

Fig. S67. (a) Schematic of A9-TAMRA digestion by the C_{16}DPA•Zn^{2+}-ALP complex, showing time-dependent change (b) in fluorescence emission spectra and (c) anisotropy value. (d) Schematic of G9-TAMRA digestion by the C_{16}DPA•Zn^{2+}-ALP complex, showing time-dependent change (e) in fluorescence emission spectra and (f) anisotropy value. Experimental conditions: [ALP] = 100 nM, [C_{16}DPA•Zn^{2+}] = 50 μM, [oligonucleotides] = 5 μM, ex/em slit width 5/5 nm, Excitation wavelength = 555 nm, [HEPES] = 5 mM, pH 7.0, T = 25 °C.

10. Binding and Catalysis Studies through ITC (Isothermal Titration Calorimetry)

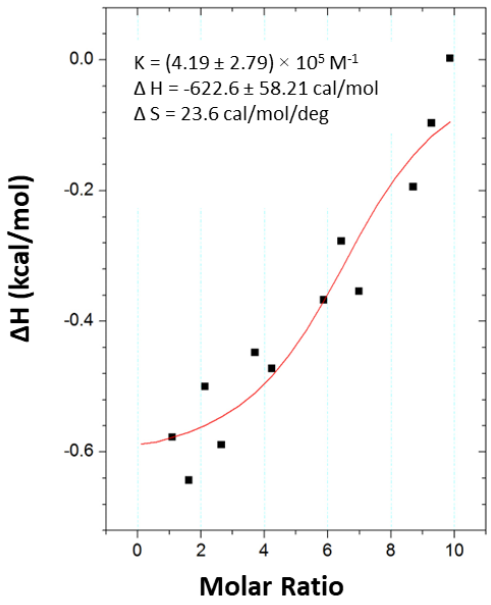

Fig. S68. Isothermal Titration Calorimetry (ITC) isotherm of (a) C_{16}DPA•Zn^{2+} (in the cell) with ALP (in syringe). Experimental conditions: [C_{16}DPA•Zn^{2+}] = 300 µM, [ALP] = 3 µM, [HEPES] = 5 mM, pH 7.0, T = 25 °C.

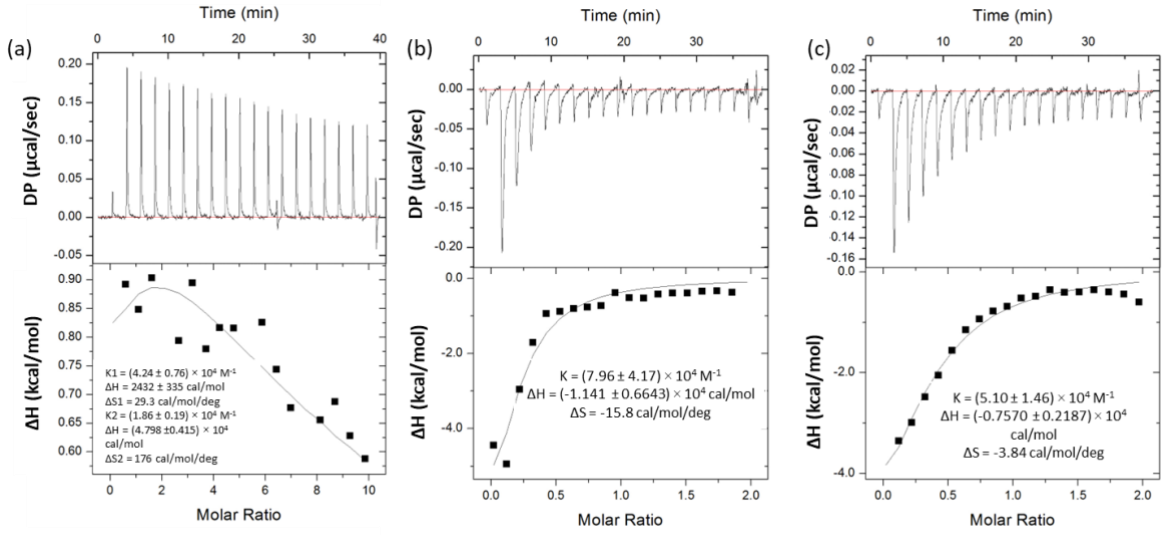

Fig. S69. Isothermal Titration Calorimetry (ITC) isotherm of (a) ALP + $Zn(NO_3)_2$ (in the cell) with Na_3PO_4 (in syringe), fitted in sequential binding fit model[S3-S4] and (b) C_{16}DPA•Zn^{2+} (in the cell) with Na_2HPO_4 (in syringe) (c) C_{16}DPA•Zn^{2+} + ALP (in the cell) with Na_2HPO_4 (in syringe). Experimental conditions: [C_{16}DPA•Zn^{2+}] = 60 µM, [$Zn(NO_3)_2$] = 60 µM [Na_3PO_4] = 600 µM (for fig. a) [Na_2HPO_4] =600 µM (for fig. b and c), [ALP] = 12 µM (for fig. a), 120 nM (for fig. c), [HEPES] = 5 mM, pH 7.0, T = 25 °C.

Table. S10 Thermodynamic aspects of phosphate binding with ALP, $C_{16}DPA•Zn^{2+}$, and $C_{16}DPA•Zn^{2+}$-ALP conjugate.

System	K (M^{-1})	ΔH (cal/mol)	ΔS(cal/mol/deg)
ALP-Zn^{2+}+ Na_3PO_4	K1 = (4.24 ± 0.76) × 10^4 K2 = (1.86 ± 0.19) × 10^4	ΔH1 = 2432 ± 335 ΔH2 = (4.798 ±0.415) × 10^4	ΔS1 = 29.3 ΔS2 = 176
$C_{16}DPA•Zn^{2+}$ + Na_2HPO_4	(7.96 ± 4.17) × 10^4	(-1.14 ± 0.6643) × 10^4	-15.8
$C_{16}DPA•Zn^{2+}$- ALP + Na_2HPO_4	(5.10 ± 1.46) × 10^4	(-0.7570 ± 0.2187) × 10^4	-3.84

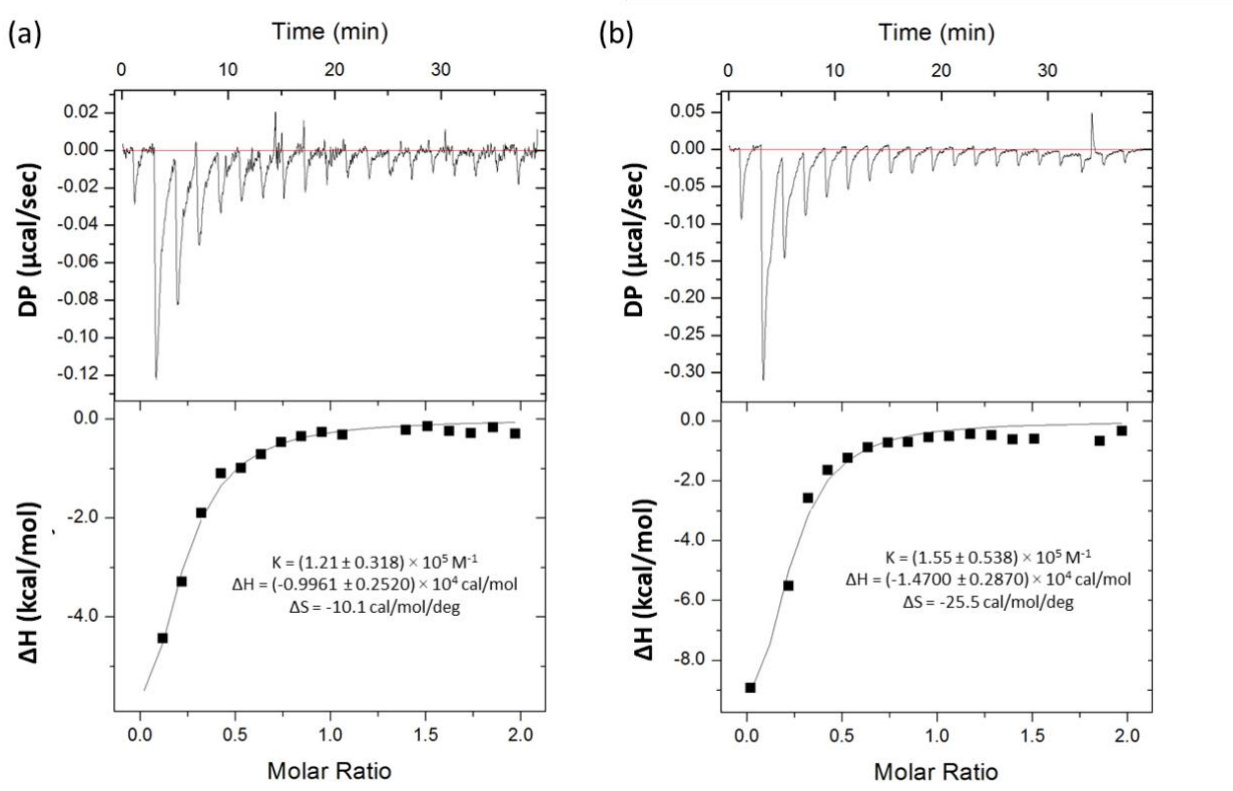

Fig. S70. Isothermal Titration Calorimetry (ITC) isotherm of (a) $C_{16}DPA•Zn^{2+}$ (in the cell) with AMP (in syringe), and (b) $C_{16}DPA•Zn^{2+}$ (in the cell) with GMP (in syringe). Experimental conditions: [$C_{16}DPA•Zn^{2+}$] = 60 µM, [Nucleotides] = 600 µM, [HEPES] = 5 mM, pH 7.0, T = 25 °C.

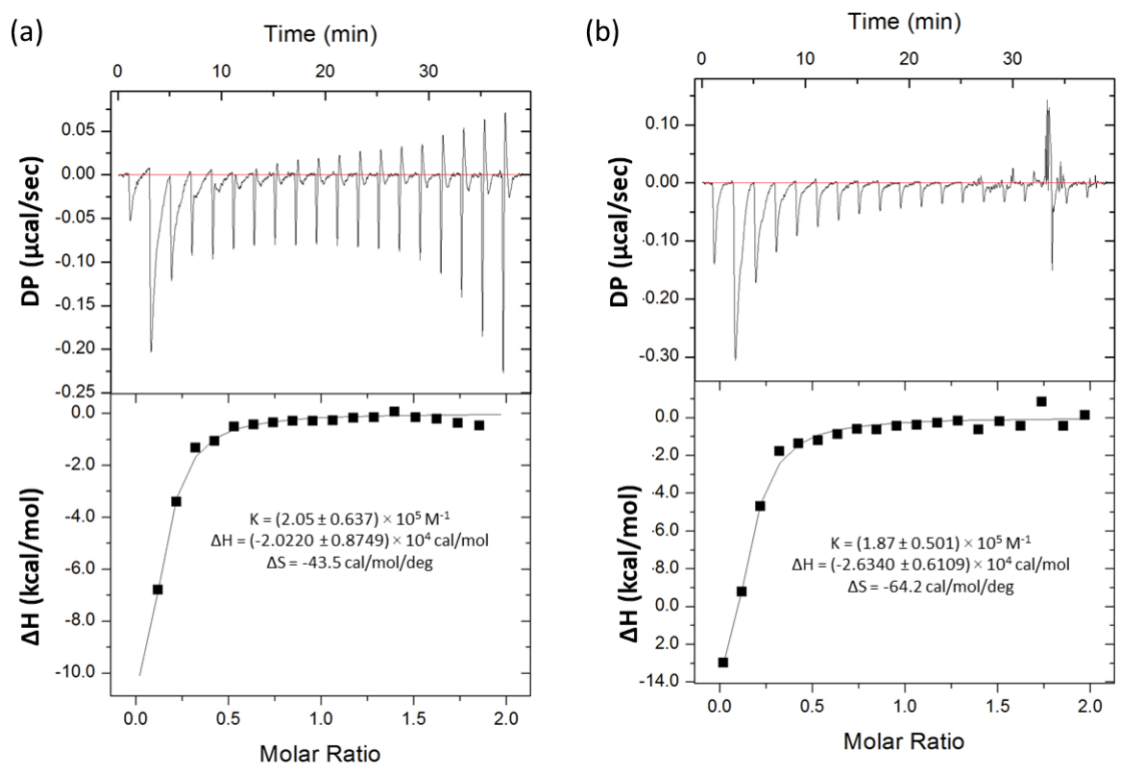

Fig. S71. Isothermal Titration Calorimetry (ITC) isotherm of (a) C_{16}DPA•Zn^{2+}+ ALP (in the cell) with AMP (in syringe), and (b) C_{16}DPA•Zn^{2+}+ ALP (in the cell) with GMP (in syringe). Experimental conditions: [C_{16}DPA•Zn^{2+}] = 60 µM, [ALP] = 120 nM, [Nucleotides] = 600 µM, [HEPES] = 5 mM, pH 7.0, T = 25 °C.

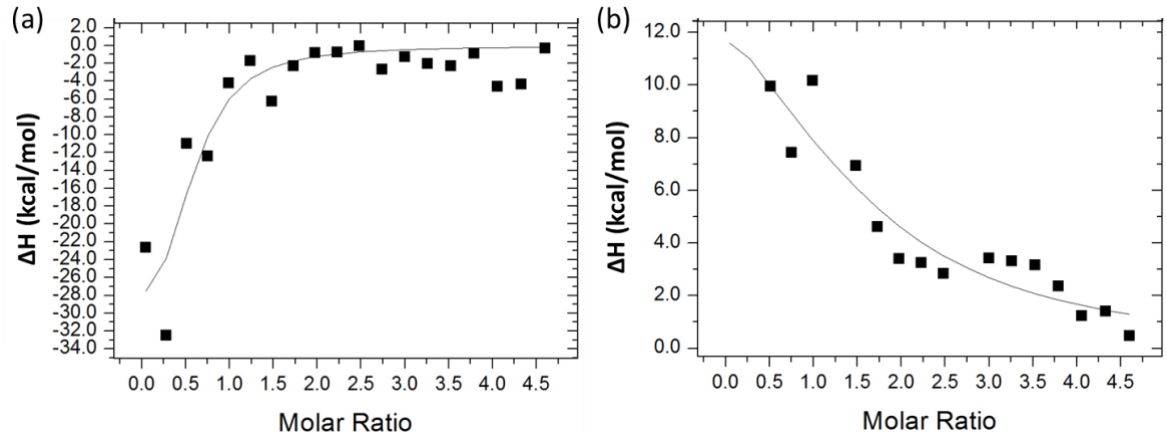

Fig. S72. Isothermal Titration Calorimetry (ITC) isotherm of (a) ALP (in the cell) with A9 (in syringe), and (b) ALP (in the cell) with G9 (in syringe). Experimental conditions: [ALP] = 1.2 µM, [Nucleotides] = 28 µM, [HEPES] = 5 mM, pH 7.0, T = 25 °C.

Table. S11 Thermodynamic aspects of ALP binding with A9 and G9.

	N	K (M^{-1})	ΔH (cal/mol)	ΔS(cal/mol/deg)
ALP + A9	0.502 ± 0.155	(4.85 ± 3.76) × 10^6	(- 3.76 ± 1.43) × 10^4	-95.8
ALP + G9	1.45 ± 0.761	(8.25 ± 6.94) × 10^5	(1.98 ± 1.36) × 10^4	93.6

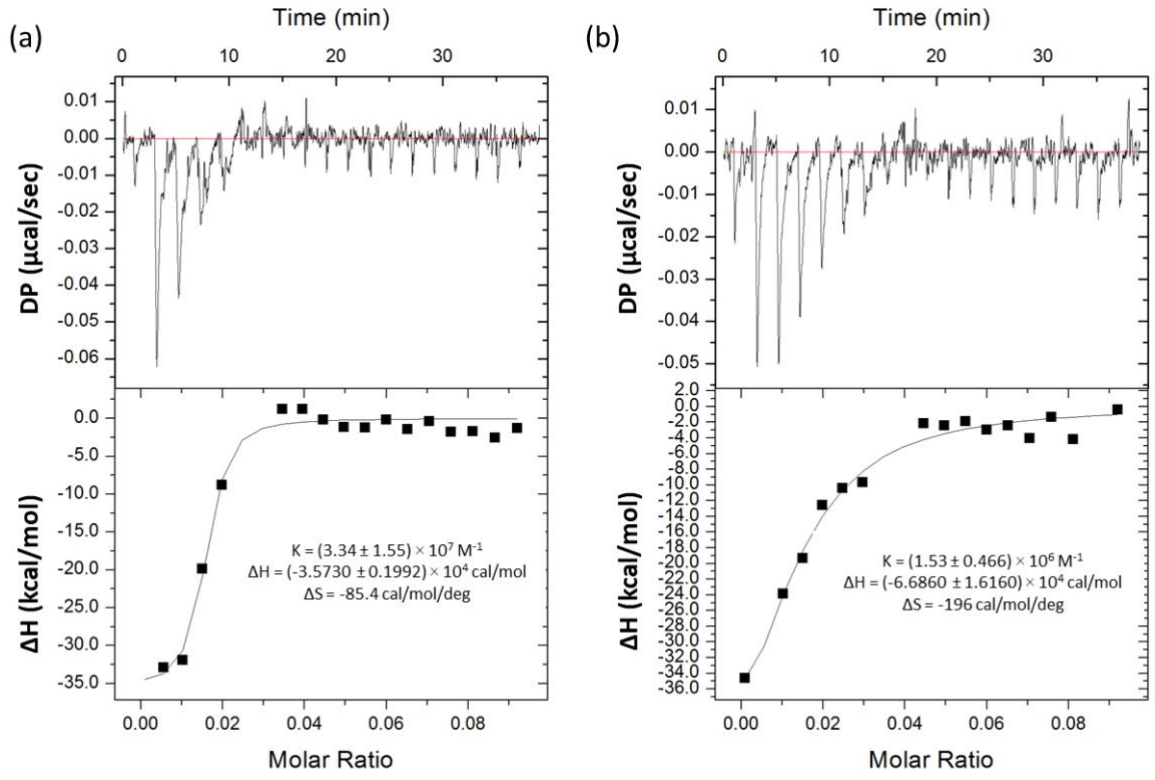

Fig. S73. Isothermal Titration Calorimetry (ITC) isotherm of (a) C_{16}DPA•Zn^{2+} (in the cell) with A9(in syringe), and (b) C_{16}DPA•Zn^{2+} (in the cell) with G9 (in syringe). Experimental conditions: [C_{16}DPA•Zn^{2+}] = 60 µM, [oligonucleotides] = 28 µM, [HEPES] = 5 mM, pH 7.0, T = 25 °C.

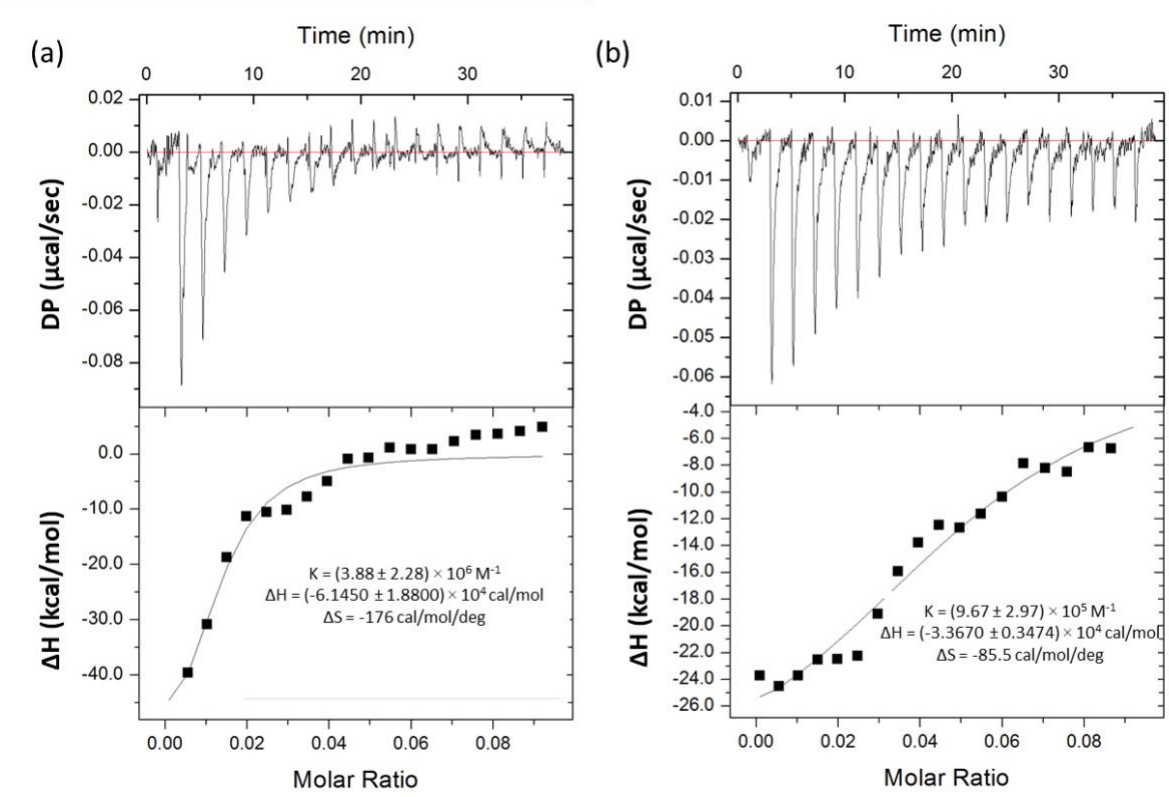

Fig. S74. Isothermal Titration Calorimetry (ITC) isotherm of (a) C_{16}DPA•Zn^{2+}+ ALP (in the cell) with A9 (in syringe), and (b) C_{16}DPA•Zn^{2+}+ ALP (in the cell) with G9 (in syringe). Experimental conditions: [C_{16}DPA•Zn^{2+}] = 60 µM, [ALP] = 120 nM, [Oligonucleotides] = 28 µM, [HEPES] = 5 mM, pH 7.0, T = 25 °C.

11. References

S1 Micsonai, F. Wien, É. Bulyáki, J. Kun, É. Moussong, Y.-H. Lee, Y. Goto, M. Réfrégiers, J. Kardos, *Nucleic Acids Res.* **2018**, *46*, W315–W322.

S2. Priyanka, S. Kaur Brar, S. Maiti, *ChemNanoMat* **2022**, 8, e202100498.

S3. M. L. Applebury, B. P. Johnson and J. E. Coleman, *J. Biol. Chem.*, 1970, **245**, 4968–4975.

S4. D. R. Banerjee, D. Dutta, B. Saha, S. Bhattacharyya, K. Senapati, A. K. Das and A. Basak, *Org. Biomol. Chem.*, 2014, **12**, 73–85.